Anna Eibel, BSc

Toward Enhancing the Scope of Photoinitiating Compounds

MASTER'S THESIS

to achieve the university degree of

Master of Science

Master's degree programme: Chemistry

submitted to

Graz University of Technology

Supervisor

Univ.-Prof. Mag.rer.nat. Dr.phil, Georg Gescheidt-Demner

Institute of Physical and Theoretical Chemistry (PTC)

Graz, March 2016

AFFIDAVIT

I declare that I have authored this thesis independently, that I have not used other than the declared sources/resources, and that I have explicitly indicated all material which has been quoted either literally or by content from the sources used. The text document uploaded to TUGRAZonline is identical to the present master‘s thesis.

Date	Signature

The important thing is not to stop questioning –

Curiosity has its own reason for existence.

Albert Einstein

Abstract

One subject of this work was the investigation of novel photochemical reaction pathways of bisacylphosphane oxide (BAPO) photoinitiators in aqueous media and in presence of nucleophiles. Upon photolysis of BAPOs in samples containing water or alcohols, an additional long-lived radical was observed in time-resolved EPR (TR-EPR) experiments, appearing together with the well-established benzoyl and phosphanoyl radicals. In samples containing BAPO and nucleophilic salts, only the benzoyl radical, but no phosphanoyl radical was found in TR-EPR spectra. These findings were attributed to an electrophilic behavior of the phosphanoyl radical formed upon photoinduced *α*-cleavage of BAPOs. The observed reactivity might be relevant with respect to the development and application of water-soluble BAPO photoinitiators and further investigations were performed using chemically induced dynamic nuclear polarization (CIDNP) spectroscopy and ^{31}P-NMR spectroscopy. Based on the experimental results and DFT calculations, reaction mechanisms have been established, comprising a nucleophilic attack at the BAPO-based phosphanoyl radical, which occurs either at the carbonyl group or directly at the phosphorous center.

Further, novel photoinitiators composed of a bisacylphosphane oxide (BAPO) and a α-hydroxy ketone were tested for their applicability as trifunctional photoinitiators utilizing UV-Vis spectroscopy, NMR spectroscopy, mass spectrometry, and gel permeation chromatography (GPC). Evidence for a wavelength-selective stepwise cleavage of the two benzoyl (mesitoyl) moieties from the BAPO and the α-hydroxy ketone moiety was gained from trapping experiments using a disulfide as well as a sterically congested monomer as radical scavengers (proof of principle). The sequential reactivity at three different wavelengths was successfully applied for the synthesis of polymers containing three distinct polymer blocks. It has been shown that multi-wave photoinitiators allow the synthesis of block copolymers by means of free radical photopolymerization, paving the way for novel applications in polymer design.

Kurzfassung

Ein Gegenstand dieser Arbeit war die Untersuchung photochemischer Reaktionswege von Bisacylphosphanoxid-Photoinitiatoren (BAPOs) im wässrigen Medium und in Gegenwart von Nukleophilen. Experimente mittels zeitaufgelöster Elektronenspinresonanz (TR-EPR) zeigen, dass in wässrigen oder alkoholhaltigen Proben zusätzlich zum bekannten und gut charakterisierten Phosphanoyl- und Benzoylradikal eine neue, langlebige radikalische Spezies entsteht. In Gegenwart von nukleophilen Salzen wurde hingegen nur das Benzoylradikal beobachtet, jedoch kein Phosphanoylradikal und auch keine zusätzliche Spezies. Diese Beobachtungen könnten einer elektrophilen Reaktivität des Phosphanoylradikals (welches durch photoinduzierte *α*-Spaltung von BAPOs entsteht) zugrunde liegen, was speziell für die Entwicklung und Anwendung von wasserlöslichen BAPO-Photoinitiatoren von Relevanz ist. Weitere Experimente wurden mittels CIDNP (chemisch induzierter dynamischer Spinpolarisation) und ^{31}P-NMR Spektroskopie durchgeführt. Basierend auf den experimentellen Ergebnissen und quantenmechanischen Berechnungen werden Reaktionsmechanismen vorgeschlagen, welche aus einem nukleophilen Angriff auf das Phosphanoylradikal bestehen, der entweder an der Carbonylgruppe oder direkt am Phosphoratom stattfinden kann.

Weiters wurden neue Photoinitiatoren bestehend aus einer BAPO-Einheit und einer α-Hydroxyketon-Einheit als trifunktionelle Photoinitiatoren getestet. Dafür wurden die Methoden UV-Vis Spektroskopie, NMR Spektroskopie, Massenspektrometrie und Gel-Permeations-Chromatografie (GPC) eingesetzt. Photolyse-Experimente in Gegenwart von Radikalfängern zeigen, dass die zwei Benzoyl-Einheiten vom BAPO und die α-Hydroxyketon-Gruppe wellenlängenselektiv stufenweise gespalten werden können. Als Radikalfänger wurden ein Disulfid sowie ein sterisch gehindertes Monomer eingesetzt. Die stufenweise Reaktivität bei drei verschiedenen Wellenlängen konnte erfolgreich für die Synthese von Polymeren bestehend aus drei unterschiedlichen Polymerblöcken verwendet werden. Es wurde gezeigt, dass „Multi-wave“ Photoinitiatoren die Synthese von Blockcopolymeren mittels freier radikalischer Photopolymerisation erlauben, was neue Anwendungen in der Polymerentwicklung ermöglichen könnte.

Acknowledgement

I would like to thank everyone who has contributed to this work. Especially I want to thank…

…. my supervisor Prof. Georg Gescheidt for his guidance, for numerous important discussions and – most importantly – for the fun and joy I have had working on my projects.

… David Fast for always having an open door for me and all my countless questions. I thank him for his support and patience and the time he has spent explaining everything to me or performing my MALDI-MS experiments. I really enjoy working with David and I appreciate very much all the things I have learned.

… Dmytro Neshchadin for his support and all the inspiring scientific conversations we have had. Dimi is always there to help me with the interpretation of my results and he is the one to ask whenever one of the instruments doesn't work properly – Dimi would always fix all the instruments I "broke" again and I value his help a lot.

… Max Schmallegger for being an awesome colleague. We have gone through our studies together, resulting in a friendship which I value a lot.

…. Eduard Stadler, Roman Geier, Yasmin Bürkl and Anne-Marie Kelterer for valuable discussions and the nice working atmosphere.

… Prof. Grützmacher at ETH Zürich for providing the photoinitiators and for useful discussions.

… Prof. Breinbauer for a very inspiring discussion about reaction mechanisms, and for motivating me during the time of my bachelor and master studies with each of his lectures.

… my parents for their support, love, patience and time throughout the last (almost) 23 years. Especially I want to thank my mum for always being there for me, always listening to me, always encouraging me and always believing in me.

Contents

1 General Introduction

Photoinitiated polymerizations play an important role in polymer chemistry. The reactions are widely applied in industrial processes, since curing can be performed in solvent-free formulations at high speed, low temperatures, and at spatially well-defined regions.[1,2] Common fields of applications include coatings (on wood, plastic, paper or metal surfaces), adhesives, stereolithography, microelectronics, optics, as well as medicine (e.g. tissue engineering, dental fillings and ophthalmology).[3,4]

The photoinitiator is a crucial component of every photopolymerized formulation. Upon absorption of light, it generates reactive species starting the polymerization process. These reactive species may be free radicals as well as ions (e.g. in cationic photopolymerization), the free radical process being most frequently applied.[3,5,6]
The development of new radical photoinitiators is still an ongoing field of research and particular interest is nowadays paid on water-soluble systems, which are important for biomedical applications as well as the development of hydrogel materials.[7,8] Apart from good solubility, biocompatibility and storage stability, high reactivity is a crucial property of such photoinitiators.[8] Hence, in order to design new and efficient water-soluble photoinitiators, it is essential to fully understand the photochemistry of the initiating species in aqueous media.

An important class of radical photoinitiators comprise mono- and bisacylphosphane oxides (MAPOs and BAPOs) and recently, water-soluble derivatives have been developed.[7,8] The basic photochemistry of MAPOs and BAPOs is well established. Photolysis of the compounds leads to the formation of a benzoyl and a phosphanoyl radical pair via *α*-cleavage, both radicals being reactive towards the double bonds of monomers.[9,10] However, little is known about the reactivity of these radicals in aqueous media and in presence nucleophiles. This work addresses the characterization of such systems by time-resolved electron paramagnetic resonance (TR-EPR) as well as NMR-based techniques and mass spectrometry.

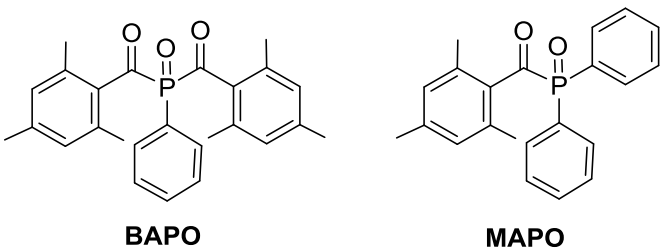

BAPO **MAPO**

Figure 1. Structures of a typical BAPO and a typical MAPO.

Another less commonly regarded feature of BAPOs is their ability to act as “multiwave-photoinitiators”. If BAPOs are irradiated with light of sufficiently high wavelength, only one of the two benzoyl groups is cleaved, and polymers bearing a photoactive MAPO end group can be obtained. These polymers can act as macroinitiators in a second irradiation step in presence of a different monomer, yielding a diblock copolymer.[11] In the present work, BAPO-based photoinitiators featuring a third photoactive group (which cleaves at lower wavelengths than BAPOs and MAPOs) are characterized and tested for the synthesis of triblock polymers.

2 Theoretical Background

2.1 Radical Photopolymerization

Photoinitiated radical polymerizations consist of three main steps: initiation, propagation and termination.[6] In the initiation step, the photoinitiator absorbs energy from a photon and subsequently yields the radicals which may add to the first monomer unit. By the addition of further monomer units, an oligomer or polymer chain is formed (propagation reaction). Termination of the chain reaction mainly occurs via combination of two polymer radicals or via disproportionation.[6] Side reactions, such as quenching of the radicals by molecular oxygen can also terminate the polymerization process. A simple scheme of the polymerization reaction is shown below on the example of a cleavage type photoinitiator A–B and the monomer M.

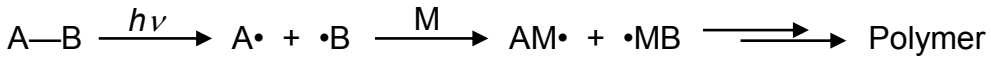

Scheme 1. General mechanism of radical photopolymerizations.

In most cases, the initiating radicals are formed from the excited triplet state (T_1) of the photoinitiator, which is reached upon light excitation into the excited singlet state (S_1) followed by intersystem crossing (ISC).[5] Depending on the photochemical reaction mechanism, radical photoinitiators (PIs) are divided into two main classes: one-component (type I) and two-component (type II).[2,12] Also, multicomponent initiating systems are known.[5]

Type I PIs undergo homolytic bond cleavage and are applied alone. Type II PIs, on the other hand, work in a bimolecular process together with a coinitiator. The initiating radicals are produced either by direct hydrogen abstraction between the excited PI and the coinitiator (a hydrogen donor) or by electron transfer followed by a proton transfer, which is more common.[2] In general, important requirements for an efficient photoinitiator are a good match between its absorption properties and the emission spectrum of the light source, as well as a high quantum efficiency of radical formation and a high reactivity of the resulting radicals towards the monomers.[2,4] Sometimes, direct photoexcitation of the PI is not possible (e.g. in colored or pigmented media, where the absorption spectra of the pigment and the PI overlap). In such a case, a suitable photosensitizer (PS) may be applied. The PI is then excited indirectly via energy transfer from the excited sensitizer.[5]

All individual components required to yield radicals in the initiation step of the photopolymerization (photoinitiator and/or coinitiator and/or sensitizer) together are referred to as the photoinitiating system.[5]

2.1.1 Overview of Type I and Type II Photoinitiating Systems

Typical type I photoinitiators feature a benzoyl moiety as the chromophore.[13] These compounds absorb light in the UV and near-UV range due to the *n,π** transition of the carbonyl group at around 320 – 360 nm and the *π,π** transition at around 280 – 300 nm.[4] Examples include benzoin ether or ester derivatives as well as alpha-hydroxy ketones, which fragment via *α*-cleavage, as shown in Scheme 1.[4,14] The scission of the bond next to the carbonyl group is also known as Norrish type I reaction.[2]

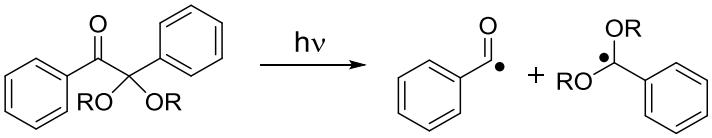

Scheme 2. Typical type I photoinitiator (a benzoin ether) undergoing *α*-cleavage.

Other important type I PIs are phosphane oxides, which absorb light in the UV-near visible range (see section 2.1.2).
Some type I PIs are known to undergo *β*-cleavage, since they feature a weak bond in the *β* position of the carbonyl group. An example are *α*-haloketones.[4]

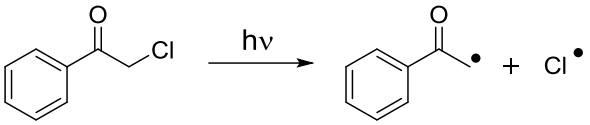

Scheme 3. Type I photoinitiator (an *α*-haloketone) undergoing *β* -cleavage.

Concerning type II photoinitiating systems, the light absorbing molecules are usually based on benzophenone, thioxanthone, camphorquinone, anthraquinone, benzil or ketocumarin derivatives. Typical coinitators are amines, alcohols, silanes or germanes, serving as the electron donor and/or hydrogen source.[4] Recently, one-component type II systems, consisting of both the photoinitiator and the coinitiator within one molecule have been developed.[15]

The mechanism is shown in Scheme 4 on the example of benzophenone and an amine. The excited triplet state of benzophenone accepts an electron from the amine, forming a radical ion pair, which is transformed into two radicals via subsequent proton transfer.[4]

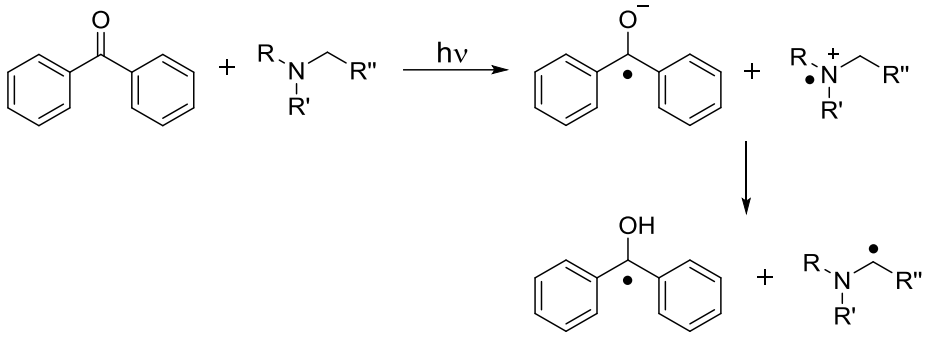

Scheme 4. Electron transfer followed by proton transfer in a type II photoinitiating system.

Another possible reaction mechanism for type II systems is direct hydrogen transfer from the donor molecule (Scheme 5). This is only possible from *n,π** triplet states (not from *π,π**).[4] Donors are usually alcohols or ethers like tetrahydrofuran (THF), which is therefore not a suitable solvent for type II photopolymerizations.

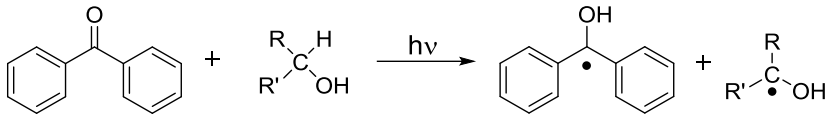

Scheme 5. Type II photoinitiating system working via direct hydrogen transfer.

2.1.2 Acylphosphane Oxide Photoinitiators

In this work, mono- and bisacylphosphane oxides (MAPOs and BAPOs) are studied, which are an important class of type I PIs.[9,10] Upon irradiation, they undergo *α*-cleavage to produce a benzoyl and a phosphanoyl radical with high efficiency ($\varphi \approx 0.6$).[16] The bond cleavage occurs from an excited triplet state, as was shown by chemically induced nuclear polarization (CIDNP) studies.[17] The triplet lifetimes have been found to be quite short (100 – 300 ps), resulting in high rate constants for bond cleavage.[18] Computational studies indicate that the efficiency of *α*-cleavage might be influenced by conformational dynamics of the excited molecules.[19] This is in line with the similar time scales for bond rotations, intersystem crossing and the kinetics of bond cleavage.[20]

Both phosphanoyl and benzoyl radicals can add to double bonds of monomers and initiate polymerization processes, while phosphanoyl radicals are more reactive than benzoyl radicals.[21–24] Scheme 6 depicts the reaction sequences involved in radical photo-polymerizations initiated by BAPOs.

Notably, it has been shown that the first additions of the initiator radicals to the monomer double bonds occur in a reversible way.[25]

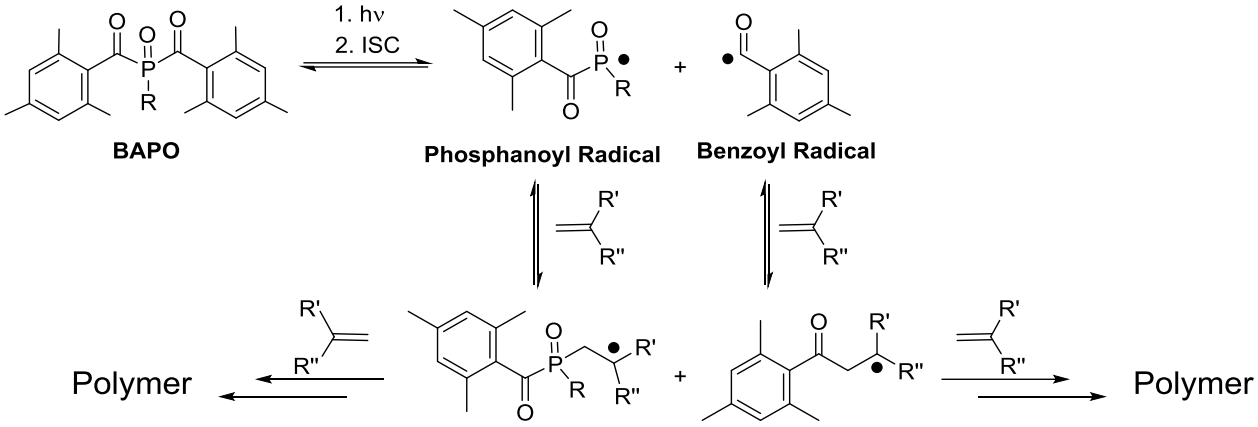

Scheme 6. Reaction scheme of radical photopolymerizations initiated by BAPOs.

An advantage of BAPOs over MAPOs is the production of altogether four initiating radicals in a stepwise way.[17] Scheme 6 shows that the addition product of a BAPO-based phosphanoyl radical to a double bond (or a different radical scavenger) is a MAPO derivative, which can undergo another *α*-cleavage reaction, producing a second benzoyl radical and a MAPO-based phosphanoyl radical. The cleavage of the first benzoyl moiety can be achieved at higher wavelengths than the cleavage of the resulting MAPO photoproduct, as is explained by the absorption properties of the compounds.

Due to the rather large conjugated electronic system caused by the presence of two benzoyl moieties, the absorption spectrum of BAPOs extends well into the visible range (*n*-*π** transition at around 400 nm). In comparison, the *n*-*π** transition of MAPOs is shifted to lower wavelengths (hypsochromic shift), since the conjugated system is smaller. Therefore, light of higher energy (lower wavelengths) is needed for the *α*-cleavage of a MAPO. This is also the basis for the applicability of BAPOs as “multi-wave photoinitiators” (chapter 4).

Moreover, the higher efficiency in the absorption of visible light makes BAPOs more favorable than MAPOs in many industrial applications. Visible light photoinitiators are for example desired for the curing of pigmented coatings as well as for clear coatings in the automotive industry, where UV stabilizers are added to the formulation, making the use of a PI absorbing only in the UV range unfavorable.[9,10] For the curing of white pigmented coatings and thick clear layers, BAPOs (and MAPOs) show superior performance over other visible light photoinitiators, since they display the photobleaching effect. BAPOs are yellowish compounds, but upon light irradiation, the chromophore is broken, resulting in colorless photoproducts required for applications such as clear coatings.[9,10]

2.2 Experimental Techniques

Short-lived radical species can be detected using several techniques. Time-resolved electron paramagnetic resonance (TR-EPR) and chemically induced dynamic nuclear polarization (CIDNP) spectroscopy are powerful methods based on magnetic field effects. In TR-EPR, radicals are observed directly, while from CIDNP spectroscopy (which is based on NMR), information about the products formed via radical pathways is obtained. Both methods have been extensively applied to study MAPO and BAPO photoinitiators.[17,22,23,26]

Another common technique to study radical reactions is transient optical spectroscopy (nanosecond laser flash photolysis), which is especially useful for kinetic investigations (determination of reaction rate constants).[27] As an example, phosphanoyl radicals generated from MAPO or BAPO photoinitiators can be very well observed by laser flash photolysis (LFP) due to their absorbance in the UV-Vis range.[23] Benzoyl radicals, on the other hand, can be detected by TR-IR spectroscopy.[21]

This chapter gives a short overview of TR-EPR and CIDNP spectroscopy, which represent the techniques mainly used in this work.

2.2.1 Time-resolved Electron Paramagnetic Resonance

Time-resolved electron paramagnetic resonance (TR-EPR) spectroscopy allows the detection of radicals in a nanosecond–microsecond timescale.[28] At such short timescales, the intensities of the EPR signals differ from what is predicted by a Boltzmann distributed population of the spin energy levels and signals with enhanced absorption or enhanced emission are observed. The appearance of these spin-polarized signals is due to a phenomenon called chemically induced dynamic electron polarization (CIDEP). Comprehensive theoretical descriptions of CIDEP can be found in a number of publications.[29–33] In general, CIDEP may originate from two mechanisms: the triplet mechanism (TM) and the radical pair mechanism (RPM).[29,30] Often, a combination of both mechanisms is observed in TR-EPR spectra. For completeness, it should be mentioned that recently, also a third mechanism giving rise to CIDEP was discovered, called the radical triplet pair mechanism (RTPM).[33]

From CIDEP spectra, one can obtain information about the multiplicity of the precursor molecules (singlet or triplet precursors) as well as the structure of the primarily formed radicals. By applying the line-width method, kinetic studies are possible as well.[26,34]

Technically, TR-EPR spectra can be recorded in two ways, either via a modified continuous-wave (cw) EPR experiment or via Fourier transform (FT) EPR (pulsed mode).[35] In our group, the first method is used. The experimental setup consists of a Nd:YAG laser serving as the pulsed light source (ns pulses), a X-band EPR spectrometer, a digital oscilloscope for data acquisition and a sample flow system. The oscilloscope is synchronized to the laser trigger and a PC program controls the whole setup. The spectra are recorded directly and not in the derivative mode, since the application of the field modulation (used to improve the S/N ratio in conventional EPR experiments) would not allow the desired time resolution.[36]

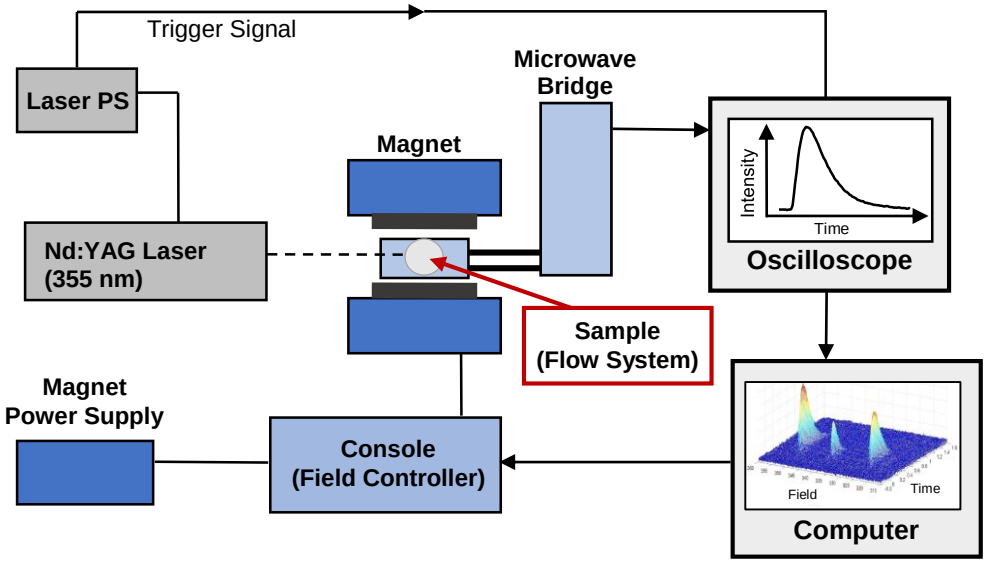

Figure 2. Block diagram of the TR-EPR setup used in this work.

2.2.1.1 Triplet Mechanism and Radical Pair Mechanism

CIDEP originating from the triplet mechanism (TM) may be detected when radicals are generated photochemically (since a triplet precursor is required). The TM is based on anisotropic intersystem crossing to preferentially populate one of the three triplet states, which are nondegenerate in a magnetic field. Notably, the polarization is created before the formation of the radicals.[28] Therefore, spin-polarized radicals can only be observed if the kinetics of radical formation from the polarized triplet state can compete with the physical process of spin lattice relaxation (SLR), leading to equally populated triplet states. Figure 3 depicts the processes involved in the TM.

In Figure 3, a preferential population of the T_{+1} triplet state is shown. This will lead to emissive signals in TR-EPR spectra, whereas enhanced absorption will be observed if the T_{-1} state is populated. Accordingly, CIDEP originating from the TM shows either totally absorptive or totally emissive signals.

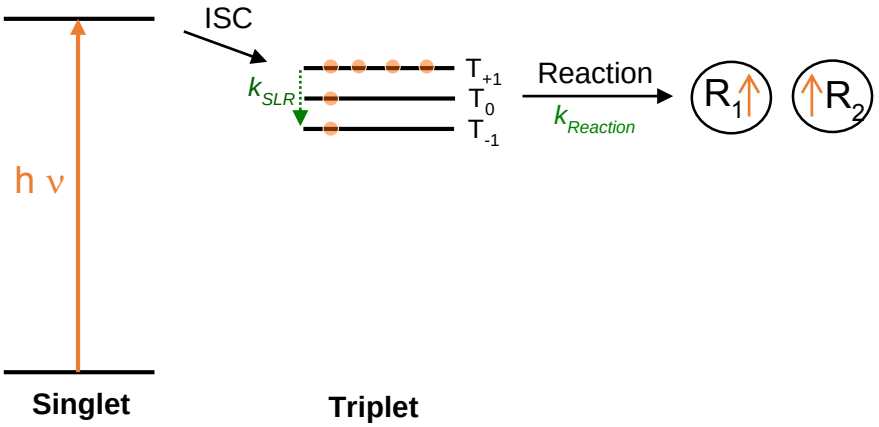

Figure 3. The triplet mechanism: selective population of one of the three triplet states.

In contrast, mixed absorption-emission patterns are observed in CIDEP caused by the radical pair mechanism.[28] In general, the RPM involves a spin-sorting process based on singlet-triplet mixing. A radical pair is either produced from a singlet precursor (in thermal reactions) or a triplet precursor (in photochemical reactions) and it has the same multiplicity as the precursor molecule.[37] The energies of singlet and triplet radical pairs in an external magnetic field are distance dependent, as shown in Figure 4.[38]

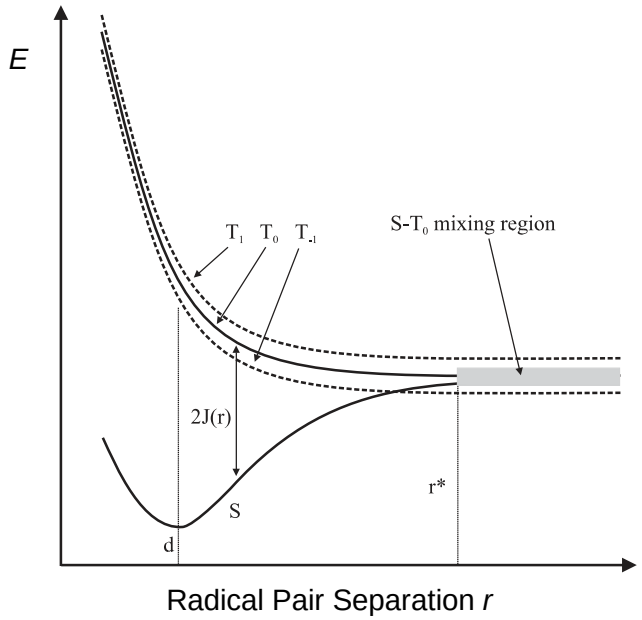

Figure 4. Energy levels of singlet and triplet radical pairs as a function of the distance between the radicals.

At a certain distance $r > r^*$, the exchange interaction $J(r)$ is small enough so that mixing between the singlet state S and the T_0 triplet state becomes energetically possible. Therefore, a radical pair originally formed in the triplet state may be interconverted to a singlet radical pair after diffusing apart to a distance of at least r^* between the two radicals. The S-T_0 mixing

process is represented by the vector model depicted in Figure 5.[38] Mixing of the spin states is possible due to slight deviations in the Larmor frequency of the two spins, caused by small magnetic field variations.[29]

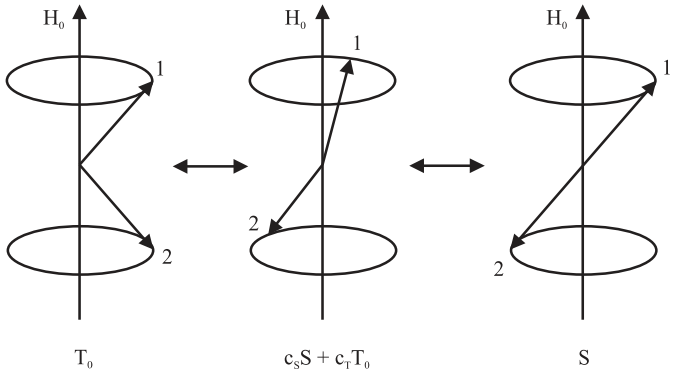

Figure 5. Vector representation of S-T_0 mixing (shown for the electron spins 1 and 2).

In CIDEP caused by the RPM, net effects (one radical is in emission and the other one in absorption or vice versa) and multiplet effects (emission and absorption are observed for the same radical) are distinguished.[29] Net polarizations are due to the influence of the electron exchange interaction, which leads to the accumulation of more *α* spins in one radical and more *β* spins in the other. Multiplet effects are generated due to hyperfine interactions, since nuclear spin configurations influence the rate of intersystem crossing.[33]

2.2.2 Chemically Induced Dynamic Nuclear Polarization

Chemically Induced Dynamic Nuclear Polarization (CIDNP) is observed in NMR experiments when fast radical pair reactions take place. In contrast to CIDEP, the radical species are not detected directly, but polarized signals of the follow-up products are detected, providing insight into radical reaction pathways.

The CIDNP effect is explained by the radical pair mechanism.[39,40] Due to interactions between the unpaired electron and nuclear spins, the populations of the nuclear spin energy levels are no longer in thermal equilibrium according to the Boltzmann distribution. Thus, signals showing enhanced absorption or emission signals are observed in the NMR spectra.[41,42]

Scheme 7 presents the radical pair mechanism leading to CIDNP effects. Three main steps are involved in the CIDNP effect. First, a radical pair (indicated by the overbars) is generated from a singlet or a triplet precursor. Then, the radical pair may undergo nuclear spin selective singlet-triplet mixing. The last step comprises different subsequent reactions of singlet and triplet pairs, forming the products observed via NMR.

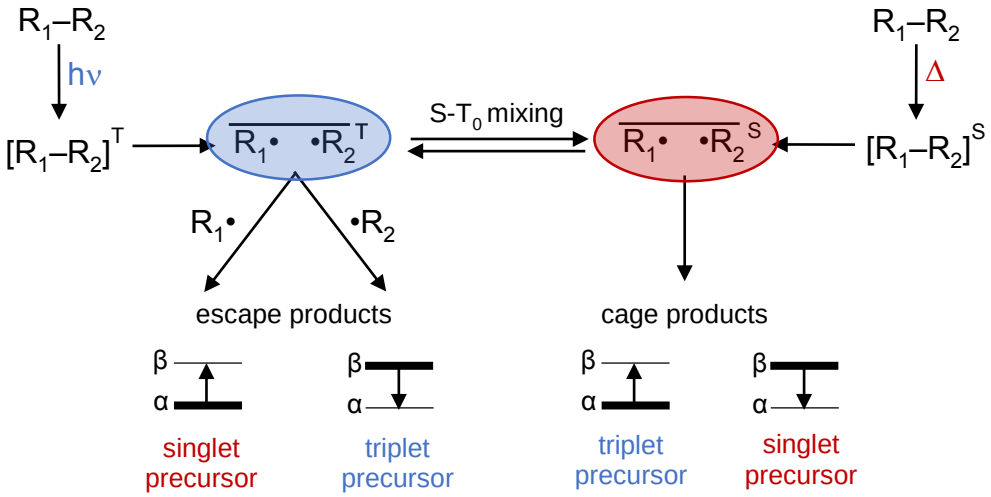

Scheme 7. General CIDNP reaction scheme.

So called “cage products” (or “recombination products”) are formed if the initial radical pair recombines, while “escape products” are observed if the radicals escape the solvent cage. Generally, recombination reactions can only occur from the singlet state (due to the Pauli principle). Therefore, singlet-triplet mixing is required for the formation of cage products from triplet radical pairs.[41] This process is analogous to the one occurring in CIDEP and can be described with the vector model presented in Figure 5. The rate of S-T_0 mixing is proportional to the difference in the Larmor frequencies $\Delta\omega$ of the two electron spins (equation 1).[43] A higher value of $\Delta\omega$ corresponds to a faster S-T_0 mixing.

$$\Delta\omega = \omega_1 - \omega_2 = \frac{1}{2}\left[H_0\,\Delta g\,\beta_e\,h^{-1} + \sum_{i=1}^{n} a_{1i}\,m_{1i} - \sum_{j=1}^{k} a_{2i}\,m_{2i}\right] \qquad (1)^{a}$$

Equation 1 shows that the rate of S-T_0 mixing depends on the magnetic field, the *g* factor difference of the two radicals, the magnitude of the hyperfine coupling constant and the nuclear spin orientation, reflected by the magnetic quantum number *m*. For example, for a nucleus with a spin of 1/2 (like a proton) the value of *m* can be +1/2 (α) or -1/2 (β).

In order to rationalize the spin-selective reaction pathways shown in Scheme 7, equations 2 and 3 (which are valid for a radical pair where only one radical carries a magnetically active nucleus with a spin of 1/2) can be considered.

[a] ω_1 and ω_2: Larmor frequencies of unpaired electron spin of R_1 and R_2, H_0 - strength of magnetic field, Δg – difference of g-factors of radical R_1 and R_2, β_e - Bohr magneton, a_{1i} and m_{1i}, a_{2j} and m_{2j}: hyperfine coupling constant and magnetic quantum number of nuclei i and j in radical R_1 and R_2.

$$\alpha;\ m_{1i} = +\frac{1}{2}: \qquad \Delta\omega_{+} = \frac{1}{2}\left[H_0\,\Delta g\,\beta_e\,h^{-1} + \frac{1}{2}a_{1i}\right] \qquad (2)$$

$$\beta;\ m_{1i} = -\frac{1}{2}: \qquad \Delta\omega_{-} = \frac{1}{2}\left[H_0\,\Delta g\,\beta_e\,h^{-1} - \frac{1}{2}a_{1i}\right] \qquad (3)$$

For *α* nuclear spins, the rate of S-T_0 mixing is higher than for a *β* spin, since $\Delta\omega_+$ is larger than $\Delta\omega_-$ (assuming that *Δg* and the hyperfine coupling constants *a* are positive).
Therefore, triplet radical pairs with *α* nuclear spins reach the singlet state faster than triplet radical pairs with *β* spins. This explains why cage products formed from triplet precursors show enhanced absorption (*α* spin levels overpopulated), while the corresponding escape products show enhanced emission (*β* spin levels overpopulated). Accordingly, the polarization of the CIDNP signals is opposite for the products formed from singlet precursors.

A tool for the qualitative interpretation of CIDNP spectra are Kaptein's rules, which allow the prediction of the sign of the polarizations. Both net effects (signals show either enhanced emission or absorption) and multiplet effects (different polarizations are observed in the same multiplet) can be analyzed using these rules.[44]

To summarize, CIDNP spectroscopy is a method to indirectly observe radicals via the follow-up products formed in radical reactions. The chemical shifts observed in the spectra are the same as in conventional NMR spectra, providing structural information about the products formed, whereas the polarization of the signals contains information about the reaction pathways.

3 Photochemistry of BAPOs in Presence of Nucleophiles

3.1 Introduction

The photochemistry of mono- and bisacylphosphane oxide (MAPO and BAPO) photoinitiators has been extensively investigated utilizing TR-EPR (and an array of other methodologies) by the group of Prof. Turro, as well as by our group.[22,23,26,45,46] As mentioned before, photolysis of MAPOs and BAPOs yields a phosphanoyl radical (**P•**) and a (substituted) benzoyl radical (**B•**)[b] via a Norrish type I reaction (*α*-cleavage).

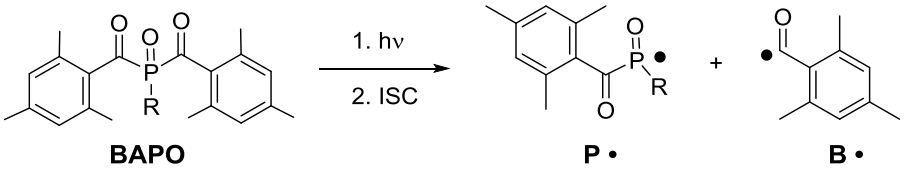

Scheme 8. Photoinduced *α*-cleavage of a BAPO photoinitiator.

A TR-EPR spectrum typical for these compounds is presented in Figure 6 on the example of bis(2,4,6-trimethylbenzoyl)phenylphosphane oxide, which is a commercially available BAPO. In the spectrum, three peaks are observed. The central peak is assigned to the benzoyl radical, while the two outer lines belong to the phosphanoyl radical, displaying a doublet due to the nuclear spin of 1/2 of the ^{31}P nucleus. The hyperfine coupling constant is determined to be 26.0 mT (measured in toluene).

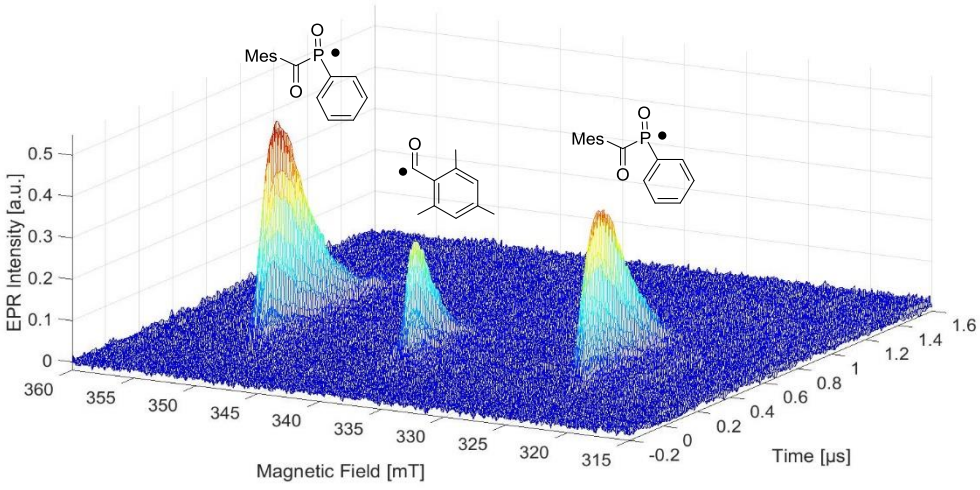

Figure 6. TR-EPR spectrum recorded upon laser flash photolysis (355 nm) of bis(2,4,6-trimethylbenzoyl)phenylphosphane oxide (10 mM solution in argon-saturated toluene).

[b] Sometimes, the substituted benzoyl radical is also referred to as mesitoyl radical.

Figure 7 depicts the same spectrum in the time span of 200 – 300 ns after the laser flash. It can be clearly seen that the triplet mechanism is the dominant CIDEP effect.

.

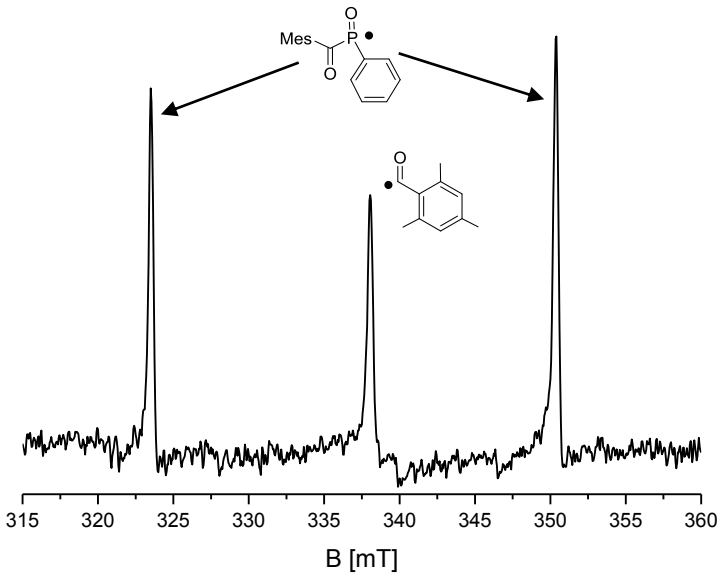

Figure 7. TR-EPR spectrum of bis(2,4,6-trimethylbenzoyl)phenylphosphane oxide observed 200 – 300 ns after the laser flash (10 mM solution in argon-saturated toluene).

Interestingly, a new radical species with a much smaller coupling constant of around 2.9 mT has been observed by Woodward and coworkers when recording the TR-EPR spectra of the same BAPO in alcoholic solvents.[47] The signals of the original phosphanoyl radical have been found to show decreased intensity when compared to the spectra measured in toluene or acetonitrile. Similar solvent effects have earlier been found by Gatlik.[45] The structure of the newly formed species as well as the reaction mechanism are not clear yet. Notably, the new signals have not been observed with MAPOs.[47]

Evidence for the photoinduced reactivity of BAPOs towards water, alcohols and amines was also gained from the analysis of products formed upon long-time irradiation. These experiments were performed in the group of Prof. Grützmacher at ETH Zürich. The samples were irradiated using light from a UV lamp or a blue LED and the photoproducts were isolated and characterized by NMR.[48,49]

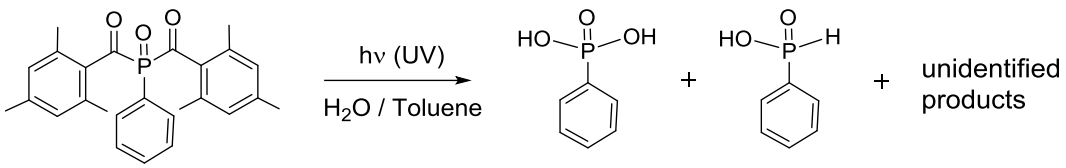

Scheme 9. Photolysis of BAPO in presence of water as reported in reference 49.

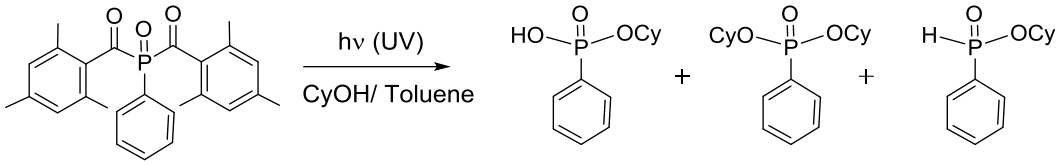

Scheme 10. Photolysis of BAPO in presence of cyclohexanol (CyOH) as reported in reference 49.

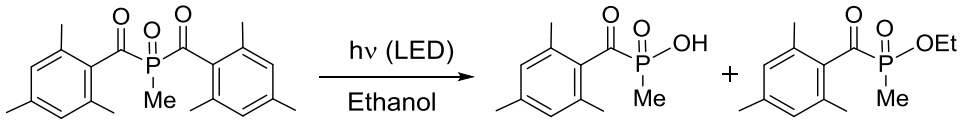

Scheme 11. Photolysis of Me-BAPO in presence of ethanol upon irradiation with a blue LED as reported in reference 49.

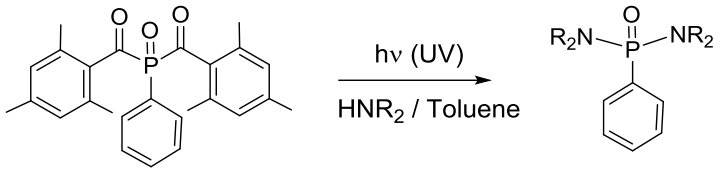

Scheme 12. Photolysis of BAPO in presence of secondary amines (HNR_2) as reported in reference 48.

The CIDEP as well as the NMR investigations mentioned above clearly suggest additional photoreaction pathways of BAPOs in presence of water or alcohols.[47] Therefore, when conducting photopolymerizations in aqueous media, there is presumably a competition between the reaction of the photoinitiator with the monomer and with the solvent. Elucidating the reaction mechanism in order to better understand the photochemistry of these systems is of interest, since nowadays, photopolymerizations in aqueous media are of growing importance. On the one hand, the water-insoluble BAPO bis(2,4,6-trimethylbenzoyl)phenyl-phosphane oxide is commercially available as a dispersion in water and on the other hand, several water-soluble BAPO derivatives have recently been synthesized by Grützmacher and coworkers.[7,8]

We want to test whether the different photochemistry of BAPOs in aqueous media can be traced back to an electrophilic behavior of the phosphanoyl radical. Therefore, the photoinduced reactivity of BAPOs towards various nucleophiles (including water and alcohols as well as anions) has been investigated in the course of this work, mainly by means TR-EPR and CIDNP spectroscopy.

3.2 Experimental

Investigated Photoinitiators, Materials and Solvents.

Compound **1** (bis(2,4,6-trimethylbenzoyl)phenylphosphane oxide, "Irgacure 819") was purchased from Ciba Specialty Chemicals. Compounds **2** and **3** were provided by the group of Prof. Grützmacher (ETH Zürich). Compound **4** (bis(2,6-dimethoxy-benzoyl)-2,4,4-trimethyl-pentylphosphane oxide, "CGI 403") and compound **5** ((2,4,6-trimethylbenzoyl)diphenyl-phosphane oxide, "Lucirin TPO") were obtained from Ciba.

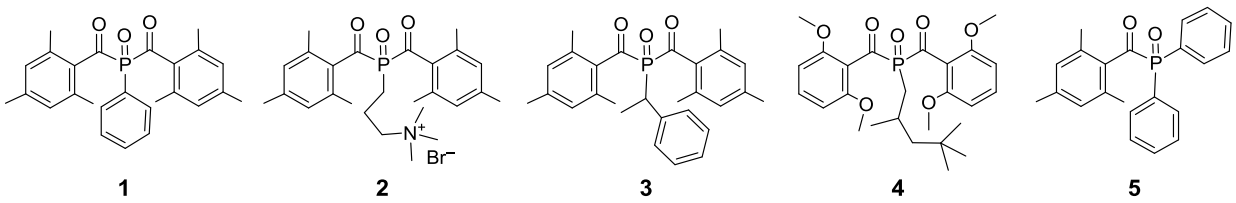

Figure 8. Structures of BAPO and MAPO photoinitiators

Tetrabutylammonium iodide ($Bu_4N^+I^-$, ≥99%), tetrabutylammonium bromide ($Bu_4N^+Br^-$, >99%), tetrabutylammonium hexafluorophosphate ($Bu_4N^+PF_6^-$, 98%), sodium iodide (NaI, ≥99%), sodium tetrafluoroborate ($Na^+BF_4^-$, 98%) were purchased from Fluka and used as received. Tetrabutylammonium chloride ($Bu_4N^+Cl^-$, ≥99%), tetrabutylammonium fluoride hydrate ($Bu_4N^+F^-\cdot xH_2O$, 98%) and sodium perchlorate ($Na^+ClO_4^-$, ≥98%) were obtained from Sigma Aldrich and dried under vacuum before use. Potassium iodide (K^+I^-, Roth, 98.5%) and diphenyliodonium hexafluorophosphate ($Ph_2I^+PF_6^-$, Sigma Aldrich 98%) were used without additional treatment. The solvents acetonitrile (MeCN, Sigma Aldrich, ≥ 99.9%), ethanol (EtOH, Sigma Aldrich, ≥99.8%) and acetonitrile-d_3 (Euriso-top) were employed as received.

TR-EPR.

Continuous-wave time-resolved EPR experiments were performed on a Bruker ESP 300E X-band spectrometer (unmodulated static magnetic field) equipped with a 125 MHz dual channel digital oscilloscope (Le Croy 9400). As the light source, the frequency triplet light of a Nd:YAG laser was used (InnoLas Spitlight 400, 355 nm, operating at 20 Hz, ca. 7 mJ/pulse, 8 ns). The setup is controlled by the fsc2 software developed by Dr. J. T. Toerring (Berlin). Spectra were recorded by acquiring the accumulated (20 – 50 accumulations) time responses to the incident laser pulses at each magnetic field value of the chosen field range (field steps: 0.5 G). Argon-saturated solutions of the samples in acetonitrile (~ 15 mM in photoinitiator concentration) were pumped through a quartz flat cell positioned in the cavity of the EPR spectrometer using a flow system (flow rate: 2-3 mL/min). The recorded data were analyzed using the Matlab software.

CIDNP Spectroscopy.

^{31}P-CIDNP spectra were recorded on a 200 MHz Bruker AVANCE DPX spectrometer featuring a custom-made CIDNP probehead. A Quantel Nd:YAG Brilliant B laser (355 nm, ~ 60 mJ/pulse, pulse length ~ 8−10 ns) operating at 20 Hz was employed as the light source. The timing sequence of the experiment consists of a series of 180° radiofrequency (RF) pulses (applied to suppress the normally present NMR intensities), the laser flash, the 90° RF detection pulse and the acquisition of the FID. The spectra were recorded with ^{1}H decoupling and "dummy" CIDNP spectra employing the same pulse sequence but without the laser pulse were always measured. Samples were prepared in deuterated acetonitrile and deoxygenated by bubbling with argon before the experiment.

Analysis of Photoproducts by NMR Spectroscopy.

Deoxygenated samples of the photoinitiator in presence of salts or water and ethanol were prepared in deuterated acetonitrile and irradiated for different time spans (40 s – 4 min) using a Hg-Xe UV lamp (Hamamatsu Lightningcure LC4, 3500 mW/cm², λ_{max} = 365 nm). The photoproducts were analyzed using standard ^{31}P and ^{13}C NMR spectroscopy. The spectra were recorded on a 200 MHz Bruker AVANCE DPX spectrometer.

MALDI-MS.

Matrix-assisted laser desorption/ionization time-of-flight (MALDI-TOF) mass spectra were recorded on a Micromass TofSpec 2E Time-of-Flight Mass Spectrometer. Trans-2-[3-(4-tert-Butylphenyl)-2-methyl-2-propenylidene]malononitrile (DCTB) was used as matrix substance. Sample solutions have been prepared by mixing solutions of DCTB (10 mg/mL in THF), sodium trifluoroacetate (1 mg/mL in THF) and the sample (NMR solutions diluted 1:10 with THF) in a ratio of 7/2/2 (v/v/v). Calibration was done externally with polyethylene glycol standards (5 mg/mL in THF).

Quantum chemical calculations.

Density functional theory (DFT) calculations were carried out on the B3LYP level of theory using the program ORCA.[50] The def2-TZVPP basis set was chosen for geometry optimization, while EPR parameters were calculated using the IGLO-III basis set. The conductor-like screening (COSMO) solvation model was employed to account for interactions of the calculated species with the solvent (acetonitrile).[50]

3.3 Results and Discussion

3.3.1 TR-EPR of BAPOs in Presence of Water and Ethanol

Figure 9 presents the TR-EPR spectra obtained upon laser flash photolysis (LFP, 355 nm excitation) of mixtures of compound **1** (15 mM) and water (0.25 M – 7.5 M) in acetonitrile. The spectra are dependent on the water concentration and all signals are (mainly) triplet polarized, showing enhanced absorption.

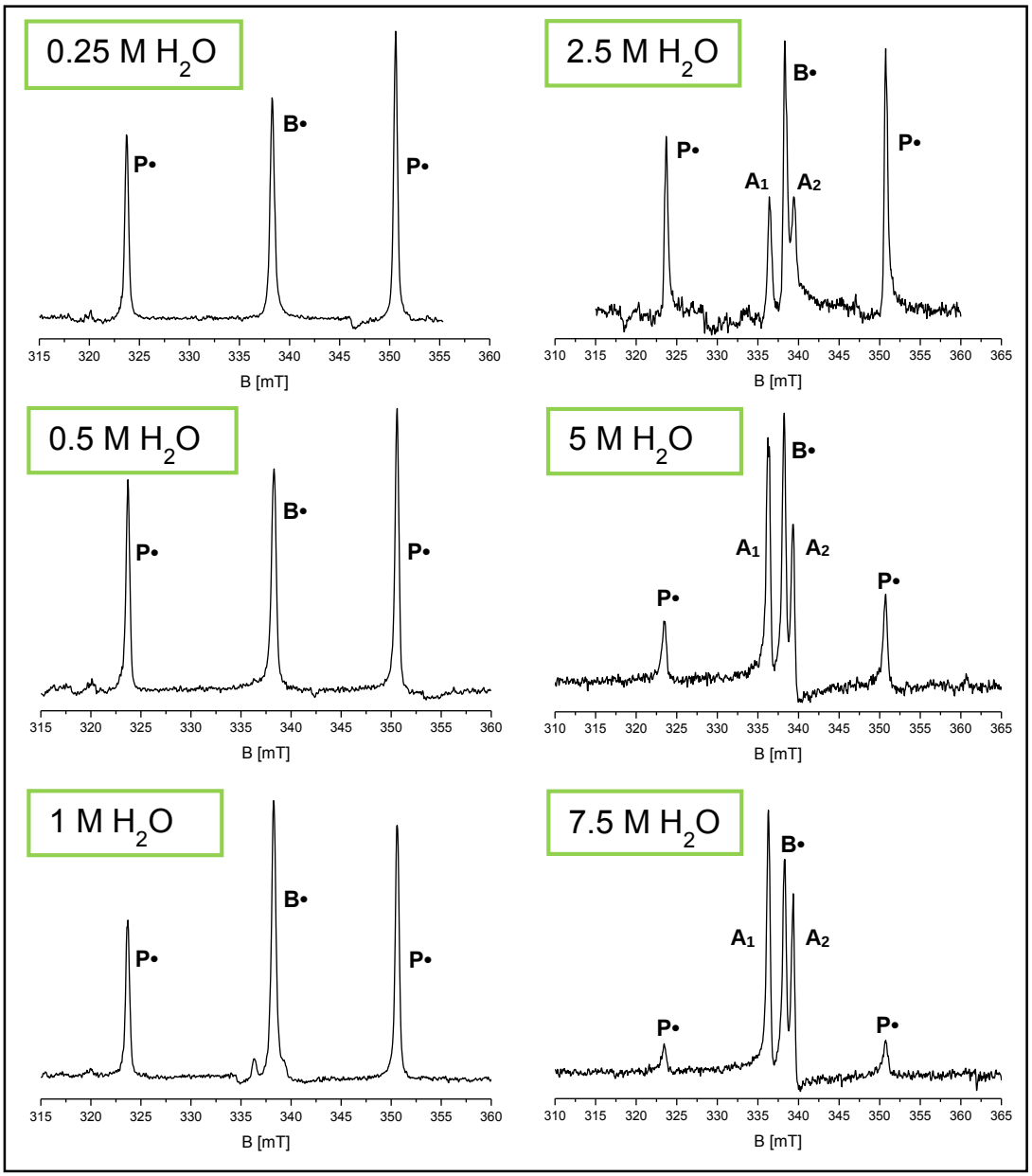

Figure 9. Dependence of the TR-EPR spectra of compound **1** on water concentration. The spectra have been recorded 200 – 300 ns after the laser flash in argon-saturated acetonitrile solutions (15 mM compound **1**).

Starting from a water concentration of 1 M (67-fold molar excess with respect to the BAPO), two additional lines are observed in the spectra. These lines are referred to as **A_1** and **A_2** in Figure 9 and they appear alongside the central peak of the benzoyl radical **B•** with a line distance of around 3 mT. With increasing water concentration, the signal intensities of the new lines increase while the peaks of the phosphanoyl radical **P•** (exhibiting a doublet with a hyperfine coupling constant of ~ 27 mT) decrease.

The lines **A_1** and **A_2** appear at the same time after the laser flash and they show an intensity ratio of ~ 1:1 (see Figures 10-12). Based on these observations and previous interpretations[47] we assume that **A_1** and **A_2** can be assigned to a doublet belonging to a so far unknown radical species. Table 1 summarizes the hyperfine coupling constants observed in the spectra presented in Figure 9.

Table 1. Hyperfine coupling constants determined from the TR-EPR spectra of BAPO (compound **1**) in presence of water

c_{H2O} [M]	Hyperfine Coupling Constant [mT]	
	Phosphanoyl Radical (**P•**)	Doublet **A_1A_2**
0.25	26.90	–
0.5	26.85	–
1	26.90	–
2.5	27.05	3.05
5	27.20	2.95
7.5	27.30	3.05

Remarkably, the radical exhibiting the doublet **A_1A_2** is formed later in time than the original radical pair and is observed for a longer time span, as shown in Figures 10 and 11.

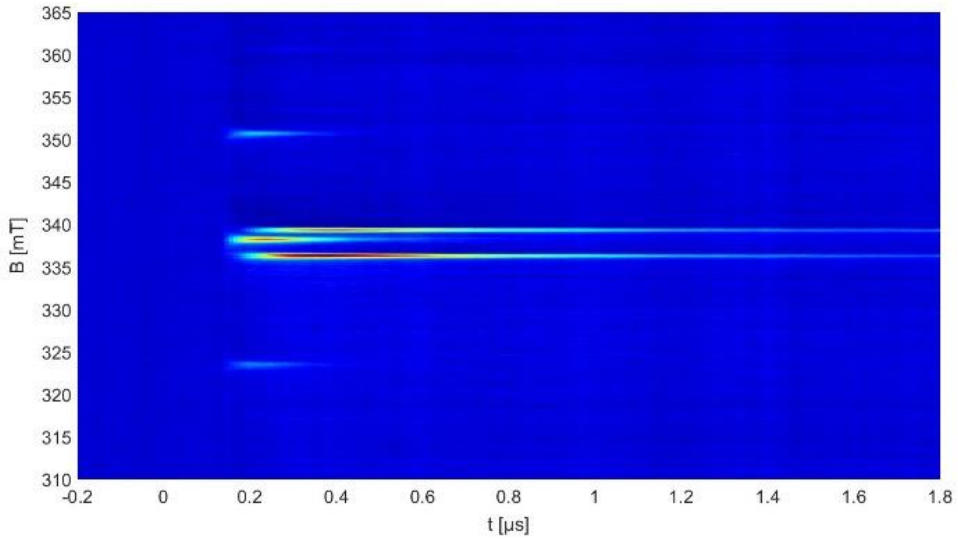

Figure 10. TR-EPR spectrum recorded upon LFP of compound **1** in presence of H_2O (sample: 15 mM **1**, 5 M H_2O in deoxygenated acetonitrile).

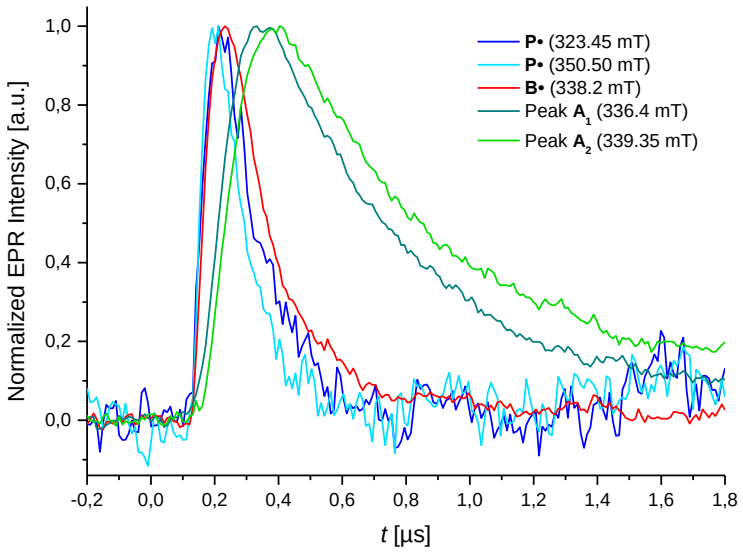

Figure 11. Time dependence of the (normalized) signal maxima observed in the TR-EPR spectrum of compound **1** in presence of H_2O (sample: 15 mM 1, 5 M H_2O).

The intensity maximum of the signals assigned to the benzoyl and phosphanoyl radical is found around 220 ns after the laser flash, as compared to ~ 400 ns in case of the new peaks **A_1** and **A_2**. The time delay in the appearance of the new doublet, as well as the decreased signal intensities of the phosphanoyl radical **P•** imply that the new radical might be a secondary species, formed upon reaction of primary **P•** with water. A similar assumption was made by Woodward and coworkers.[47]

Notably, the time traces of the signal maxima shown in Figure 11 are not exactly the same for the two peaks belonging to one doublet. The reason for this observation still has to be found.

Figure 12 presents the time evolution of the spectra is presented in a different way.

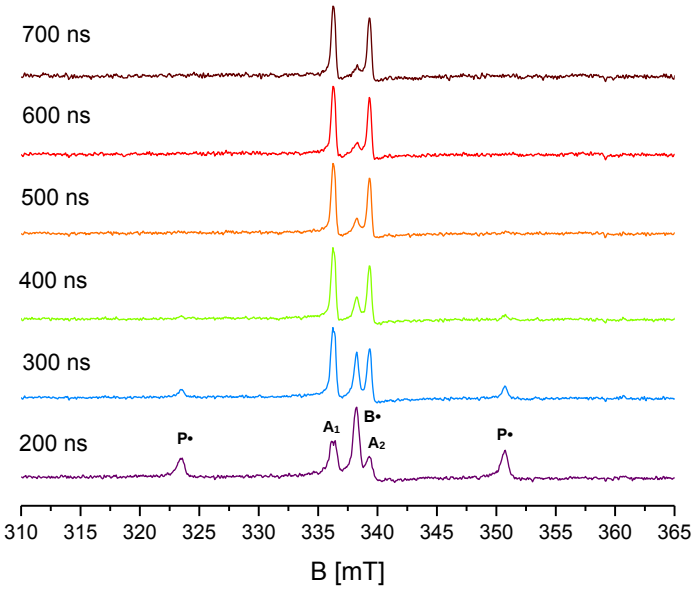

Figure 12. Slices of the TR-EPR spectrum of compound **1** in presence of H_2O at different time points after the laser flash. The spectra are normalized by signal intensity.

The signals of the phosphanoyl radical **P•** have disappeared in the spectrum recorded 400 ns after the laser flash, whereas the peaks assigned to the new radical are still clearly visible even after 700 ns. From the TR-EPR spectra, no direct conclusion about the lifetime of the observed radicals can be drawn, since only polarized signals are observed. However, the longevity of the polarization of the signals belonging to the new radical strongly suggests that the radical itself is long-lived and accordingly very stable.

Figure 13 depicts TR-EPR spectra of other phosphorous-based photoinitiators (compounds **3**, **4** and **5**) recorded in samples containing water at a concentration of 5 M. Compound **3** displays the same behavior as compound **1**, the new doublet exhibiting a hyperfine coupling constant of 2.8 mT.
In the case of compound **4**, several differences are observed. Most notably, the spectrum has a rather low quality which could not be improved by reproducing the experiment. Secondly, only the signal on the left side of the benzoyl peak is clearly visible, while the second peak of the new doublet seems to overlap with the benzoyl radical. In addition to that, a zoom into the central part of the spectrum and the plot of the time evolution indicates that the signals of the unknown species are again split into a doublet.

Concerning the spectrum of the MAPO (compound **5**), no additional signals are present, which is in line with previous investigations.[47] Accordingly, the MAPO-based phosphanoyl radical does not seem to be attacked by water. This might be one of the reasons for the superior photoinitiating performance of water-soluble MAPOs over water-soluble BAPOs, as was found by Benedikt et al. in photo-DSC experiments applying light in the range of 320 – 500 nm.[8]

From TR-EPR experiments in presence of ethanol (EtOH) instead of water, very similar results are obtained. The CIDEP spectra of acetonitrile solutions containing compound **1** and ethanol at different concentrations are depicted in Figure 14. The doublet of the phosphanoyl radical **P•** is only barely visible in the spectra measured at a concentration of 5 M EtOH, while these signals are larger in the analogous spectrum with water. Therefore, it can be tentatively suggested that ethanol is more reactive towards the phosphanoyl radical than water. The corresponding hyperfine coupling constants measured for **P•** and the small doublet of the unknown species are summarized in Table 2.

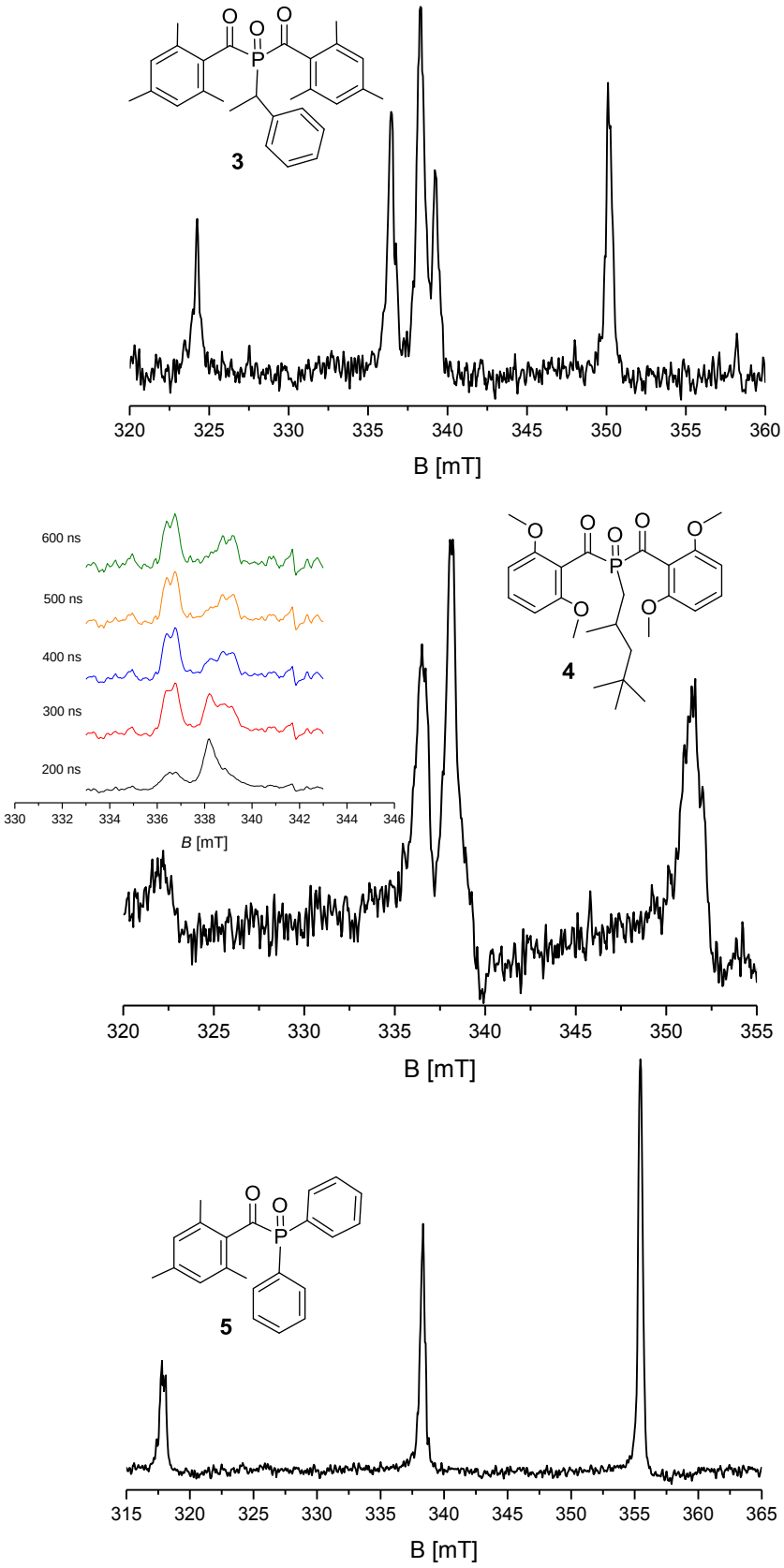

Figure 13. TR-EPR spectra of compounds **3 – 5** in presence of water, observed 200 – 300 ns after the laser flash (sample: 15 mM photoinitiator, 5 M H_2O). The inset in the spectrum of compound **4** shows a zoom into the central part (100 averages).

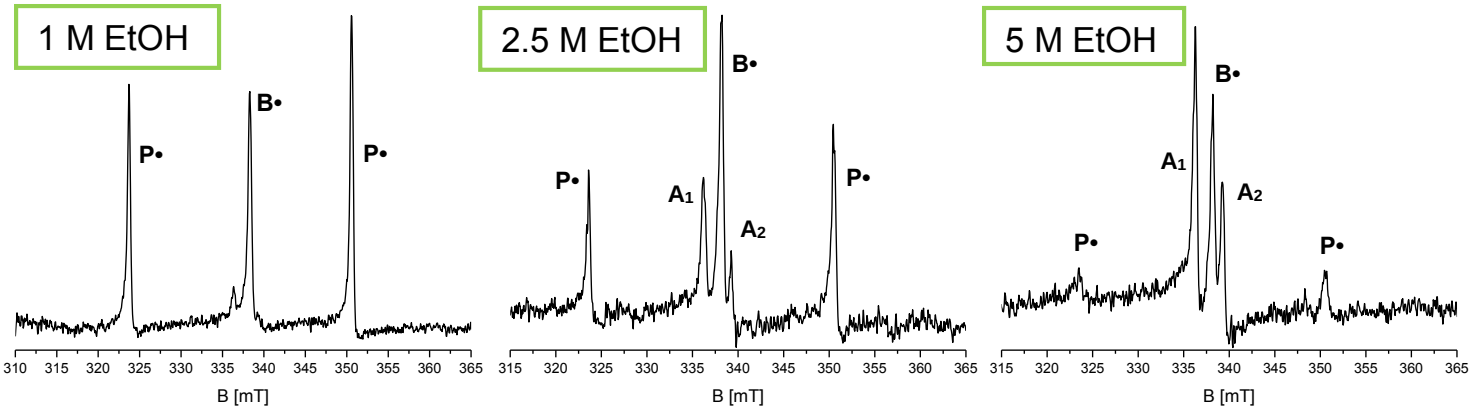

Figure 14. Dependence of the TR-EPR spectra of **1** on ethanol concentration. The spectra have been recorded 200 – 300 ns after the laser flash (15 mM compound **1**).

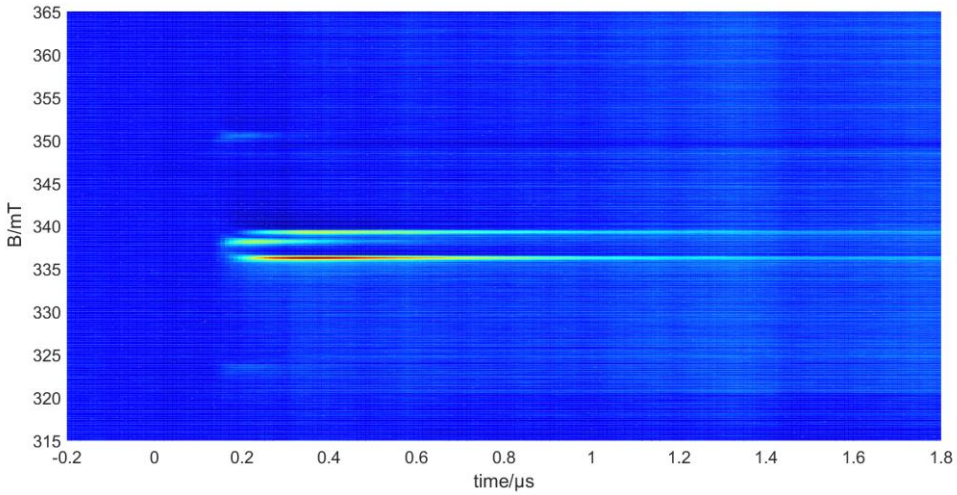

Figure 15. TR-EPR spectrum recorded upon LFP of **1** in presence of ethanol (sample: 15 mM **1**, 5 M H_2O in deoxygenated acetonitrile).

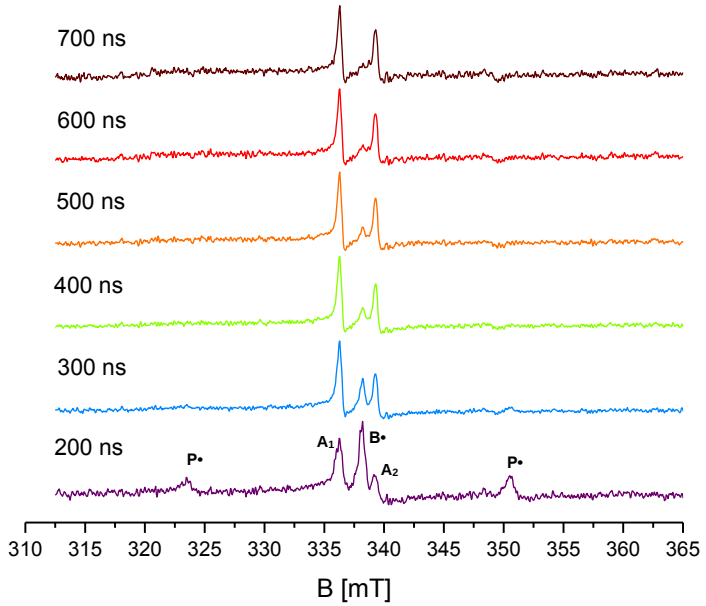

Figure 16. Slices of the TR-EPR spectrum of **1** in presence of ethanol at different time points after the laser flash. The spectra are normalized by signal intensity.

Table 2. Hyperfine coupling constants determined from the TR-EPR spectra of BAPO (compound **1**) in presence of ethanol

C_{EtOH} [M]	Hyperfine Coupling Constant [mT]	
	Phosphanoyl Radical (**P•**)	Doublet A_1A_2
1	26.85	–
2.5	26.95	3.1
5	26.95	3.0

The reactivity observed with alcohols does not seem to occur with thiols. Laser flash photolysis of compound **1** in the presence of 1-octanethiol did not result in additional peaks in the CIDEP spectra. Interestingly, the additional doublet exhibiting the small hyperfine coupling constant was observed in samples containing compound **1** and triethylamine (Et_3N). Hyperfine coupling constants have been determined to be 26.75 mT and 2.3 mT for the phosphanoyl radical and the new doublet (see supporting information, chapter 6.1). In this context, a TR-EPR spectrum of compound **1** was measured in a sample containing triphenylphosphane (Ph_3P), resulting in no additional signals.

3.3.2 TR-EPR of BAPOs in Presence of Salts

As mentioned in the introduction, the new species observed in the CIDEP spectra of BAPOs in presence of alcoholic solvents might be formed upon nucleophilic attack at the phosphanoyl radical **P•**, which is assumed to show electrophilic behavior. In order to further test this hypothesis, the photochemistry of BAPOs was studied in presence of nucleophilic salts. Photolysis of a mixture of BAPO (compound **1**) and iodide or bromide salts in acetonitrile solutions resulted in TR-EPR spectra exhibiting only the peak of the benzoyl radical (no phosphanoyl radical and no additional signals). This behavior has been found to be independent of the choice of the cation and was not observed in presence of non-nucleophilic anions. Remarkably, one equivalent of iodide is sufficient to completely consume the phosphanoyl radical, while in the case of water and alcohols, a huge excess is required (section 3.3.1). In contrast to bromide and iodide salts, additional signals are observed in the case of chloride, while the peaks of the phosphanoyl radical are still absent from the spectrum.

Table 3 summarizes the investigated salts and the observations made in the TR-EPR spectra. The samples typically contained 15 mM of compound **1** and 50 mM of the salt in deoxygenated acetonitrile solutions.

Table 3. Phosphanoyl radical peaks of **1** in presence of salts (qualitative summary)

Salt	P• in TR-EPR spectrum
$Bu_4N^+I^-$	No
$Bu_4N^+Br^-$	No
$Bu_4N^+Cl^-$	No (but additional signals)
$Bu_4N^+PF_6^-$	Yes
$Ph_2I^+PF_6^-$	Yes
Na^+I^-	No
$Na^+BF_4^-$	Yes
$Na^+ClO_4^-$	Yes
K^+I^-	No

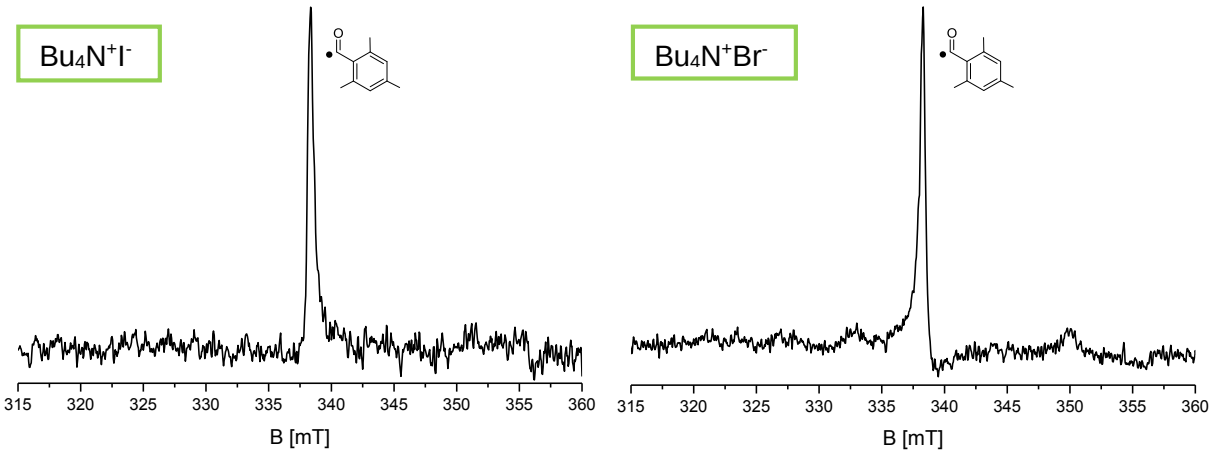

Figure 17. TR-EPR spectra of **1** in presence of Bu_4NI and Bu_4NBr observed 200 – 300 ns after the laser flash (sample: 15 mM **1**, 50 mM salt).

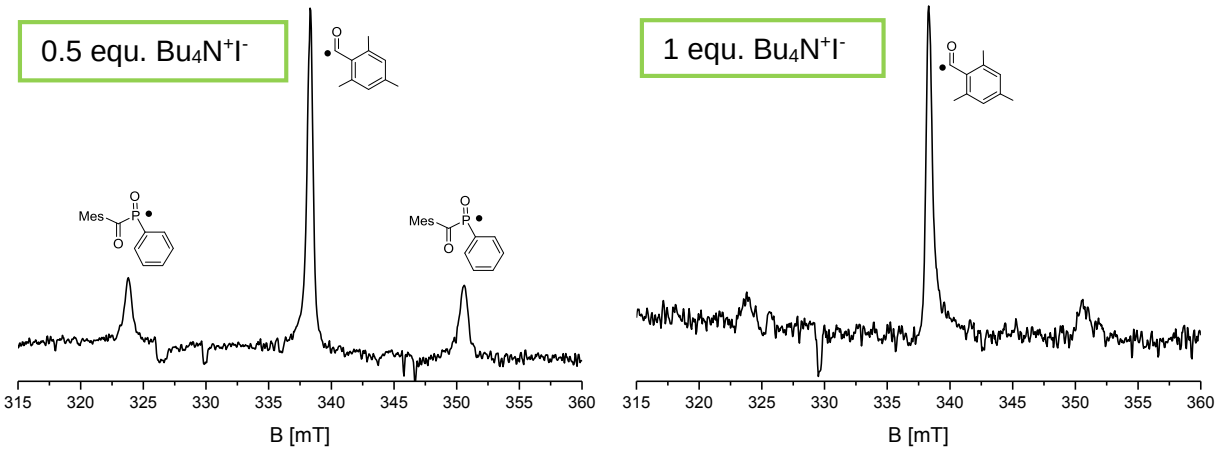

Figure 18. Dependence of the TR-EPR spectra of **1** on the concentration of Bu_4NI (15 mM **1**, 0.5 equiv. or 1 equiv. Bu_4NI). The spectra were recorded 200 – 300 ns after the laser flash.

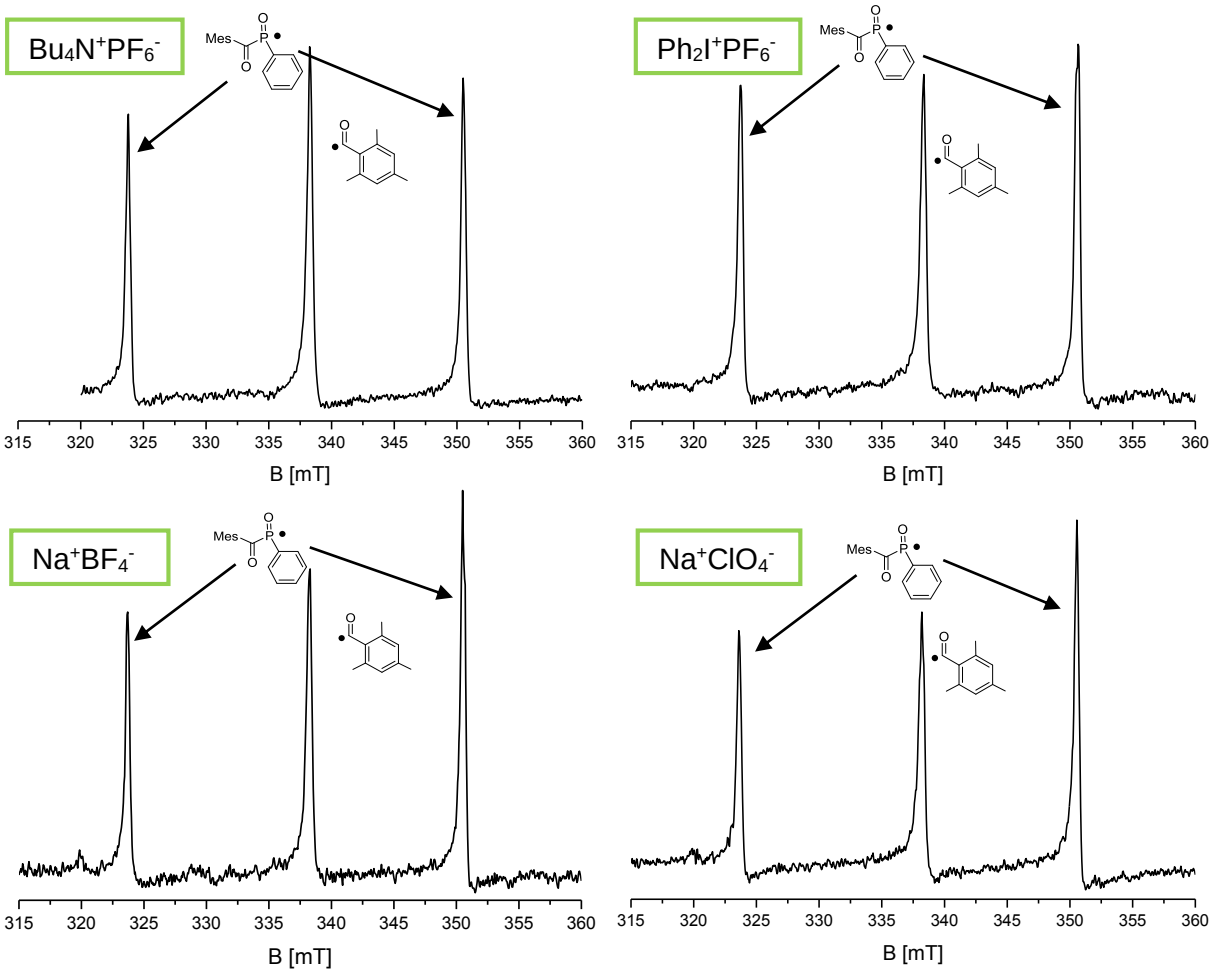

Figure 19. TR-EPR spectra of **1** in presence of non-nucleophilic salts. The spectra were recorded 200 – 300 ns after the laser flash (sample: 15 mM **1**, 50 mM salt).

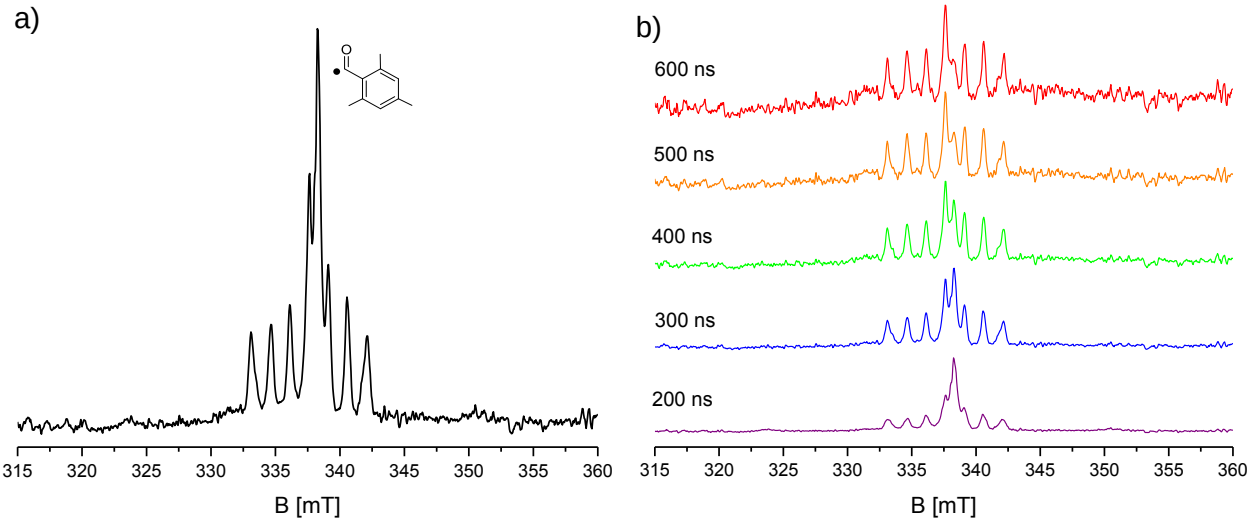

Figure 20. TR-EPR spectra of **1** in presence of Bu_4NCl: a) Spectrum recorded 200 – 300 ns after LFP. b) Slices of the spectrum at different time delays. (Sample: 15 mM **1**, 50 mM Bu_4NCl)

The spectrum shown in Figure 20 features eight peaks, the central one being assigned to the benzoyl radical. The seven additional lines appear in a distance of ~1.5 mT, and the peak in

the middle exhibits roughly twice the intensity of the six other signals (signal ratio of 1:1:1:2:1:1:1). Based on the nuclear spin of 3/2 for ^{35}Cl and ^{37}Cl, four lines with a 1:1:1:1 splitting are expected for a radical featuring a Cl substituent. Possibly, the observed lines stem from a radical bearing a chloride as well as a phosphorous atom, with the phosphorous hyperfine coupling constant being three times the one of the Cl coupling (4.5 mT).

Interestingly, compound **2**, which features an intramolecular salt moiety in the side chain does not show any phosphanoyl radical peaks in the TR-EPR spectrum, either (Figure 21).

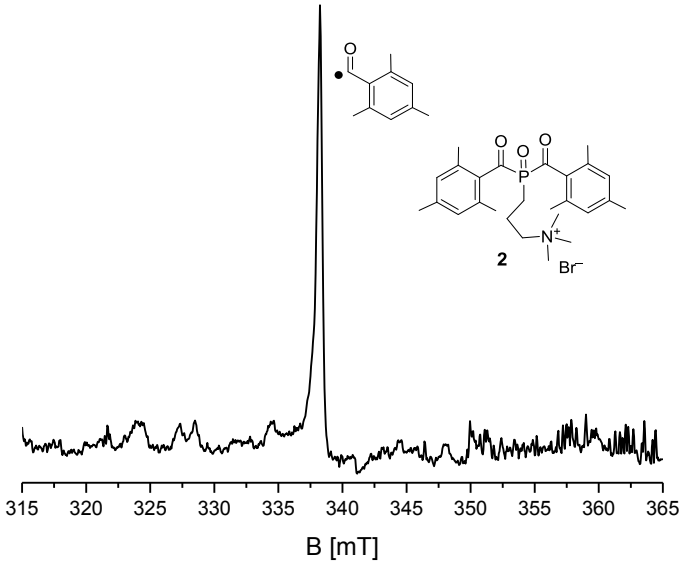

Figure 21. TR-EPR spectrum of compound **2** observed 200 – 300 ns after the laser flash (sample: 10 mM compound **2**).

Further, the TR-EPR spectrum of a mixture of a MAPO (compound **5**) and Bu_4NI was measured. The spectrum shows broadened lines as well as decreased signal intensities of the phosphanoyl radical peaks when compared to the spectrum obtained without salt, indicating some reactivity of the MAPO-based phosphanoyl radical towards iodide (Figure 22).

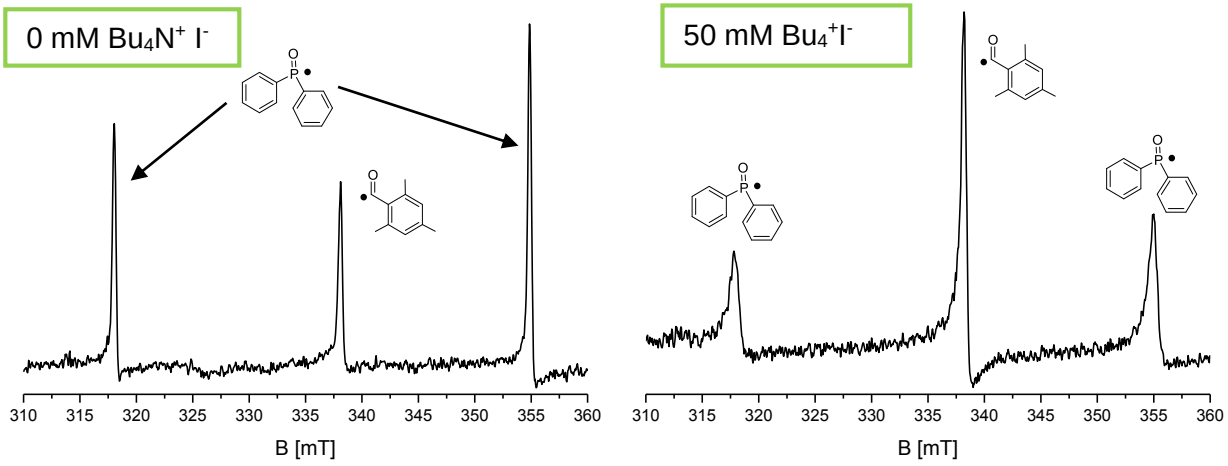

Figure 22. TR-EPR spectrum of compound **5** in presence of Bu_4NI, observed 200 – 300 ns after the laser flash (sample: 15 mM **5**, 0 mM or 50 mM Bu_4NI).

The MAPO-based phosphanoyl radical is supposed to be less electrophilic than the BAPO-based phosphanoyl radical, due to the lack of the electron withdrawing carbonyl group. Accordingly, a nucleophilic attack at the MAPO-derived phosphanoyl radical is assumed to be less likely and slower when compared to the BAPO. This is in line with the results of the TR-EPR experiments in presence of iodide and water.

3.3.3 ^{31}P-CIDNP

CIDNP spectroscopy has proven to be a powerful technique for the investigation of reaction pathways of MAPO and BAPO photoinitiators.[17,38,51]

The phosphanoyl and benzoyl radical pair formed upon light induced *α*-cleavage of the precursor molecules may form cage and escape products. Cage products are formed by the recombination of the primary radical pair and require singlet-triplet mixing, since the radical pair is formed in the triplet state (photochemical reaction), but only singlet radical pairs may recombine (as is explained by the Pauli principle). Escape products are generated if the primary radicals leave the solvent cage via diffusion and encounter other radicals. For example, two benzoyl or two phosphanoyl radicals may recombine.[51]

The possible reaction pathways for BAPO photoinitiators are summarized in Scheme 13.

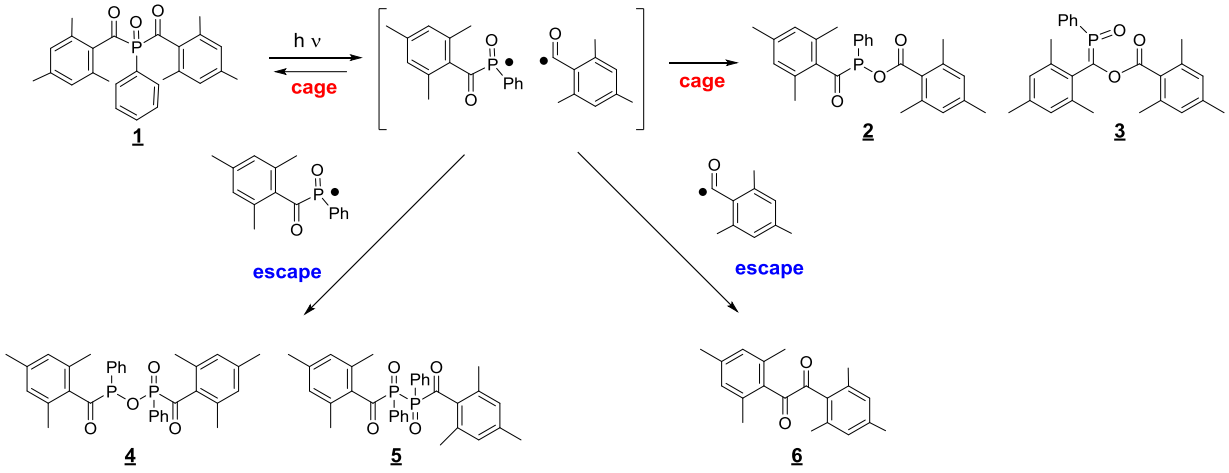

Scheme 13. Formation of cage and escape products of a BAPO (the scheme is drawn according to reference 51).

For both cage and escape products, “polarized” signals (showing enhanced emission or absorption) are observed in CIDNP spectra, since a spin-sorting process occurs due to the interaction of nuclear spins with the unpaired electron, resulting in a non-Boltzmann population of the spin states, as is explained by the radical pair mechanism (see section 2.2.2).[38] The chemical shifts measured in CIDNP experiments correspond to conventional NMR spectra, however, from the polarization pattern, knowledge of the type of product (cage or escape), the

difference between the g-factors and the sign of the phosphorus-phosphorus coupling constant (hfc) can be gained.[38] Spectra are usually analyzed using Kaptein's rules.[51]

The ^{31}P-NMR and CIDNP spectra can be roughly divided into two regions: from 0 – 50 ppm pentavalent phosphorus species are detected, whereas trivalent phosphorus compounds are found around 100 ppm.[51]

Figure 23 shows the ^{31}P-NMR and ^{31}P-CIDNP spectra of compound **1**. All phosphorous containing cage and escape products presented in Scheme 13 can be found in the CIDNP-spectrum. Species **4** exhibits two signals with and A/E (absorption/emission multiplet effect) pattern due the presence of P(III) and P(V) in the molecule. The formation of species **3** can be explained by drawing a resonance structure of the phosphanoyl radical **P•** with a double bond between the phosphorous and the carbonyl carbon, the radical center then being at the oxygen of the carbonyl group. This radical may recombine with the benzoyl radical to yield species **3** in a cage reaction.

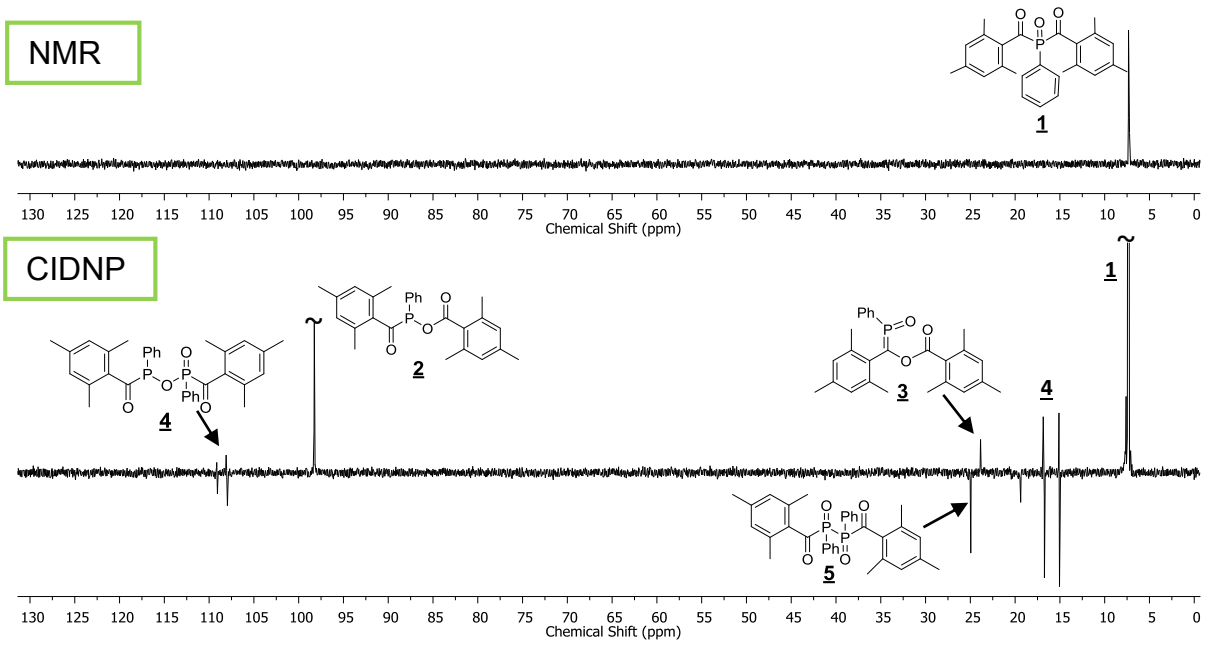

Figure 23. ^{31}P-NMR and ^{31}P-CIDNP spectra (64 scans) of compound **1** (sample: 25 mM BAPO in deoxygenated acetonitrile-d_3).

Figure 24 presents the CIDNP spectra of BAPO (compound **1**) measured in presence of water. An analogous "titration" study as performed in the TR-EPR experiments (Figure 9) was conducted.

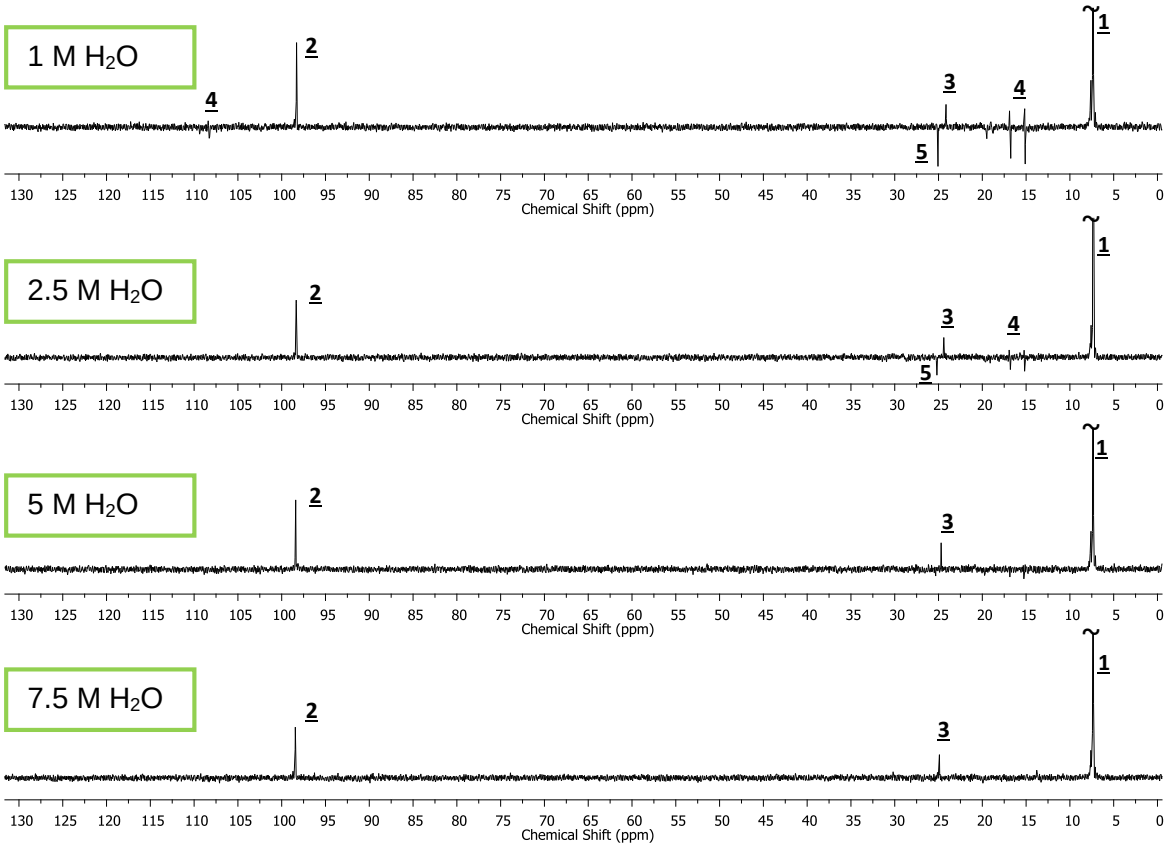

Figure 24. ^{31}P-CIDNP spectra (64 scans) of compound **1** in presence H_2O (sample: 25 mM **1** in deoxygenated acetonitrile-d_3, concentrations of H_2O are indicated in the plot).

At a water concentration of 1 M, all products observed in the samples without water are still visible. However, the escape products show decreased signal intensity. Increasing the water concentration results in the disappearance of all signals assigned to escape products. Only the cage products **1**, **2** and **3** are visible in samples containing water at a concentration of 5 M and 7.5 M. This observation supports the idea that phosphanoyl radicals generated via *α*-cleavage of BAPOs are "consumed" by water.

When measuring the ^{31}P-CIDNP spectra of compound **1** in presence of tetrabutylammonium salts of iodide, bromide and chloride similar results are obtained. With the chloride, only the three cage products are found in the CIDNP spectra. In presence of iodide and bromide, the escape product **4** is not observed, while species **5** is found in the samples containing a twofold excess of iodide and bromide (but not in presence of an eightfold excess of iodide). Four additional (and yet unassigned) signals are observed in the samples with bromide (12.4 ppm, 12.8 ppm, 13.4 ppm and 98.3 ppm).

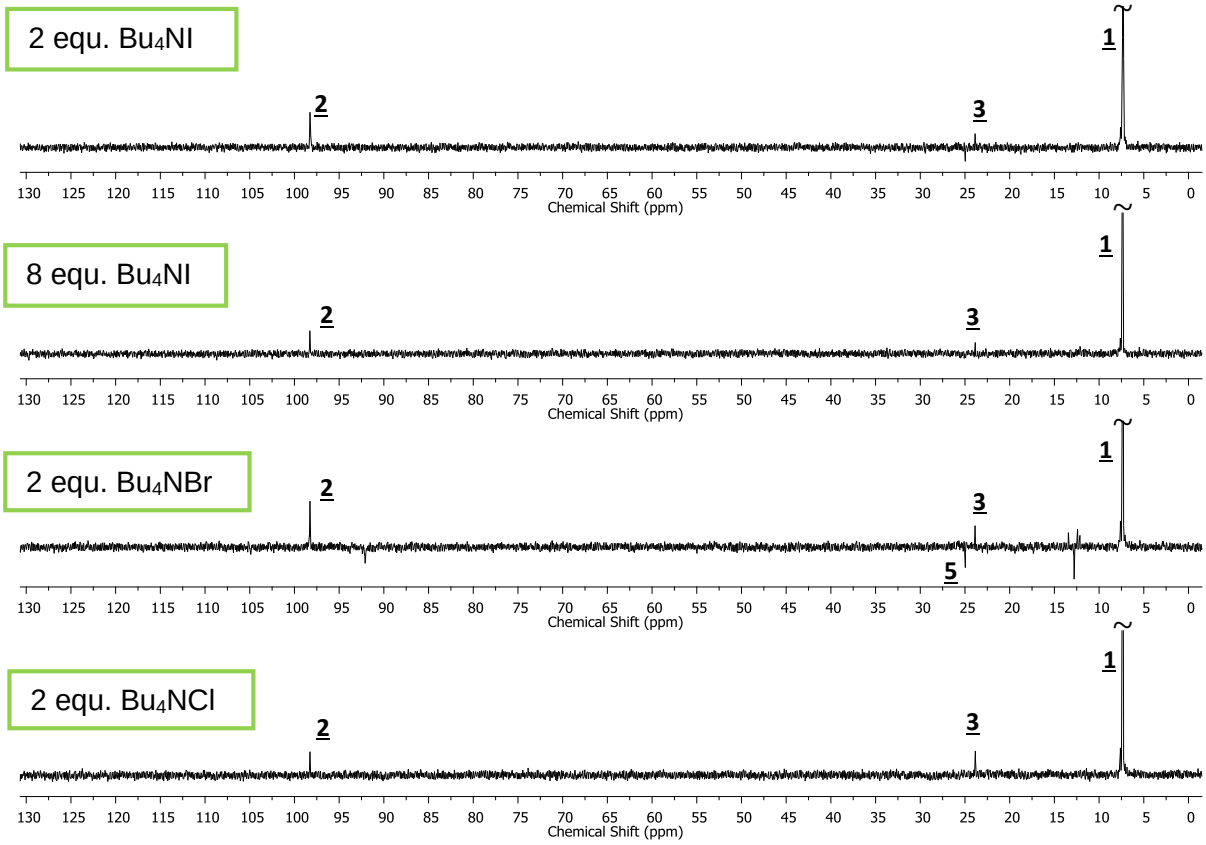

Figure 25. ^{31}P-CIDNP spectra (64 scans) of compound **1** in presence of Bu_4NI, Bu_4NBr and Bu_4NCl (25 mM **1** in deoxygenated acetonitrile-d_3).

The absence of most escape products formed from the phosphanoyl radical in the CIDNP spectra points towards the reaction of the phosphanoyl radical **P•** with the anions, yielding a non-radical species, as was already implied by the results of the TR-EPR experiments. However, cage products (as well as new signals in presence of bromide) are still observed, although no phosphanoyl peaks were found in the TR-EPR spectra. This might be explained by the higher sensitivity of the CIDNP method when compared to the TR-EPR technique.

The CIDNP experiments were also performed with ethanol and triethylamine. In the case of ethanol, analogous spectra as measured in presence of water were obtained. Interestingly, in samples containing triethylamine, all compounds apart from **1** are absent in the CIDNP spectra. Instead, a new (and yet unassigned) emission signal at 11 ppm is observed. (see supporting information, chapter 6.1).

3.3.4 ^{31}P-NMR of Photoproducts

In order to study the products formed upon photolysis of BAPOs in presence of nucleophiles, long-time irradiations (40 seconds – 4 minutes) using a Hg-Xe-UV lamp were performed inside the NMR tubes, followed by a simple 1D ^{31}P-NMR experiment.

The spectra measured upon 4 min irradiations of compound **1** in acetonitrile solutions containing water, ethanol and trimethylamine exhibit numerous signals in the range of 5 – 45 ppm (Figure 26). The simplest spectrum is obtained in presence of ethanol, showing two major peaks at 15.5 ppm and 25.8 ppm. In presence of water, large peaks are observed at 13.7 ppm, 15.4 ppm, 19.8 ppm and 35.4 ppm. With triethylamine, two distinct peaks at lower shifts are found (7.5 ppm and 11.1 ppm).

The spectra measured before the irradiations only display the signal of the parent BAPO photoinitiator, observed at 7.15 ppm, 6.85 ppm and 7.14 ppm in presence of water, ethanol and triethylamine, respectively.

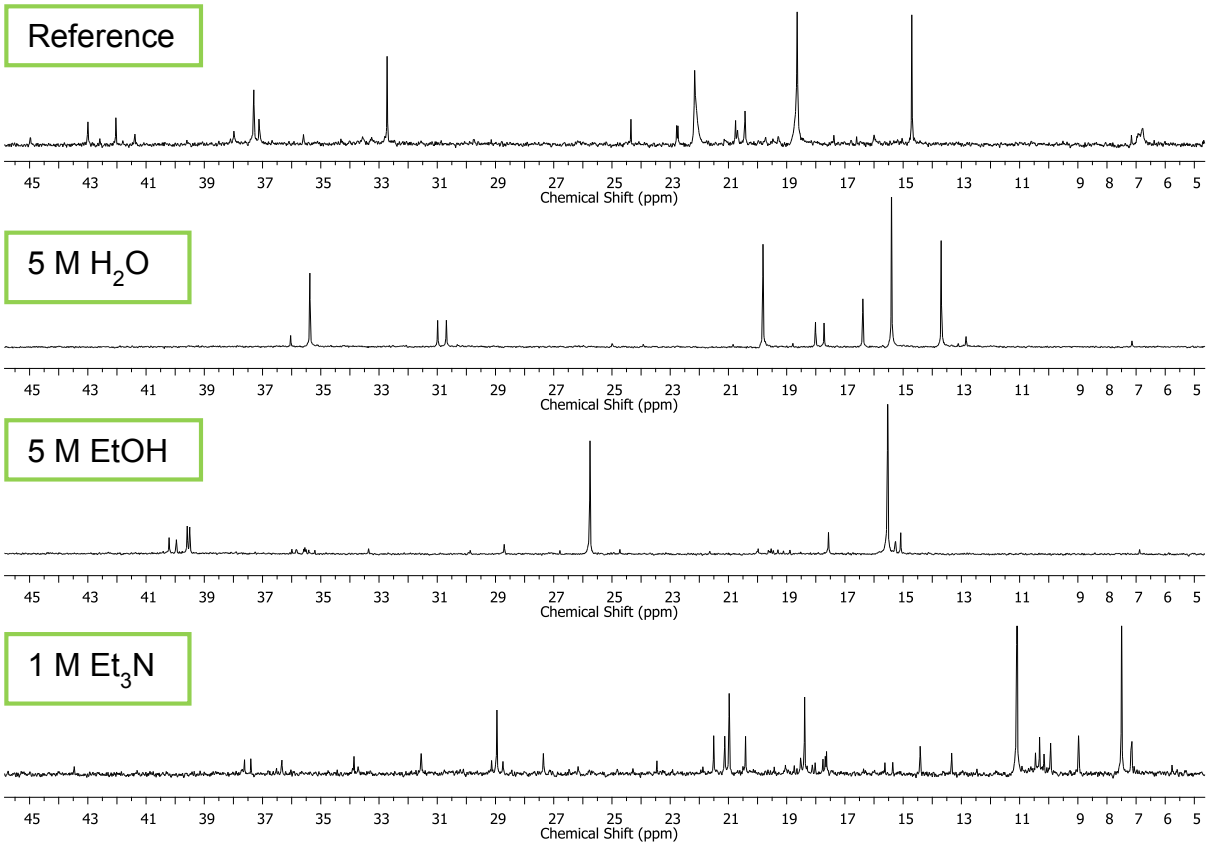

Figure 26. ^{31}P-NMR spectra of photoproducts with H_2O, EtOH and Et_3N (4 min irradiation, samples: 40 mM compound **1** in deoxygenated acetonitrile-d_3, concentrations of the reagents are indicated in the plot).

Table 4. ^{31}P-chemical shifts of photoproducts with water, ethanol and triethylamine

Spectrum	Chemical Shifts [ppm]
Reference	46.86, 46.82, 43.00, 42.04, 41.38, 37.98, 37.30, 37.12, 35.59, 32.72, 24.35, 22.78, 22.73, 22.16, 20.76, 20.43, 18.64, 17.38, 16.00, 14.70, 6.77, -18.52
5 M H_2O	36.03, 35.37, 30.99, 30.69, 19.81, 18.78, 18.01, 17.71, 16.38, 15.40, 13.69, 12.84, 7.14
5 M EtOH	40.21, 39.96, 39.58, 39.50, 35.99, 35.54, 35.41, 33.36, 28.70, 25.76, 24.73, 19.98, 19.53, 19.30, 18.89, 17.56, 15.53, 15.26, 15.08, 6.88
1 M Et_3N	37.62, 37.40, 36.34, 33.86, 31.55, 29.14, 28.95, 28.74, 27.36, 23.46, 21.51, 21.13, 20.97, 20.41, 18.52, 18.38, 18.02, 17.76, 17.63, 15.63, 15.36, 14.42, 13.33, 11.09, 10.45, 10.32, 10.16, 9.94, 8.97, 7.50, 7.18, 7.14, 4.18, 3.79

When conducting similar long-time irradiation experiments in presence of tetrabutylammonium salts, photoproducts displaying ^{31}P-NMR peaks in the range of -19 ppm – 110 ppm are formed (Figure 27). Samples contained 40 mM of compound **1** and 600 mM of the salt (150-fold excess). In the case of iodide and bromide, distinct signals are observed at around 110 ppm and -18.6 ppm, which are not found in the reference sample (BAPO without salt). These signals do not appear in presence of chloride either, pointing to a different reaction pathway when compared to iodide and bromide, as was also implied by TR-EPR experiments.

The irradiation time in the experiments described above has been chosen to reach complete photolysis of the parent BAPO. A significant drawback of this approach is that no distinction can be made in the product NMR spectra between primarily formed products and products formed in photoinduced follow-up reactions. Therefore, the experiments have been repeated applying a significantly shorter irradiation time (40 seconds instead of 4 minutes, see Figure 28). In this case, significantly less peaks are observed. The peaks at around 110 ppm are still observed in presence of Bu_4NI and Bu_4NBr and can be most likely assigned to a P(III) species. The negative peak at -18.6 ppm is only observed with the iodide but not with the bromide when applying the shorter irradiation time.

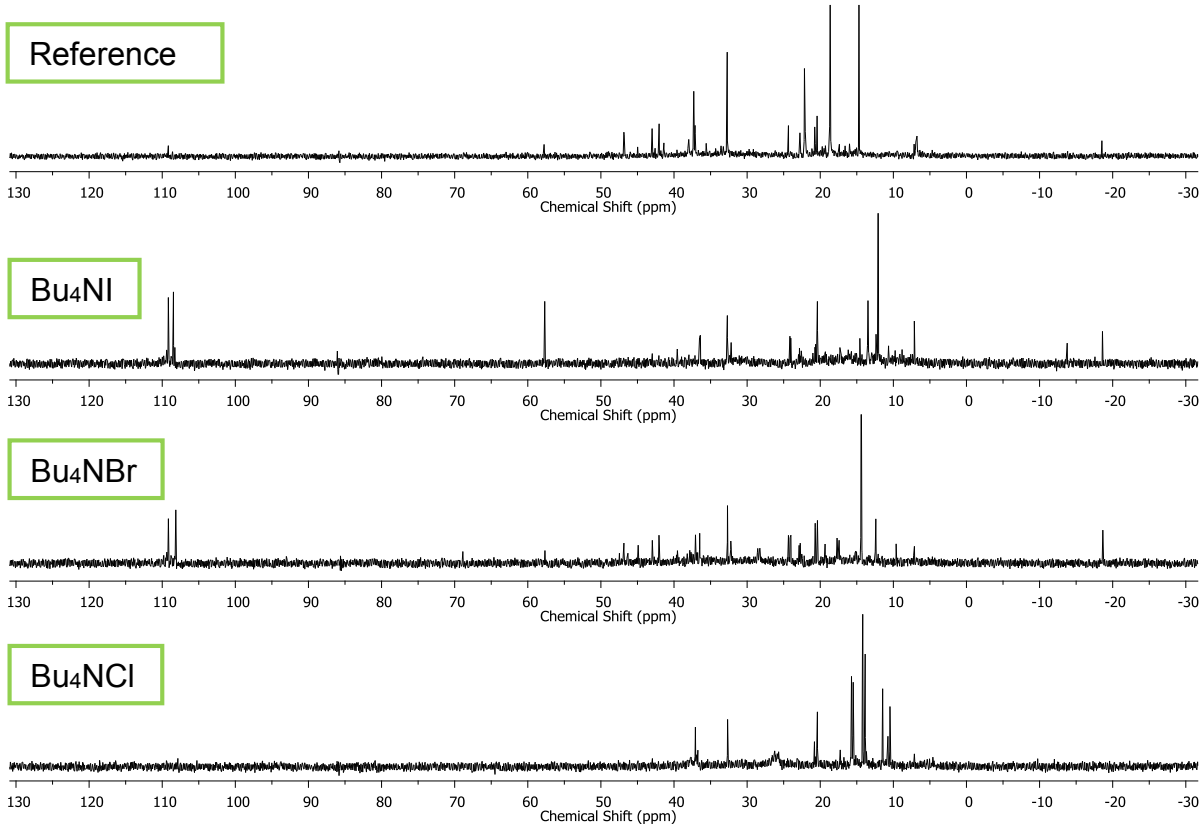

Figure 27. ^{31}P-NMR spectra of photoproducts formed in presence of salts (4 min irradiation, samples: 40 mM compound **1** and 600 mM salt in deoxygenated acetonitrile-d_3).

Table 5. ^{31}P-chemical shifts of photoproducts with salts (4 min irradiation)

Spectrum	Chemical Shifts [ppm]
Reference	46.86, 46.82, 43.00, 42.04, 41.38, 37.98, 37.30, 37.12, 35.59, 32.72, 24.35, 22.78, 22.73, 22.16, 20.76, 20.43, 18.64, 17.38, 16.00, 14.70, 6.77, -18.52
Bu_4NI	109.16, 108.46, 57.68, 36.50, 36.39, 32.71, 32.19, 24.15, 24.03, 20.39, 14.58, 13.47, 12.37, 12.07, 7.13, -13.78, -18.60
Bu_4NBr	109.16, 108.14, 46.85, 44.90, 42.97, 42.06, 37.06, 36.49, 36.38, 32.69, 32.23, 24.35, 24.12, 24.01, 22.74, 20.69, 20.38, 19.34, 17.70, 17.42, 14.40, 12.40, 9.62, -18.65
Bu_4NCl	37.07, 32.67, 20.79, 20.39, 15.72, 15.49, 14.18, 13.85, 11.46, 10.74, 10.46

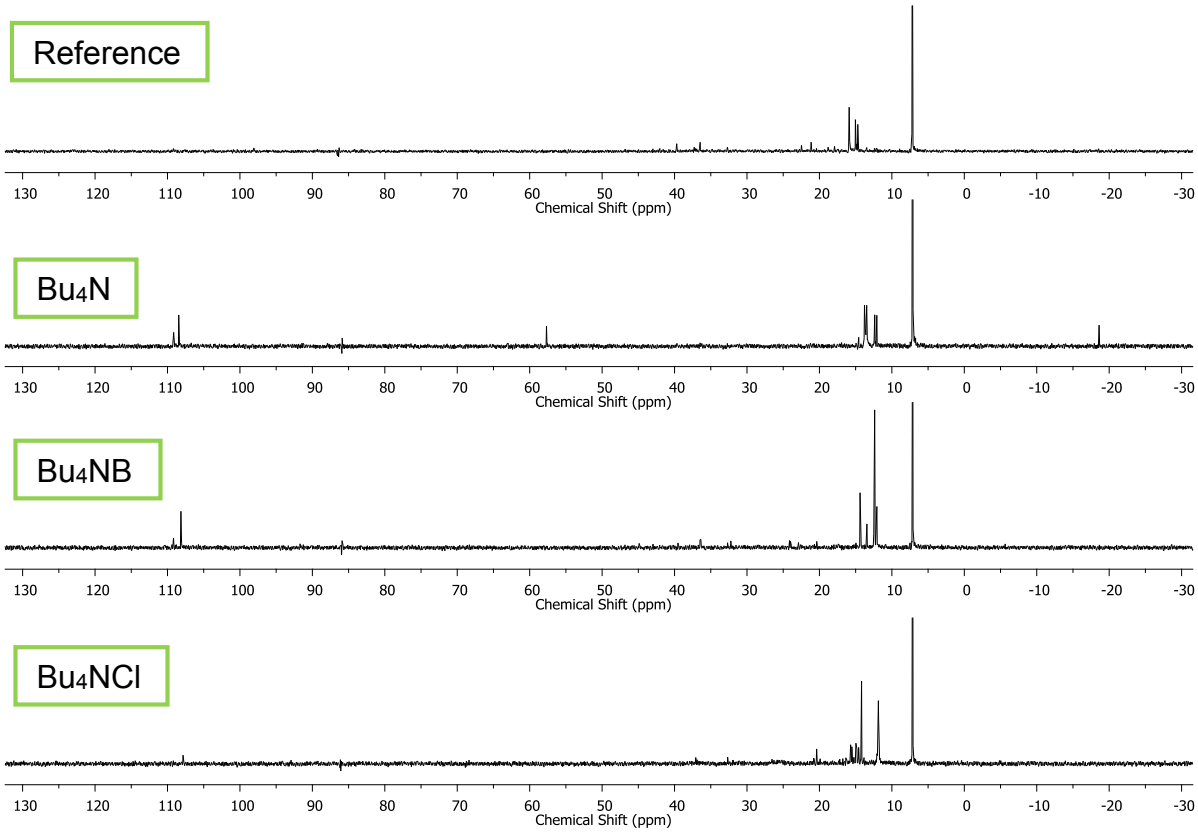

Figure 28. ^{31}P-NMR spectra of photoproducts formed in presence of salts (40 sec irradiation, samples: 40 mM compound **1** and 600 mM salt in deoxygenated acetonitrile-d_3).

Table 6. ^{31}P-chemical shifts of photoproducts with salts (40 sec irradiation)

Spectrum	Chemical Shifts [ppm]
Reference	86.13, 36.47, 22.47, 21.15, 15.89, 15.03, 14.70, 7.18
Bu_4NI	109.15, 108.44, 57.68, 14.57, 13.78, 13.47, 12.36, 12.07, 7.12, -18.61
Bu_4NBr	109.17, 108.15, 14.39, 13.44, 12.37, 12.07, 7.12
Bu_4NCl	20.38, 15.70, 15.52, 14.97, 14.82, 14.59, 14.18, 11.86, 7.12

In addition to ^{31}P NMR analysis of the photoproducts, we recorded ^{13}C-NMR spectra, but the results proved to be inconclusive so far.

3.3.5 MALDI-MS

Samples from the ^{31}P-NMR experiments in presence of water and ethanol were analyzed by matrix-assisted laser desorption mass spectrometry (MALDI-MS). The spectra were measured by David Fast (TU Graz).

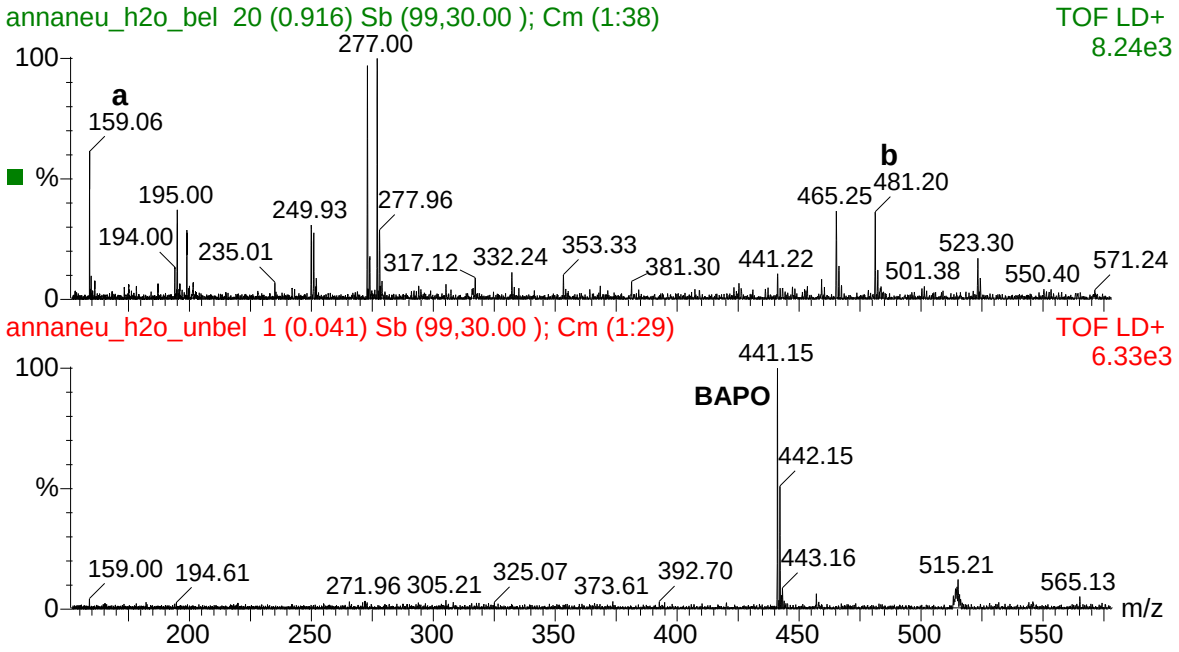

Figure 29. MALDI-MS spectrum of the photoproducts formed upon irradiation (4 min) of compound **1** in presence of water (green spectrum). The red spectrum refers to the sample before the irradiation. (Sample: 40 mM **1**, 5 M H_2O in acetonitrile)

The signal observed in the mass spectrum of the unirradiated sample (m/z 441.15) corresponds to the parent BAPO molecule, ionized by a sodium ion. The signal at m/z 159.06 observed in the irradiated sample is most likely assigned to the phosphonic acid derivative **a**, ionized by a proton. The suggestion for the structure corresponding to the signal at m/z 481.20 (species **b**) will be rationalized in the next section. For the other signals observed in the mass spectrum, an unambiguous assignment has not been possible yet.

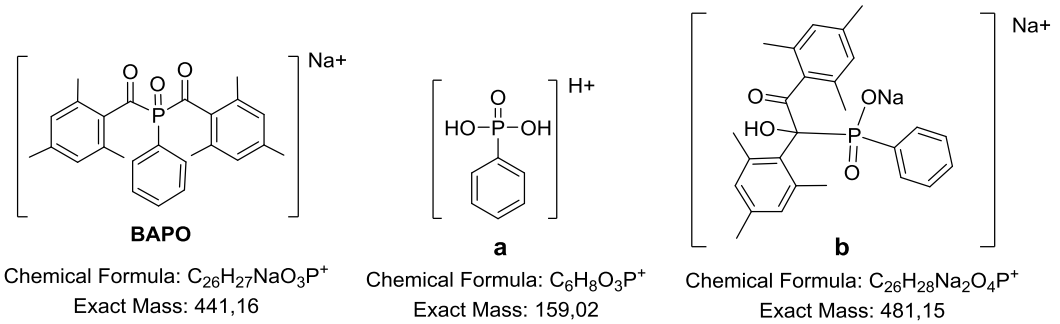

Scheme 14. Suggested structures for the species observed in the mass spectra in Figure 29.

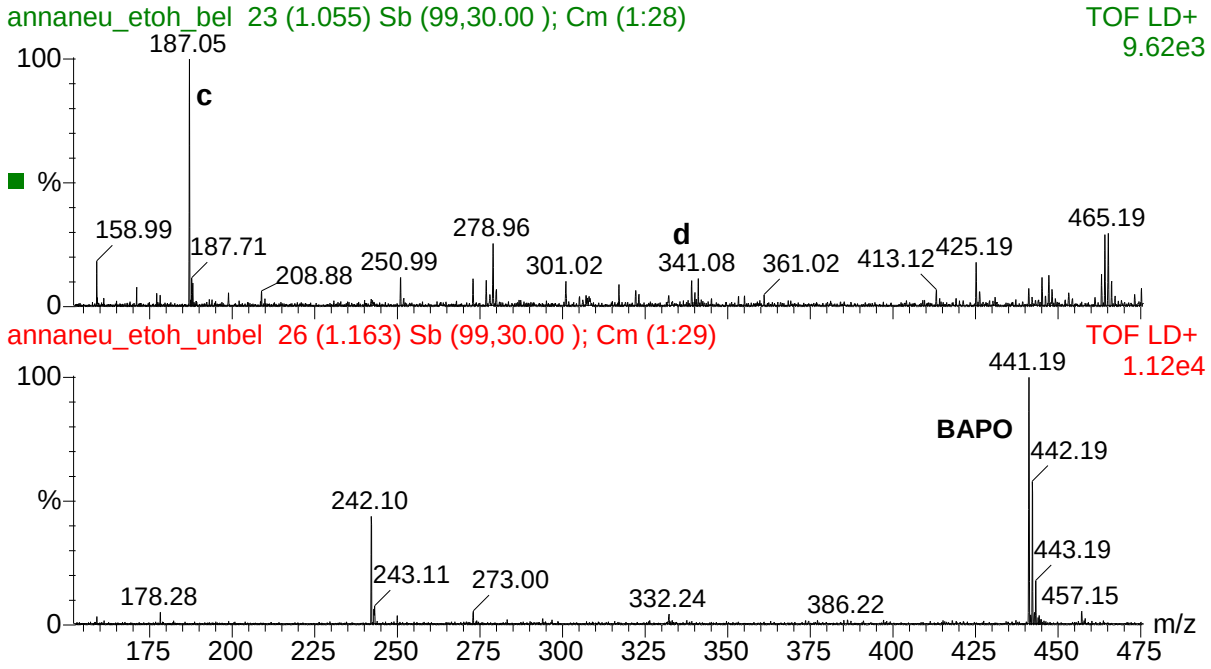

Figure 30. MALDI-MS spectrum (lower m/z) of the photoproducts formed upon irradiation (4 min) of compound **1** in presence of ethanol (green spectrum). The red spectrum refers to the sample before irradiation. (Sample: 40 mM **1**, 5 M EtOH in acetonitrile)

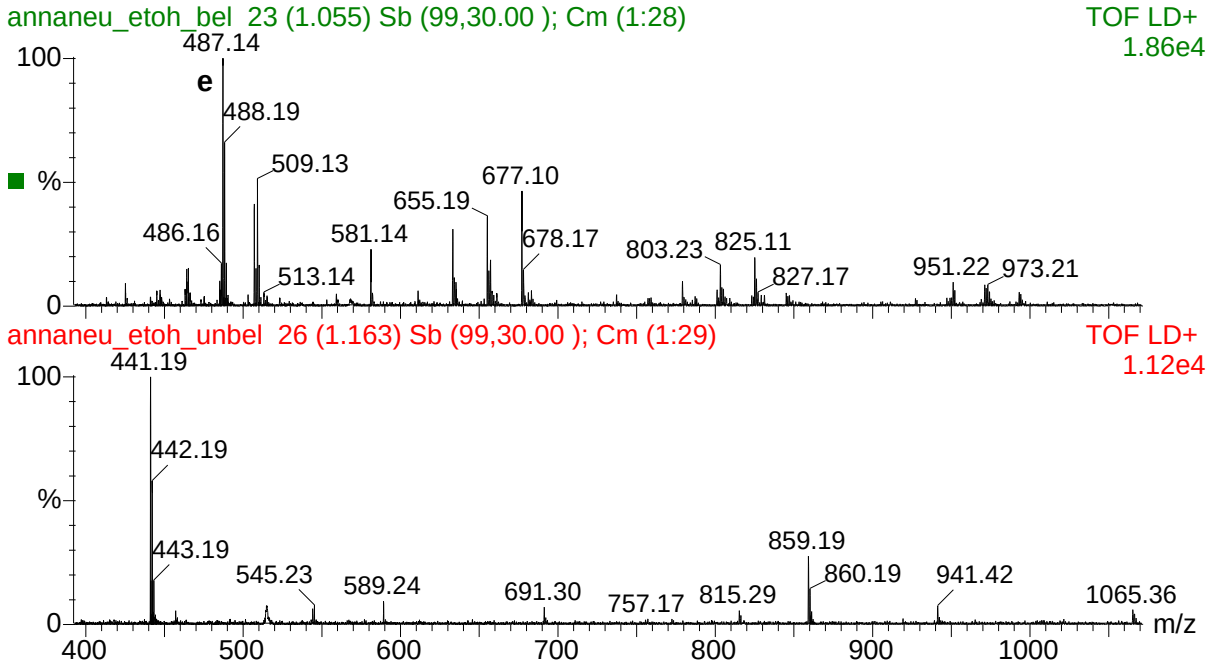

Figure 31. MALDI-MS spectrum (higher m/z) of the photoproducts formed upon irradiation (4 min) of compound **1** in presence of ethanol (green spectrum). The red spectrum refers to the sample before irradiation. (Sample: 40 mM **1**, 5 M EtOH in acetonitrile)

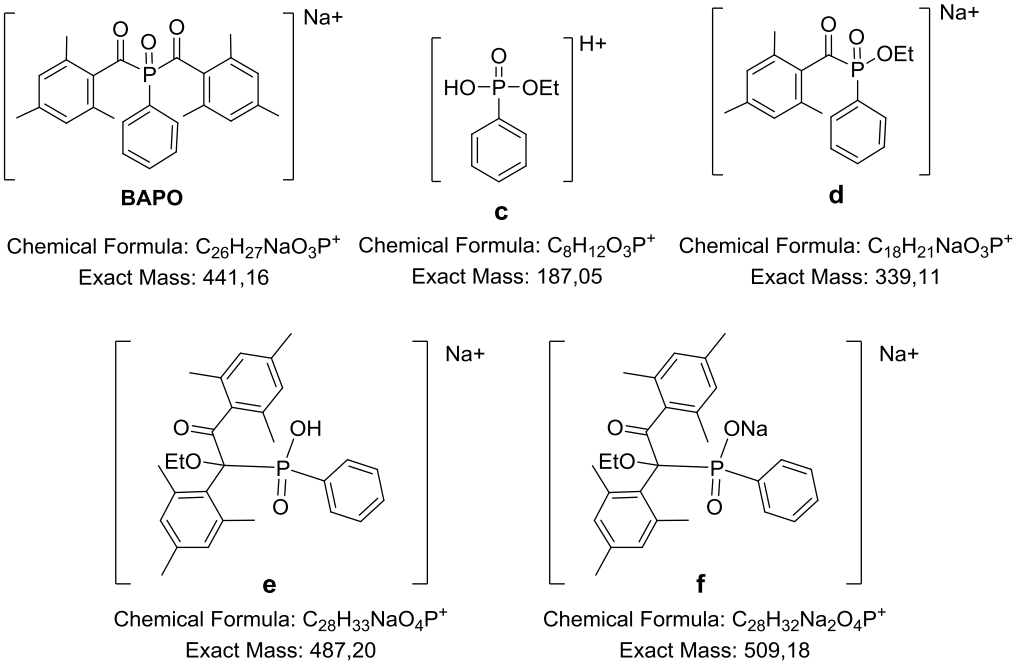

Scheme 15. Suggested structures for the species observed in the mass spectra in Figure 30 and Figure 31.

3.3.6 Summary of the Experiments

In this chapter, we briefly summarize the results described in the previous sections: The TR-EPR spectra obtained upon laser flash photolysis of BAPOs in samples containing water and ethanol feature two remarkable differences when compared to the spectra recorded in pure acetonitrile or toluene: first, an additional doublet is observed alongside the central benzoyl peak, exhibiting a hyperfine coupling constant of around 3 mT and second, the signal intensities of the phosphanoyl radical generated upon *α*-cleavage of BAPO precursors decrease with increasing concentrations of water or ethanol. The second observation as well as the time delay in the appearance of the new doublet indicate that the unknown species is a secondary radical, generated by a reaction of the primarily formed phosphanoyl radical **P•** with the water or alcohol. ^{31}P-NMR analysis of the photoproducts formed upon long-time irradiation shows that specific phosphorous-containing species are formed in presence of ethanol and water, supporting the above-mentioned assumption.

A similar reactivity as observed with water and ethanol is found in presence of triethylamine. In contrast, neither the phosphanoyl peaks nor any additional signals are visible in the CIDEP spectra of BAPOs recorded in presence of iodides and bromides. The counterion (cation) of the salts does not influence this result, suggesting that the disappearance of the phosphanoyl signals is due to a nucleophilic attack of the anion at the **P•** radical. The addition of non-

nucleophilic salts does not result in different spectra than recorded without salts. In experiments conducted with tetrabutylammonium chloride, no phosphanoyl radical is observed, but seven additional spectral lines are found around the central peak of the benzoyl radical.

In this context, the photochemistry of BAPOs in presence of fluoride salts is of interest. TR-EPR experiments were performed with compound **1** and tetrabutylammonium fluoride hydrate (see supporting information, chapter 6.1). However, ^{31}P NMR spectra indicate that the fluoride anion is already reactive towards the parent BAPO molecule in ground state. Also, tetrabutylammonium fluoride hydrate might be contaminated with HF, making the interpretation of the spectra difficult.

CIDNP-NMR spectra recorded of BAPO in samples containg iodide, bromide and chloride showed mainly signals of the cage products, while escape products are formed at a significantly lower amount when compared to the spectra measured without salts. This supports the hypothesis that the phosphanoyl radical **P•** is somehow quenched by the nucleophilic anions. ^{31}P-NMR of the photoproducts proved to be difficult to analyze due to a large amount of products formed. The most distinct features of these spectra are peaks at around 110 ppm (belonging to P(III) species) and a negative peak at around -18.6 ppm, observed in presence of iodide and bromide.

The CIDEP spectra recorded with all the different nucleophiles (water, alcohol, amines and halide anions) have in common that the phosphanoyl radicals are either observed at a significantly lower amount, or not at all. Therefore, an electrophilic reactivity of the **P•** species towards nucleophiles seems to be likely. The halide anions are significantly better nucleophiles than water or alcohols.[52,53] This is in concert with the observation that one equivalent of the anion (with respect to the BAPO) is sufficient to fully consume the phoshpanoyl radical in the TR-EPR experiments, whereas in the case of water or ethanol, a large excess is required (see section 3.3.1 and 3.3.2). The nucleophilicity of the compounds was rated according to the nucleophilicity parameter developed by Mayer and coworkers.[53]

3.3.7 Mechanistic Considerations and DFT Calculations

Concerning the structure of the so far unidentified radical formed in presence of water and ethanol, three conclusions can be drawn on the basis of the TR-EPR spectra:

- A doublet is observed, suggesting that the unknown radical presumably contains phosphorous (due to the size of the hyperfine coupling constant of ~3 mT it is very unlikely that the doublet comes from a hydrogen).
- The hyperfine coupling constant is rather small, and therefore, the unknown radical is presumably not P-centered.
- The lifetime of the unknown radical is very long. Accordingly, it must be very stable.

Concerning the second point, it should be noted that the radical anions of BAPOs are known to exhibit small hyperfine coupling constants at around 2.5 mT.[54] However, the long lifetime of the observed radical in aqueous (protic) media is a rather strong indication against the possibility that the newly observed species is a radical anion.

Assuming a nucleophilic attack of water or alcohols (denoted as Nu) at the most electrophilic position in the phosphanoyl radical (the carbonyl group), we developed the following radical reaction mechanism. Species **C•** is a C-centered radical bearing a phosphorous atom next to the radical center. The free electron can delocalize into the mesityl ring, making the proposed radical quite stable.

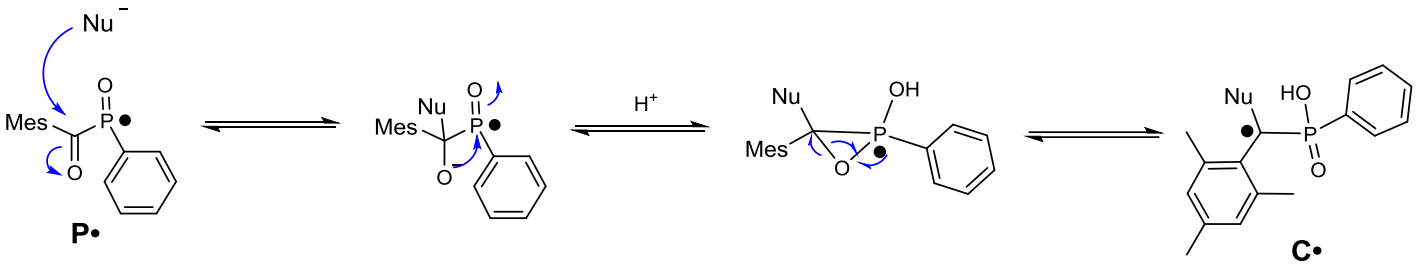

Scheme 16. Possible reaction mechanism with water and alcohols (Nu^-: OH^- or OR^-).

In order to test whether radical **C•** is a likely candidate for the species observed in the TR-EPR spectra, quantum chemical calculations on the B3LYP level of theory have been performed (Figure 32). ^{31}P hyperfine coupling constants have been calculated to be 2.81 and 3.03 mT for the radicals **C•** formed with water and ethanol, while the experimental values are 2.95 mT (H_2O) and 3.0 mT (EtOH). The good match supports the possibility that radical **C•** is the species observed in the CIDEP experiments. Further, assuming that radical **C•** recombines with a

mesitoyl radical, the formation of the species **b** (m/z 481.2), **e** (m/z 487.14) and **f** (m/z 509.13) found in the MALDI-MS spectra of the samples with water and ethanol can be explained (see section 3.3.6).

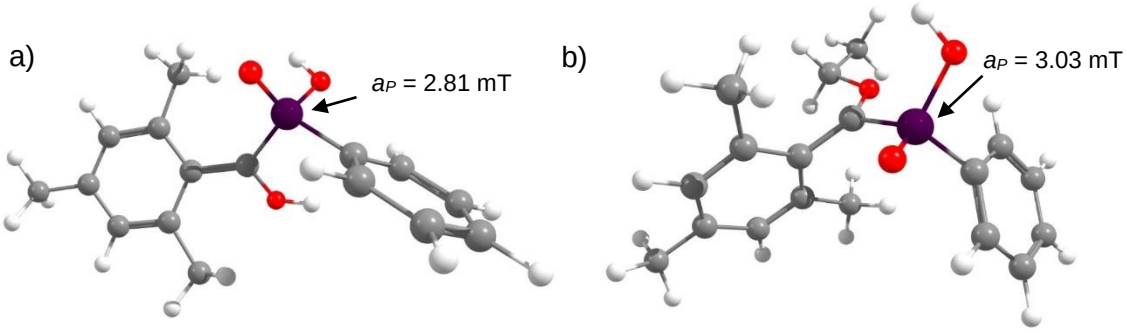

Figure 32. Optimized geometries and calculated hyperfine coupling constants a_P of radical **C•** with a) OH^- and b) EtO^- as nucleophiles.

The same reaction mechanism as shown in Scheme 15 might be conceivable for chloride as the nucleophile. However, when analyzing the experimental spectrum under the assumption that radical **C•** is observed, hyperfine coupling constants of 4.5 mT and 1.5 mT are determined for the ^{31}P and ^{35}Cl nuclei, which is not in line with calculated values of 2.9 mT and 0.9 mT.

Apart from an attack of the nucleophile at the carbonyl group, one could think of an attack occurring directly at the phosphorous atom. This might happen in the case of bromide and iodide. Both anions are considered to be “soft” in terms of HSAB theory, making an attack of at the “soft” phosphorous more likely than at the “hard” carbonyl group. The opposite is true in the case of the rather “hard” water, alcohol and chloride nucleophiles.

A mechanism which could be in line with the experimental data obtained in presence of iodide and bromide is shown below. As the final product, a P(III) species is suggested, which might fit to the observations made from the NMR spectra of the photoproducts. The P-centered radicals shown in Scheme 17 might react very fast to form the diamagnetic species, so that they are not observed within the detection speed of the TR-EPR experiment.

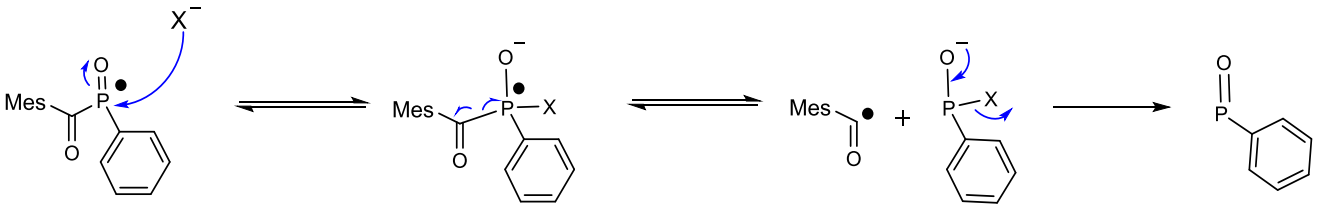

Scheme 17. Possible reaction mechanism with nucleophilic anions.

4 Multi-wave Photoinitiators

4.1 Introduction and Previous Work

Multi-wave photoinitiators (MW-PIs) are radical photoinitiators featuring at least two photoactive groups which are selectively addressed by different irradiation wavelengths.[55] This allows the synthesis of block copolymers by means of free radical photopolymerization. Other possible ways to obtain block copolymers by radical photopolymerization are photochemical coupling of two individual polymer chains as well as the application of controlled (living) radical polymerization.[13,56,57]

The multi-wave concept is based on specific absorption properties of the photoactive moieties, as shown in Scheme 18.

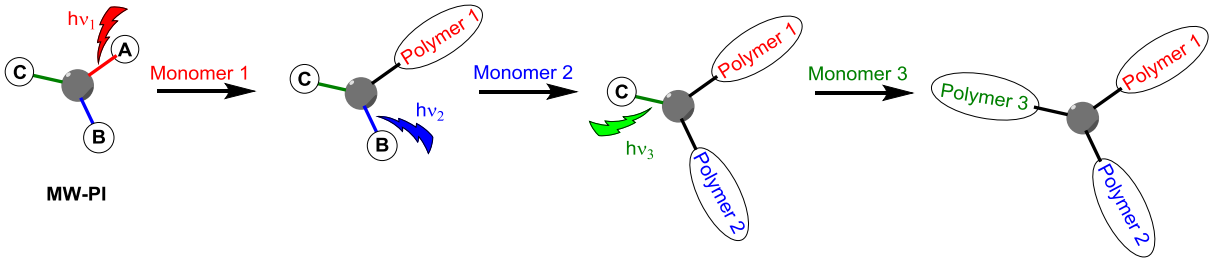

Scheme 18. Simple representation of the multi-wave concept on the example of a trifunctional photoinitiator (MW-PI) featuring the photoactive moieties A, B and C.

Light of wavelength 1 (represented in red) selectively excites group A, initiating the polymerization of the first monomer. The resulting polymer features an end group with two photoactive moieties (B and C), serving as a macroinitiator in the second polymerization step to obtain a diblock copolymer comprising still one photoactive group. In the last step, a star-shaped polymer with three linear polymer chains is formed.[c]

A star-shaped polymer is defined as a macromolecule which contains several linear polymer chains starting from one single multifunctional branching point.[58,59] Both, the multiple functionalities as well as the compact shapes (resulting in e.g. a small hydrodynamic volume) make these polymers interesting for several applications.[59]

It should be emphasized that in Scheme 18, a simplified and ideal process is drawn. Since the photoactive groups A, B and C are based on (cleavage type) radical photoinitiators, two radicals are produced upon excitation of the individual groups. Depending on the chemical structure of the photoactive group, the second radical may also initiate polymerizations, resulting in the formation of homopolymers together with the desired products.[56] The

[c] Less precisely, this polymer is also referred to as a triblock polymer in this work.

separation of the desired polymer from these “side products” may be a challenge. This problem is not encountered if block copolymers are synthesized by ionic polymerizations. However, free radical polymerizations can be performed more easily and are therefore more attractive for industrial applications than ionic polymerizations.[56] Accordingly, it is of high interest to investigate radical multi-wave photoinitiators in more detail.

In this work, bisacylphosphane oxide (BAPO) derivatives are tested as multi-wave photoinitiators. Generally, photolysis of BAPOs leads to the formation of a benzoyl and a phosphanoyl radical pair via triplet-state *α*-cleavage, both radicals being reactive towards the double bonds of monomers. The polymer chains initiated by the phosphanoyl radical comprise a monoacylphosphane oxide (MAPO) end group, capable of producing another benzoyl and phosphanoyl radical. However, if the irradiation wavelength is chosen high enough, the MAPO group cannot be cleaved, since the absorption spectrum of MAPOs is blue-shifted when compared to BAPOs. In a subsequent irradiation step applying light of lower wavelength, the polymerization of a different monomer may be initiated, yielding a diblock copolymer, as was shown by Yagci and coworkers.[11]

Herein, the stepwise reactivity of the commercially photoinitiator BAPO Irgacure 819 is investigated. Further, BAPO derivatives featuring a α-hydroxy ketone in the side chain were synthesized (Prof. Grützmacher, ETH Zürich) and are tested as trifunctional photoinitiators (Figure 33).

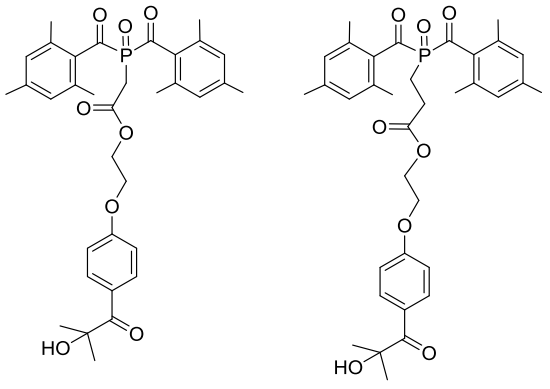

Figure 33. BAPO-based multi-wave photoinitiators MW-PI1 and MW-PI2.

On the molecular level, evidence for the wavelength-selective reactivity of MW-PI1 and MW-PI2 has been gained from CIDNP experiments performed by Michal Zalibera (TU Graz). Excitation of the compounds using light of a laser operating at 415 nm selectively resulted in polarized signals stemming from the BAPO moiety in ^{1}H-CIDNP spectra. At 355 nm excitation, signals assigned to the photoproducts formed upon cleavage of both BAPO and α-hydroxy

ketone have been observed, whereas at 266 nm, the α-hydroxy ketone was cleaved selectively.

The applicability of MW-PI1 and MW-PI2 as trifunctional photoinitiators was tested according to Scheme 19. The irradiation wavelengths were chosen in order to first excite the BAPO, followed by the MAPO and the α-hydroxy ketone, which cleaves at significantly lower wavelengths than BAPOs and MAPOs.

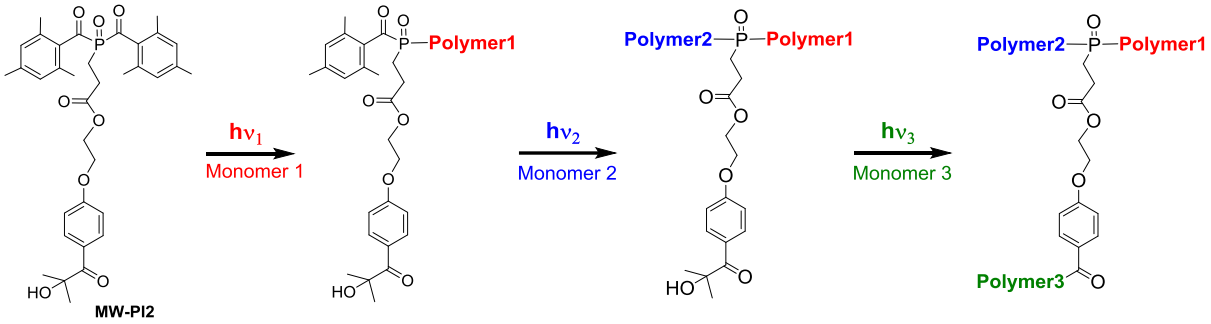

Scheme 19. Synthesis of triblock polymers initiated by MW-PI2, a trifunctional BAPO-based photoinitiator.

For diblock and triblock synthesis, methyl methacrylate (MMA) served as the monomer in the first irradiation step, since its propagation rate coefficient is suitable for bulk polymerizations.[60] Furthermore, poly(methyl-methacrylate) (pMMA) has been shown to be a convenient polymer for end group analysis using mass spectrometry, due to the molecular weight of ~100 g/mol per repeating unit.[61,62]

In addition to polymer synthesis, the photoproducts formed upon stepwise irradiation of the multi-wave photoinitiators in presence of the radical scavenger diphenyl disulfide and the non-polymerizable monomer *t*-BAM (methyl-*t*-butacrylate) were investigated utilizing NMR-spectroscopy and mass spectrometry (proof of principle).

4.2 Experimental

Compounds, solvents and light sources. The multi-wave photoinitiators were provided by the research group of Prof. Grützmacher (ETH Zürich). Bis(2,4,6-trimethylbenzoyl) phenylphosphane oxide (BAPO Irgacure 819), (2,4,6-trimethylbenzoyl)diphenylphosphane oxide (MAPO Lucirin TPO) and the α-hydroxy ketone Irgacure 2959 were purchased from Ciba and used without further purification.

The monomers methyl methacrylate (MMA, Fluka, purity ≥99.0%), styrene (S, Fluka, ≥99.5%), 1-vinyl-2-pyrollidone (VP, Fluka, ≥97.0 %), butyl methacrylate (BMA, Sigma Aldrich, 99%), benzyl methacrylate (BzMA, Sigma Aldrich, 96%) and 1*H*,1*H*,2*H*,2*H*-perfluorodecyl acrylate (FA, Sigma Aldrich, 97%) were freed from stabilizers by passing through a column of basic alumina. 3,3-Dimethyl-2-methylenbutanoat (*t*-BAM) was provided by the group of Prof. Liska (Vienna University of Technology). The radical scavenger phenyl disulfide (Ph_2S_2, 99%) was obtained from Sigma Aldrich. The solvents acetonitrile (MeCN, Sigma Aldrich, ≥99.9%), tetrahydrofuran (THF, Roth, ≥99.9%), cyclohexane (CH, puriss., Sigma Aldrich), methanol (MeOH, Roth, ≥ 99.9%), diethyl ether (Et_2O, Sigma Aldrich, ≥99%) and 1,1,1,3,3,3-hexafluoro-2-propanol (HFIP, Sigma Aldrich, ≥99%) were used as received.

As light sources, light emitting diodes (LEDs) and a Hg-Xe UV lamp (Hamamatsu Lightningcure LC4, 3500 mW/cm², λ_{max} = 365 nm) were applied. LEDs emitting light at 420 nm (15 mW output power at 20 mA, 15 nm peak half width), 400 nm (21-29 mW at 25 mA, 15 nm half width) and 385 nm (11 mW at 20 mA, 15 nm half width) were obtained from Roithner Lasertechnik. Irradiation times were controlled by an electronic device provided by Lukas Troi (TU Graz).

UV-Vis Spectroscopy. A Shimadzu UV-3101PC UV-Vis-NIR scanning spectrophotometer was used for UV-Vis measurements. Concentrations of the photoinitiators were between 0.5 mM and 0.1 mM in acetonitrile. The measurements were performed at ambient temperature.

NMR Spectroscopy. ^{1}H- and ^{31}P-NMR spectra were recorded on a 200 MHz Bruker AVANCE DPX spectrometer. ^{1}H chemical shifts (δ) are reported in ppm relative to tetramethylsilane (TMS) using the residual deuterated solvent signals as an internal reference.

MALDI-MS. Matrix-assisted laser desorption/ionization time-of-flight (MALDI-TOF) mass spectra were recorded on a Micromass TofSpec 2E Time-of-Flight Mass Spectrometer. Trans-2-[3-(4-tert-Butylphenyl)-2-methyl-2-propenylidene]malononitrile (DCTB) was used as matrix substance. Sample solutions have been prepared by mixing solutions of DCTB (10 mg/mL in THF), sodium trifluoroacetate (1 mg/mL in THF) and the sample (NMR solutions diluted 1:10 with THF or 5 mg/mL in THF) in a ratio of 7/2/2 (v/v/v). Calibration was done externally with polyethylene glycol standards (5 mg/mL in THF).

Size Exclusion Chromatography (Gel Permeation Chromatography). Size exclusion chromatography (SEC) was performed on a WGE SEC-3010 equipped with a WGE G-2010 pump and a WGE Dn-2010 refractive index (RI) detector. THF was used as eluent. For calibration polystyrene standards from Polymer Standards Service were utilized.

Analysis of Photoproducts in Presence of Radical Scavengers. Deoxygenated acetonitrile solutions of the photoinitiator (25 mM) containing a 7-fold molar excess of diphenyl disulfide or *t*-BAM were irradiated in a stepwise way at 420 nm and 400 nm (or 385 nm). In case of the multi-wave photoinitiators, a third irradiation step was performed using UV light emitted by a Hg-Xe lamp (Hamamatsu). NMR and MALDI-MS spectra were recorded after each step. Irradiations were performed in glass vials or NMR tubes (sample volume: 850 µL).

Synthesis of Diblock Copolymers. Diblock copolymers were synthesized in stepwise bulk polymerizations applying BAPO Irgacure 819 as the photoinitiator. In the first polymerization step, samples of the photoinitiator were prepared in methyl methacrylate (MMA) at a concentration of 20 mM (sample volume ~ 0.7 mL in a glass vial) and irradiated at 420 nm for 5 minutes. pMMA was isolated by precipitation in cyclohexane. For purification and removal of residual photoinitiator, the polymer was reprecipitated from THF several times. 40 mg of pMMA were dissolved in ca. 600 µL of the second monomer (styrene, 1-vinyl-2-pyrrolidone or MMA) and irradiated for 35 minutes at 385 nm. Solvents for the precipitation of the copolymers were methanol (for pMMA-pS), diethyl ether (for pMMA-pVP) and cyclohexane (for pMMA-pMMA). All solutions were deoxygenated by bubbling with argon (5 min) before irradiation.

Synthesis of Triblock Polymers. Triblock polymers were synthesized in stepwise bulk polymerizations applying MW-PI1 and MW-PI2 as photoinitiators. pMMA was obtained upon irradiation (420 nm, 4 min) of a deoxygenated sample of the photoinitiator (20 mM or 40 mM) in MMA at (sample volume ~0.7 mL, precipitation in cyclohexane). To obtain pMMA-pMMA-pMMA, samples containing 25 mg pMMA in 600 µL MMA were irradiated at 385 nm (40 min). Then, 30 mg of pMMA-pMMA were dissolved in 600 µL MMA and irradiated with a UV lamp (4 min). Alternatively, butyl methacrylate (BMA) or 1*H*,1*H*,2*H*,2*H*-perfluorodecyl acrylate (FA) were used as the second monomer and the deoxygenated samples (ca. 25 mg pMMA in 600 µL of the monomer) were irradiated for 30 minutes at 385 nm (precipitation in methanol). The triblock polymer pMMA-pBMA-pBzMA was obtained upon UV light irradiation (10 min) of a sample containing ~ 20 mg of pMMA-pBMA in 600 µL of benzyl methacrylate (precipitation in methanol). pMMA-pFA-pS and pMMA-pFA-pVP were prepared in solution polymerizations using HFIP as the solvent (ca. 30 mg of pMMA-pFA in 600 µL solvent and 300 µL monomer, 20 min UV-lamp, precipitation in MeOH and Et_2O, respectively).

4.3 Results and Discussion

4.3.1 BAPO as Bifunctional Photoinitiator

The optical spectra of BAPOs extend further into the visible range than the spectra of MAPOs (Figure 34), as is explained by the larger conjugated electronic system of BAPOs. Due to the red-shifted *n*-π^* bands of BAPOs, exclusively one of the two benzoyl (mesitoyl) moieties can be cleaved using light of 420 – 430 nm. The MAPO end group of the resulting polymer is excited at lower wavelengths, as is shown in Figure 34 on the example of a typical MAPO. For the excitation of the MAPO group, light of 385 – 400 nm is applied in this work.

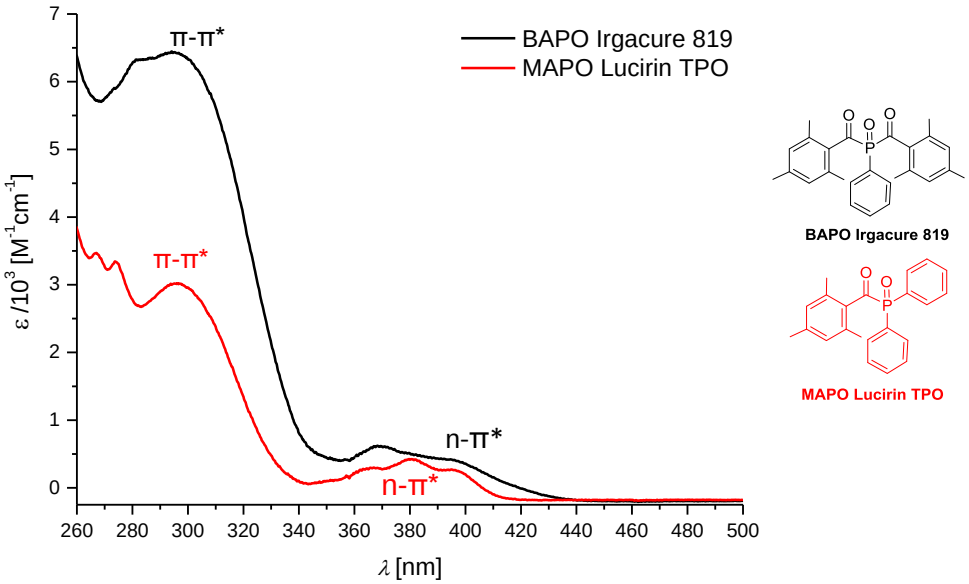

Figure 34. Comparison of the UV-Vis spectra of a typical BAPO and a typical MAPO.

4.3.1.1 Photoproducts in Presence of Diphenyl Disulfide

Clear evidence for the sequential reactivity of BAPO Irgacure 819 at two wavelengths (420 nm and 400 nm) was gained from trapping experiments using diphenyl disulfide (Ph_2S_2) as a radical scavenger (Scheme 20, see also PHD thesis of G. Müller[55]).

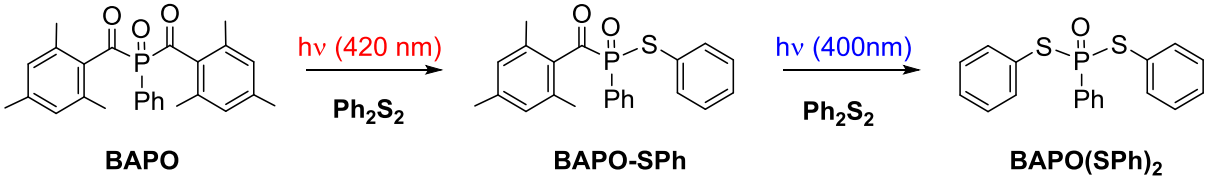

Scheme 20. Stepwise irradiation of BAPO in presence of diphenyl disulfide (Ph_2S_2).

^{31}P-NMR experiments confirm the selective formation of monothioester BAPO-SPh upon irradiation at 420 nm (LED), while subsequent irradiation at 400 nm exclusively yields the dithioester BAPO-$(SPh)_2$ (see Figure 35).

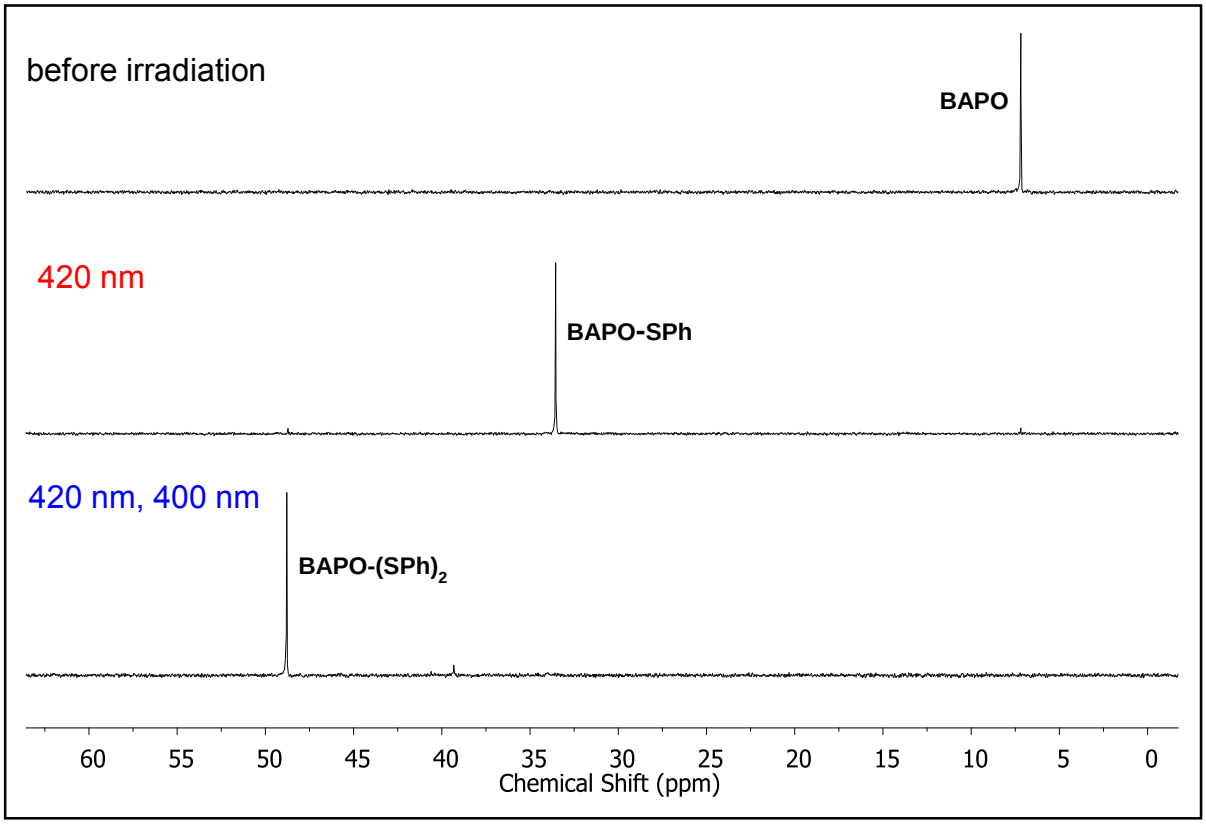

Figure 35. ^{31}P-NMR spectra of BAPO Irgacure 819 in presence of Ph_2S_2. (Sample: 25 mM BAPO, 7 equiv. Ph_2S_2 in acetonitrile-d_3, irradiation times: 5 min at 420 nm, 50 min at 400 nm.)

Further, polymerization experiments were performed using methyl methacrylate (MMA) as the first monomer. Irradiation (420 nm) of BAPO Irgacure 819 in MMA resulted in the formation of pMMA featuring MAPO end groups. Upon post-irradiation of MAPO-pMMA in presence of diphenyl disulfide, the monothioester PhS-pMMA was obtained (see Scheme 21). This was shown by end group analysis using matrix-assisted laser desorption mass spectrometry (MALDI-MS) as well as by ^{31}P-NMR spectroscopy.

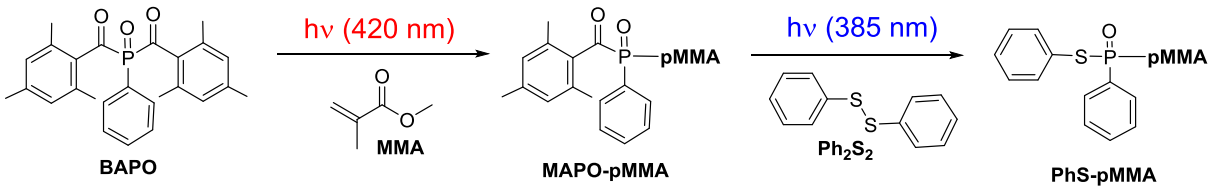

Scheme 21. Synthesis of MAPO-pMMA and subsequent irradiation in presence of Ph_2S_2.

pMMA was prepared by irradiation (420 nm, 5 min) of samples containing BAPO Irgacure 819 and MMA in a 1:78 mol:mol ratio. Post-irradiation (385 nm, 35 min) of pMMA was carried out in deoxygenated THF solutions containing 0.1 M Ph_2S_2 (concentration of pMMA ~20 g/L). The mass shifts observed in the MALDI-MS spectra upon post-irradiation clearly indicate that PhS-pMMA is formed (Figures 36 and 37).

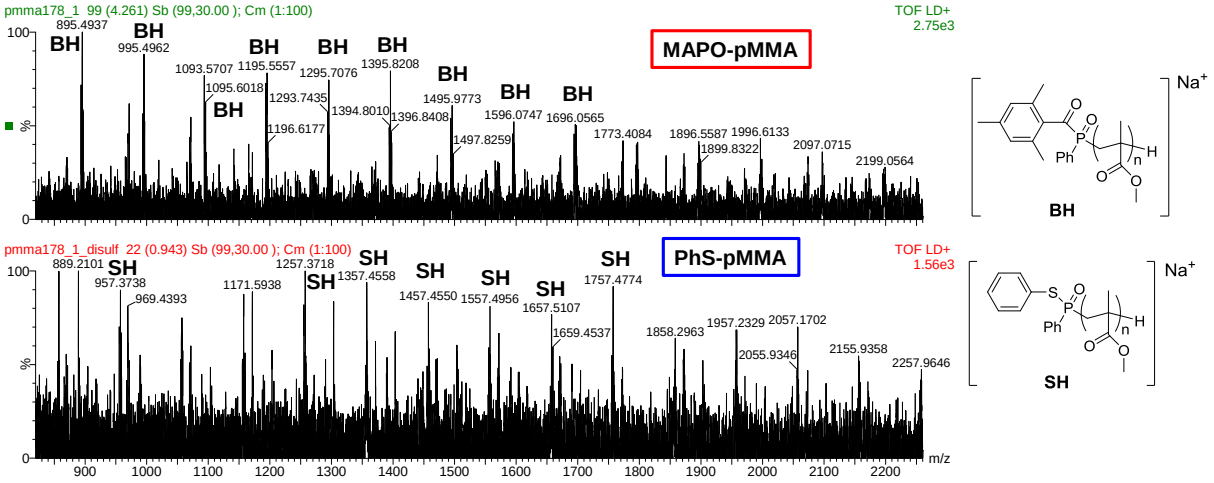

Figure 36. MALDI-MS spectra of MAPO-pMMA and PhS-pMMA.

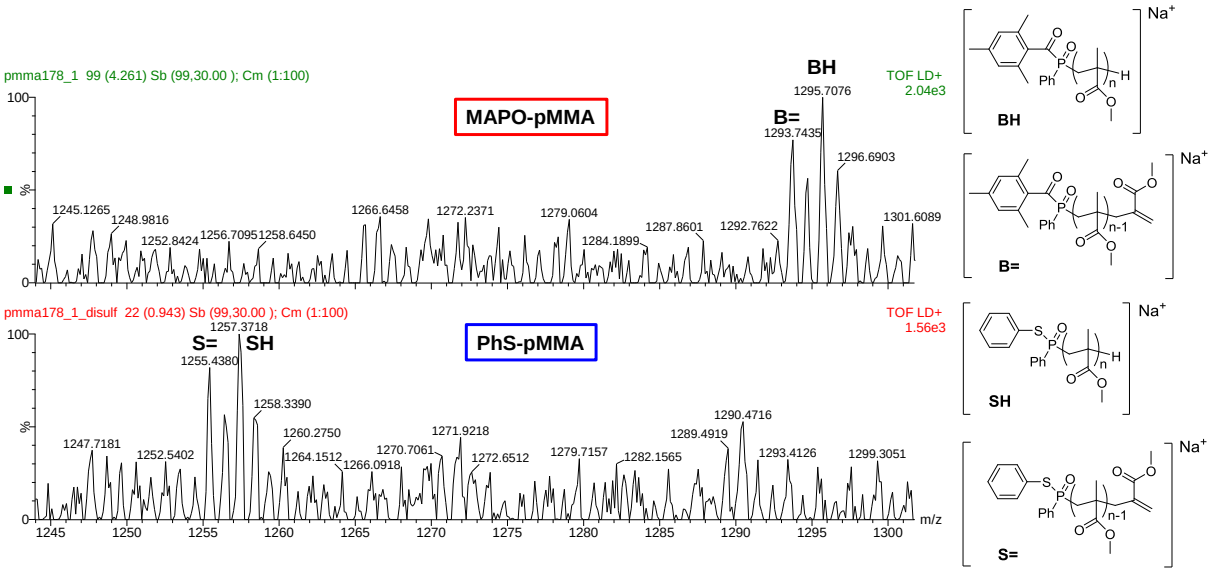

Figure 37. MALDI-MS spectra of MAPO-pMMA and PhS-pMMA (zoom).

Figure 37 presents a zoom into the MALDI-MS spectra of MAPO-pMMA and PhS–pMMA. The signals at m/z 1293.74 (B=) and m/z 1295.71 (BH) belong to MAPO-terminated pMMA chains, resulting from termination of the chain growth via disproportionation. In the sample containing PhS-pMMA, signals are observed at m/z 1255.4 and m/z 1257.37, being assigned to the

species SH and S=, which correspond to pMMA comprising a thioester end group. ^{31}P-NMR spectra of these samples are provided in the supporting information.

To summarize, photolysis of a MAPO-terminated polymer in presence of a disulfide yields a polymer featuring a thioester end group. In principle, this concept could be used to attach derivatives of the amino acid cysteine to a polymer. Irradiation of MAPO-terminated polymers in presence of the disulfide cystine might yield the desired polymer amino acid products. Further amino acids could then be added to the cysteine group by solid phase peptide synthesis, yielding a peptide functionalized polymer.

4.3.1.2 Diblock Copolymers

Diblock copolymers of pMMA and polystyrene (pS), poly-1-vinyl-2-pyrollidone (pVP) and pMMA have been synthesized according to Scheme 22.

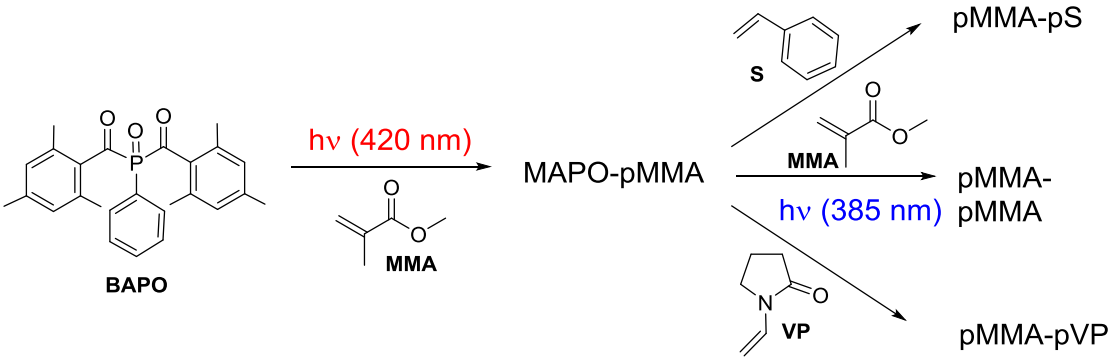

Scheme 22. Synthesis of diblock copolymers using BAPO Irgacure 819 as the photoinitiator.

Polymerizations were performed as described in the experimental section. Successful diblock copolymer formation is evidenced by gel permeation chromatography (GPC, measured by Josefine Hobisch, TU Graz). An increase in the number average molar mass M_n and the mass average molar mass M_w is observed in the copolymers when compared to pMMA (Table 7). The copolymer pMMA-pVP could not be characterized by GPC due to the high polarity of the pVP, which is not compatible with the column and solvent system available.

The obtained diblock copolymers can be successfully employed as surfactants in systems containing two immiscible solvents, as was shown for the copolymer pMMA-pS in the system cyclohexane-acetonitrile, and for pMMA-pVP in the system toluene-water. Pictures of the emulsions are presented in the supporting information.

Table 7. GPC data of diblock copolymers synthesized with BAPO Irgacure 819

Sample	M_n / 10^3 [g/mol]	M_w / 10^4 [g/mol]	M_w/M_n
pMMA	5.04	1.15	2.29
pMMA-pS	6.28	1.50	2.39
pMMA-pMMA	9.16	3.12	3.41

4.3.2 MW-PI1 and MW-PI2 as Trifunctional Photoinitiators

Figure 38 displays the UV-Vis spectra of MW-PI1, MW-PI2 and the component photoinitiators BAPO and Irgacure 2959. The spectra of MW-PI1 and MW-PI2 essentially represent a combination of the spectra of the BAPO and the α-hydroxy ketone.

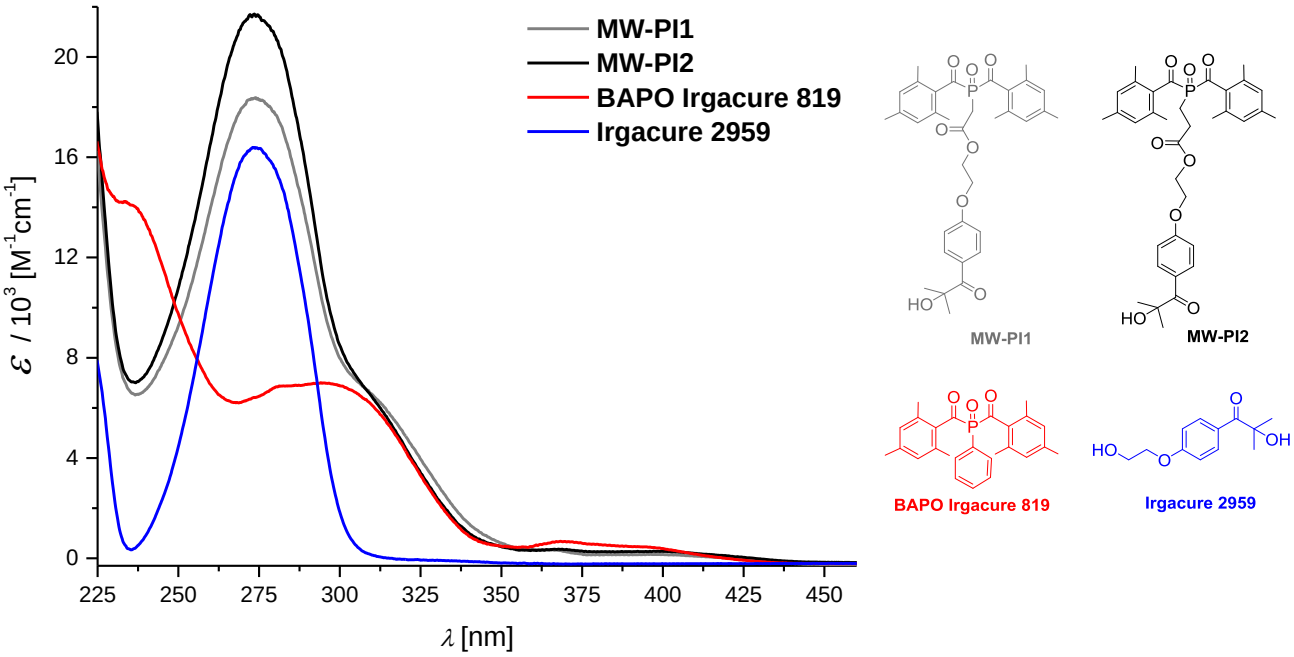

Figure 38. UV-Vis spectra of MW-PI1, MW-PI2 and the component PIs (solvent: acetonitrile).

4.3.2.1 Photoproducts in Presence of Diphenyl Disulfide

MW-PI2 was tested in the stepwise reactivity towards diphenyl disulfide (see Scheme 23). In the third irradiation step, the α-hydroxy ketone is cleaved using a Hg-Xe UV lamp emitting a broad wavelength spectrum (λ_{max} 365 nm). Of course, the light emitted by the UV lamp can also cleave the BAPO and MAPO moieties, however these groups are expected to have reacted before.

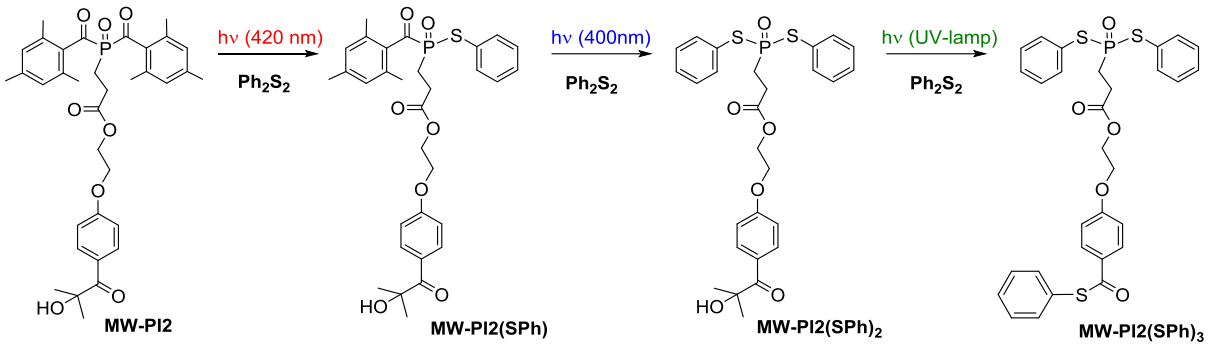

Scheme 23. Stepwise irradiation of MW-PI2 in presence of diphenyl disulfide (Ph_2S_2).

Irradiation at 420 nm (4 min) results in the exclusive formation of the monothioester MW-PI2 (SPh), which is converted to the dithioester MW-PI2(SPh)$_2$ upon subsequent irradiation at 400 nm (20 min). This was shown by ^{31}P-NMR (Figure 39). Species MW-PI2(SPh) is observed at a chemical shift of 43.36 ppm, whereas MW-PI2(SPh)$_2$ is found at 60.80 ppm. After the last irradiation step (10 min UV-lamp), no major changes are observed in the ^{31}P-NMR spectrum, which is in line with the expectation that the reaction occurs exclusively at the α-hydroxy ketone moiety, which is far away from the phosphorous atom of the BAPO group. ^{1}H-NMR spectra of can be found in the supporting information. MALDI-MS spectra are depicted in Figure 40.

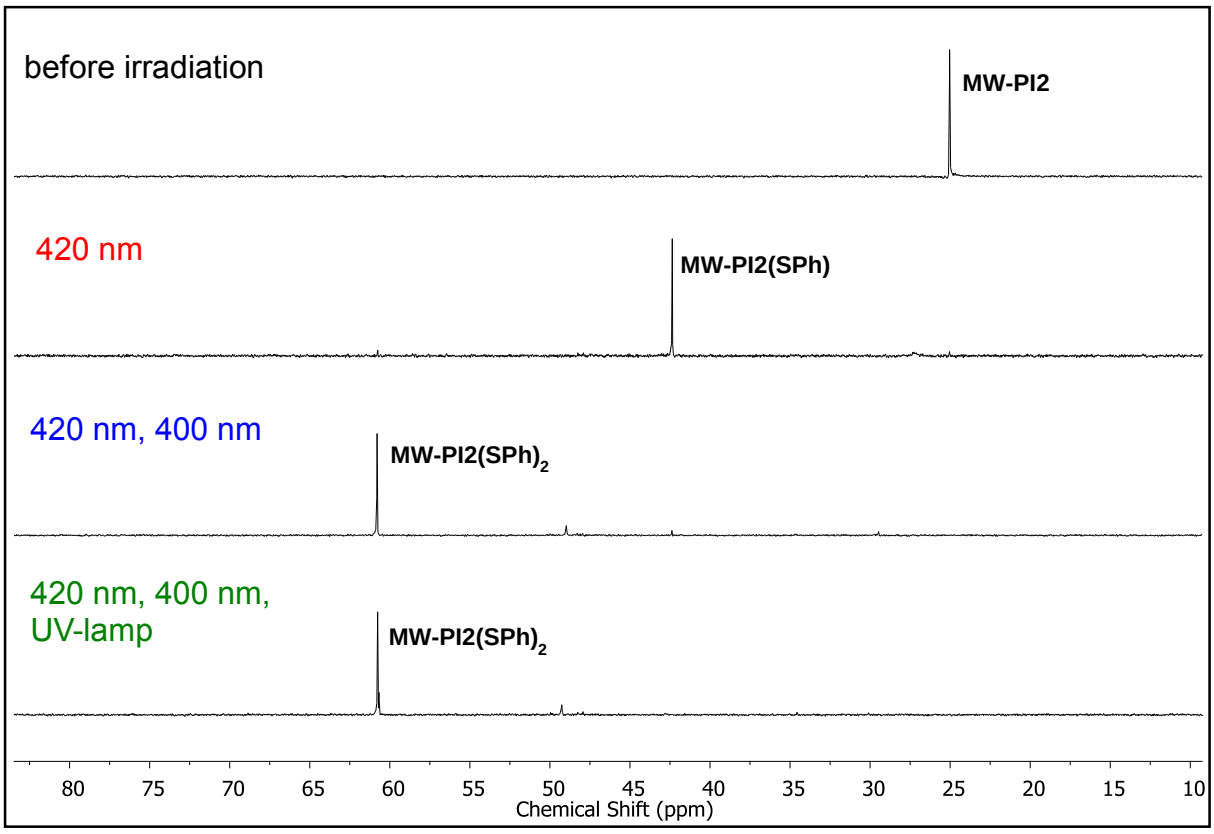

Figure 39. ^{31}P-NMR spectra of MW-PI2 in presence of Ph_2S_2. (Sample: 25 mM MW-PI2, 7 equiv. Ph_2S_2 in acetonitrile-d_3, irradiation times: 4 min at 420 nm, 20 min at 400 nm, 10 min UV lamp.)

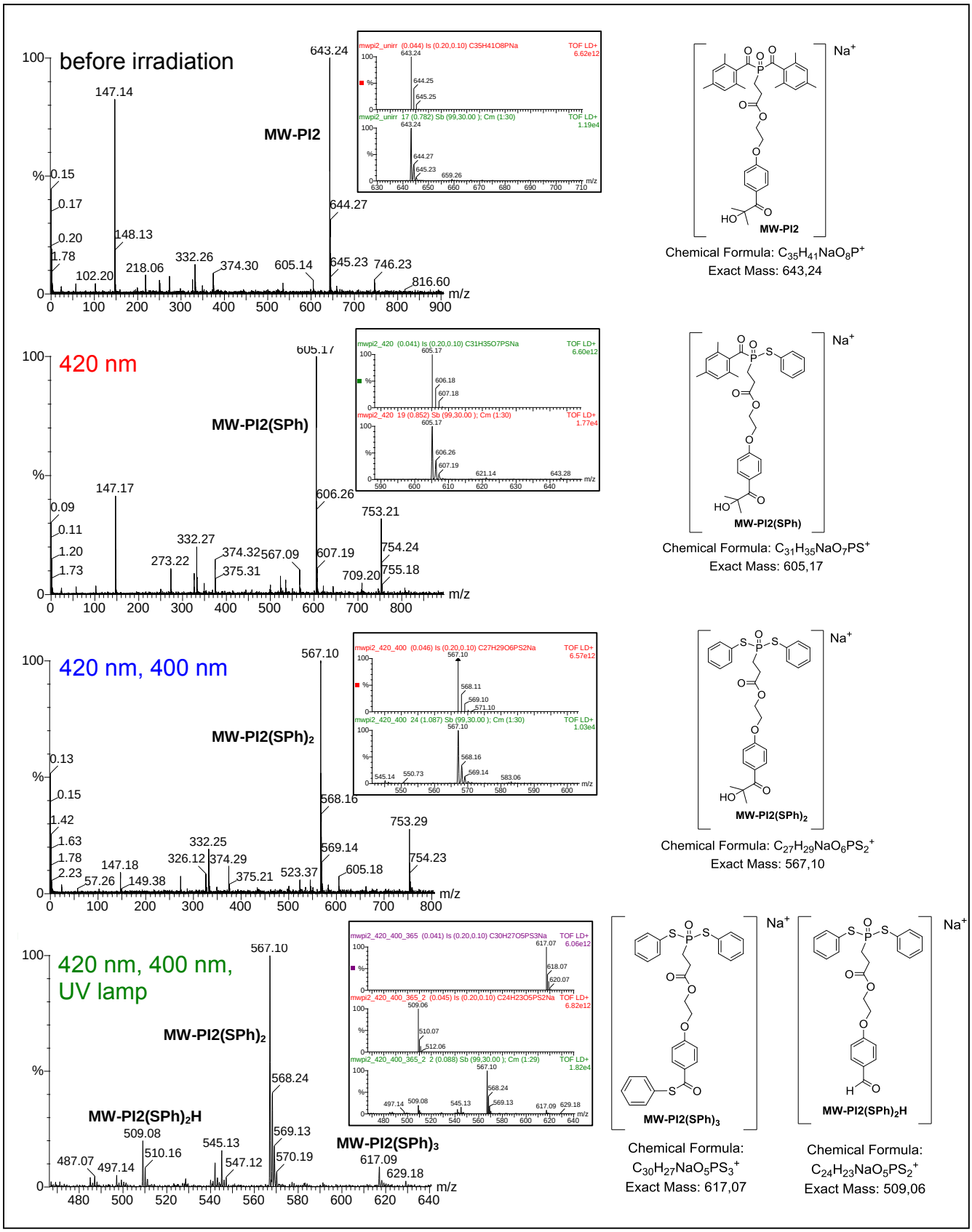

Figure 40. MALDI-MS spectra of samples containing MW-PI2 and Ph_2S_2 recorded after each irradiation step (the assigned species are shown next to the spectra). The insets present a comparison between the theoretical isotope patterns of the expected species (top) and the experimental data (bottom).

MALDI-MS experiments (Figure 40) confirm the selective formation of the monothioester upon irradiation at 420 nm and of the dithioester upon irradiation at 420 nm, followed by 400 nm. In the spectrum recorded after the third irradiation step, the thioester compound MW-PI2(SPh)$_3$ and the aldehyde MW-PI2(SPh)H are observed. The formation of both species clearly shows that the α-hydroxy ketone group is cleaved. However, residual MW-PI2(SPh)$_2$ is still found in the spectrum, indicating that full conversion to the desired species MW-PI2(SPh)$_3$ and MW-PI2(SPh)$_2$H could not be reached. It should be noted that the signal intensities in MALDI-MS spectra do not necessarily correspond to the relative concentrations of the observed species, since the ionization properties of the individual compounds might be different.

4.3.2.2 Photoproducts in Presence of a Non-polymerizable Monomer (t-BAM)

The sequential reactivity of MW-PI1 towards the non-polymerizable monomer methyl-*t*-butacrylate (*t*-BAM) was tested (see Scheme 24).

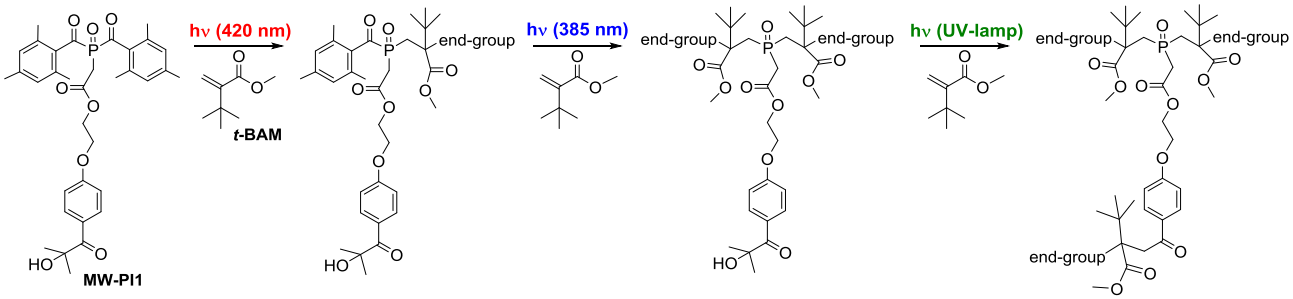

Scheme 24. Stepwise irradiation of MW-PI 1 in presence of *t*-BAM.

In the ^{31}P-NMR spectra presented in Figure 41, the sequential reactivity of the photoinitiator MW-PI1 towards *t*-BAM can be followed. ^{31}P-NMR spectra recorded after the first two irradiation steps are shown (the spectrum after the last irradiation step is now shown since the reaction does not occur next to the phosphorous atom). ^{1}H-NMR spectra are provided in the supporting information. UV-Vis spectra of diluted NMR samples clearly show stepwise photobleaching (Figure 42). MALDI-MS spectra recorded after each irradiation step are presented in Figure 43 (lower m/z) and Figure 44 (higher m/z). The full spectra are shown in the supporting information. The assigned species are color-coded according to the irradiation steps.

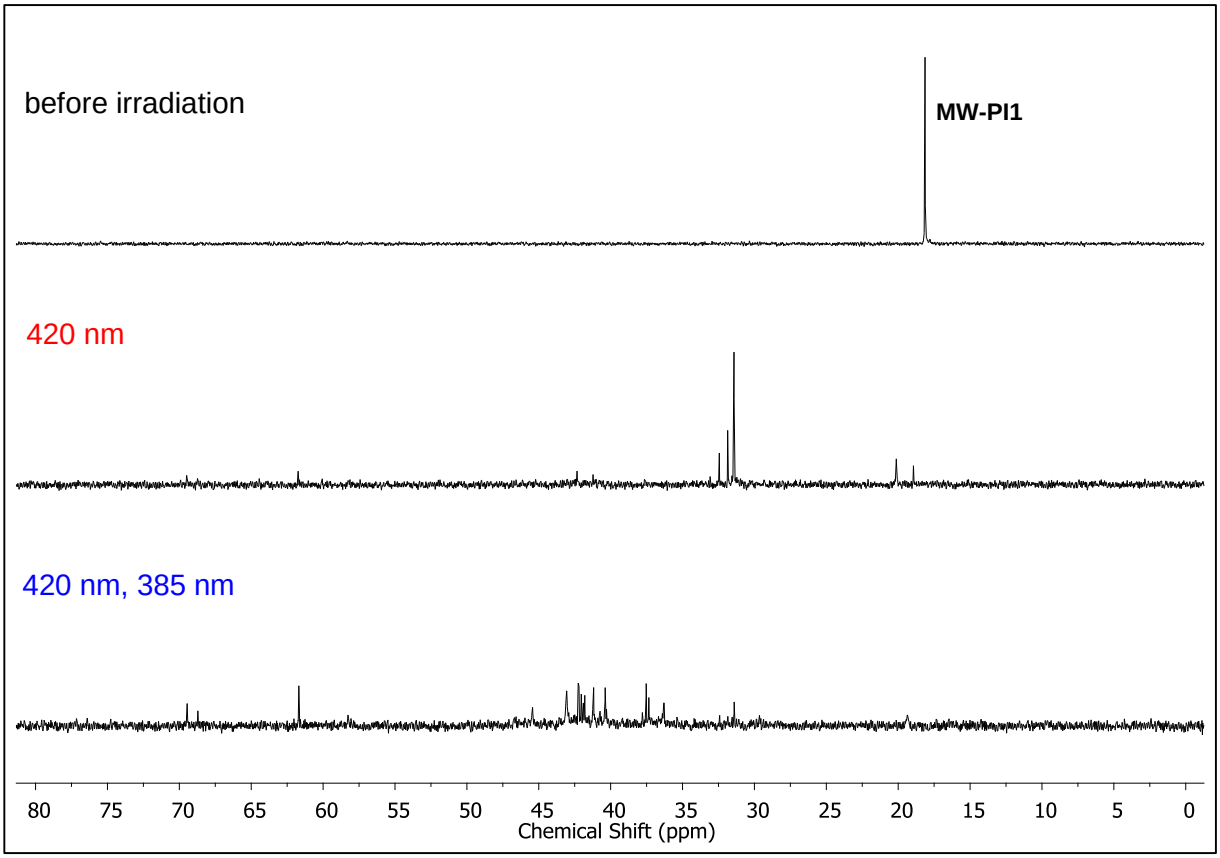

Figure 41. ^{31}P-NMR spectra of MW-PI1 in presence of *t*-BAM. (Sample: 25 mM MW-PI2, 7 equiv. *t*-BAM in acetonitrile-d_3, irradiation times: 10 min at 420 nm, 10 min at 400 nm.)

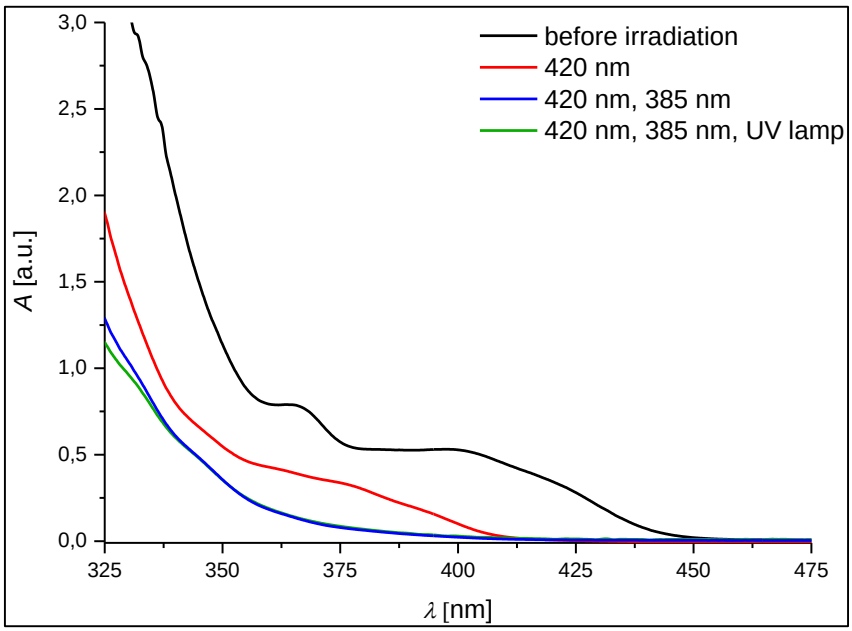

Figure 42. Photobleaching of MW-PI1 in presence of *t*-BAM. (Irradiation times: 6 min 420 nm, 12 min 385nm, 220 s UV lamp.)

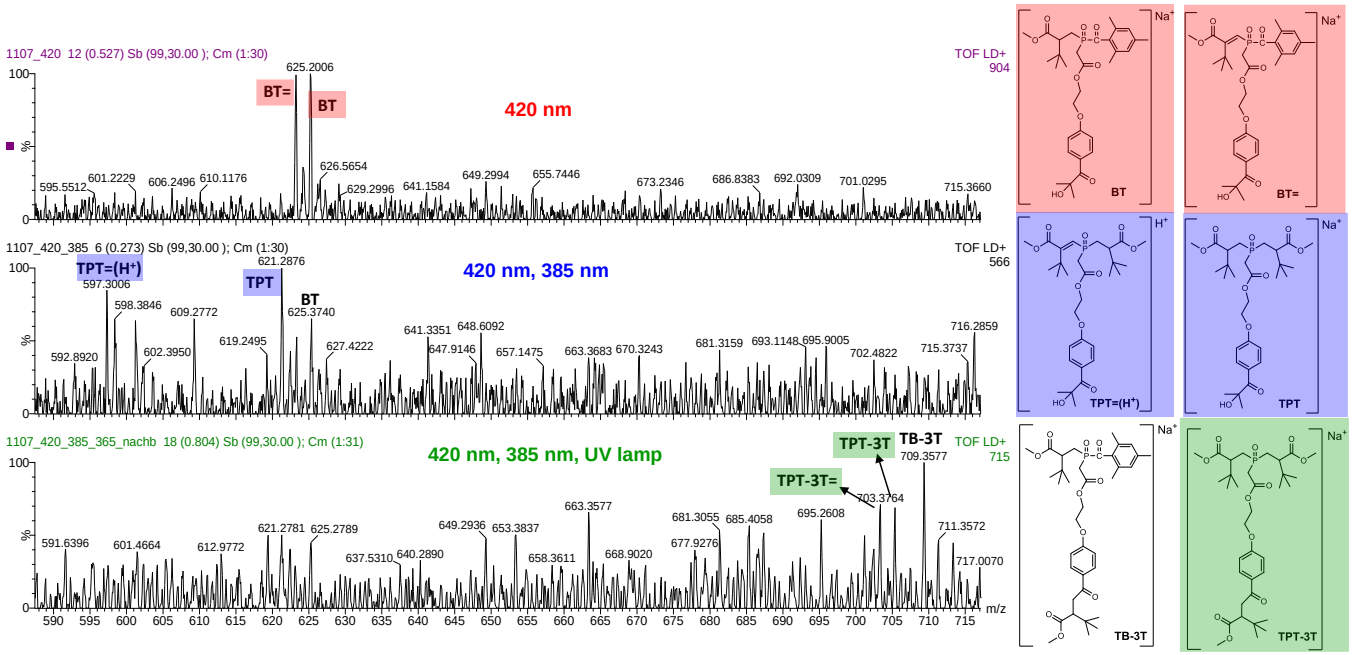

Figure 43. MALDI-MS spectra (lower m/z) of samples containing MW-PI1 and *t*-BAM, and the assigned species. (Irradiation times: 6 min 420 nm, 12 min 385 nm, 220 s UV lamp.)

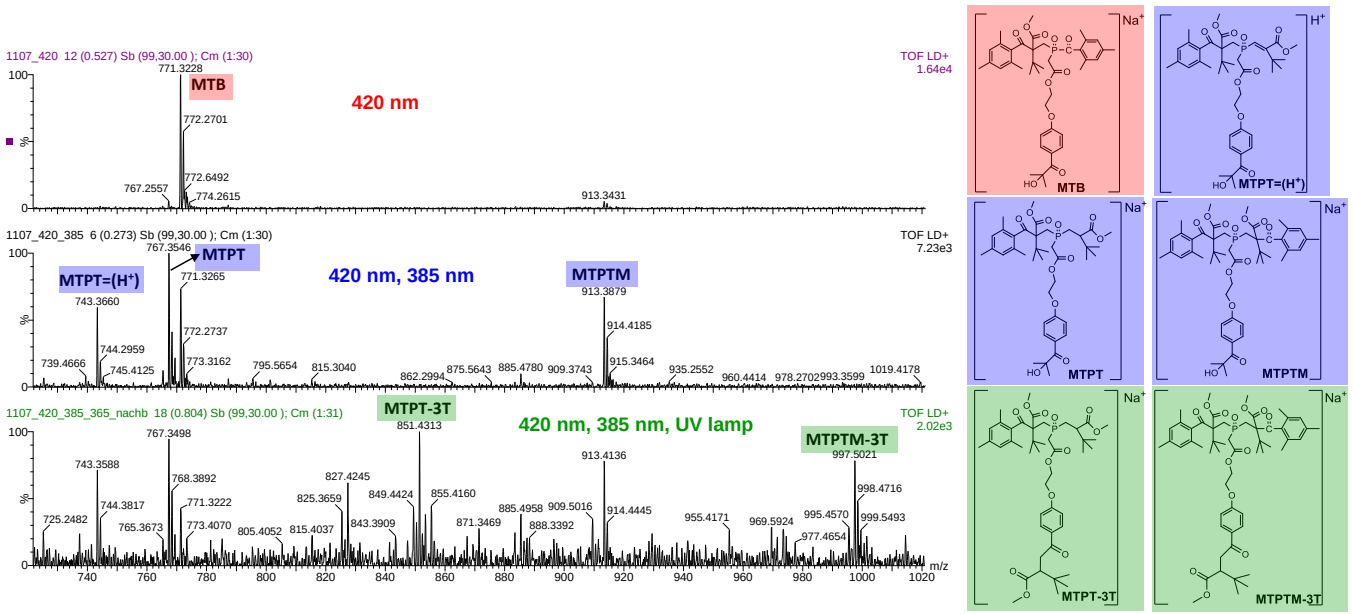

Figure 44. MALDI-MS spectra (higher m/z) of samples containing MW-PI1 and *t*-BAM, and the assigned species.

Upon irradiation at 420 nm, the species BT, BT= and MTB are observed in the mass spectra, clearly indicating that only one of the two benzoyl (mesitoyl) moieties of the BAPO is cleaved. The double bond in the species BT= results from chain growth termination via disproportionation. Species MTB is formed upon recombination of a MW-PI1-*t*-BAM radical with a mesitoyl radical. The three signals observed in the corresponding ^{31}P-NMR spectrum in the range of 31 – 32 ppm (31.4 ppm, 31.9 ppm, 32.4 ppm) are (tentatively) assigned to the products MTB, BT and BT=.

After the second irradiation step, signals assigned to the species MTPT, MTPTM and MTPT=(H^+) are found in the MALDI-MS spectra, showing that the previously formed MAPO end group has been cleaved. A signal at m/z 771.32 is still observed, belonging to remaining MTB which was not converted during the irradiation at 385 nm. In the ^{31}P NMR spectrum, ~10 new peaks appear, which might be explained the formation of *t*-BAM oligomers.

Evidence for the cleavage of the α-hydroxy ketone upon subsequent irradiation with UV light is gained from signals assigned to MTPT-3T and MTPTM-3T in the mass spectra. In the spectrum recorded after the last irradiation step, remaining MTPT and MTPTM are still found. This might be avoided by choosing a longer irradiation time. Species TB-3T and TB-3T= are found as side products, presumably resulting from incomplete cleavage of all the MAPO terminated molecules in the second irradiation step.

To summarize, the experiments with t-BAM show that the wavelength-selective reactivity of MW-PI1 can be unambiguously followed utilizing several methodologies (NMR, UV-Vis and MALDI-MS).

4.3.2.3 Triblock Polymers

A polymer containing three pMMA blocks was prepared using MW-PI1 as the photoinitiator. The corresponding GPC data are presented in Table 8. The increase in *Mn* as well as *Mw* observed after each polymerization step is a clear indication of successful diblock and triblock polymer formation.

Table 8. GPC of pMMA, pMMA-pMMA and pMMA-pMMA-pMMA synthesized with MW-PI1

Sample	M_n / 10^3 [g/mol]	M_w / 10^4 [g/mol]	M_w/M_n
pMMA	5.06	1.54	3.04
pMMA-pMMA	8.97	5.10	5.69
pMMA-pMMA-pMMA	13.14	5.69	4.33

A triblock polymer containing three different polymer blocks was synthesized with MW-PI2, utilizing the monomers MMA, butyl methacrylate (BMA) and benzyl methacrylate (BzMA). The GPC data are presented in Table 9 and Figure 45, showing that diblock and triplock polymer synthesis was successful.

Table 9. GPC of pMMA, pMMA-pBMA and pMMA-pBMA-pBzMA synthesized with MW-PI2

Sample	M_n / 10^3 [g/mol]	M_w / 10^3 [g/mol]	M_w/M_n
pMMA	4.621	14.48	3.133
pMMA-pBMA	35.23	125.7	3.568
pMMA-pBMA-pBzMA	110.2	309.5	2.808

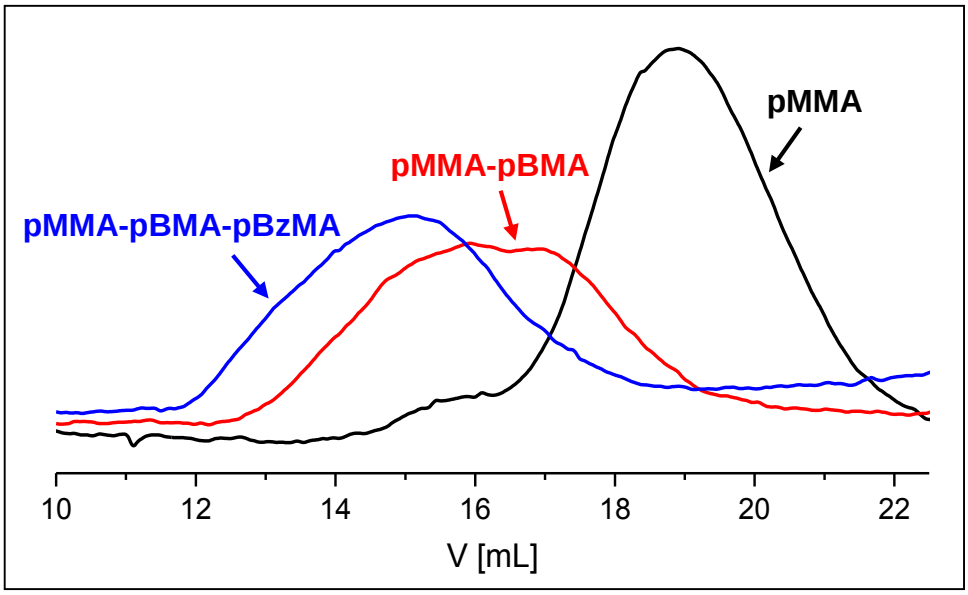

Figure 45. GPC curves of pMMA, the diblock copolymer pMMA-pBMA and the triblock polymer pMMA-pBMA-pBzMA.

Attempts to synthesize triblock polymers with polymer blocks displaying different chemical properties have been made. The goal was to obtain a triblock polymer featuring a lipophilic block (from an acrylate monomer), a water-repellant block (from a fluorinated acrylate) and a hydrophilic block (from a water soluble monomer such as 1-vinyl-2-pyrrolidone). In this respect, MAPO-pMMA (synthesized with MW-PI1) was dissolved in a fluorinated acrylate (1*H*,1*H*,2*H*,2*H*-perfluorodecyl acrylate, abbreviated as FA) and irradiated at 385 nm to obtain the copolymer pMMA-pFA. However, the characterization of this copolymer proved to be difficult, since it was insoluble in all available solvents, apart from hexafluoroisopropanol. Therefore, it was not possible to obtain NMR and GPC data of this polymer (for GPC analysis solubility in either THF or chloroform is required). In spite of that, the third polymerization step was carried out by dissolving the pMMA-pFA in hexafluoroisopropanol and adding the monomer 1-vinyl-2-pyrrolidone. Alternatively, styrene was used as the third monomer. The resulting triblock polymers could be characterized by IR spectroscopy.

4.4 Summary and Outlook

It has been found that the BAPO-based photoinitiators MW-PI1 and MW-PI2 can be successfully applied as trifunctional photoinitiators. The wavelength-selective reactivity was shown in photolysis experiments utilizing diphenyl disulfide and t-BAM as radical scavengers, as well as in the synthesis of triblock polymers.

Concerning the diblock and triblock polymer synthesis, it should be mentioned that several difficulties have been encountered. Challenges included finding the suitable solvent for the precipitation of the polymers as well as removing residual monomer from the polymer (especially in case of low volatility). Other issues were solubility problems on the one hand and rather low yields of the diblock and triblock polymers obtained in the performed bulk polymerizations on the other hand. The yields might be improved by applying more sophisticated polymerization techniques and by performing the reactions at a larger scale, using a LED reactor instead of just a single LED for irradiations.

Another important point is the separation of polymer chains initiated by the desired “multi-wave radicals” and the homopolymer chains initiated by the benzoyl radicals (in the first two steps) and the ketyl radical (in the third step). Preparative GPC might be one way to obtain pure polymer products.

5 References

(1) Yagci, Y.; Jockusch, S.; Turro, N. J. *Macromolecules* **2010**, *43* (15), 6245.

(2) Gruber, H. F. *Prog. Polym. Sci.* **1992**, *17*, 953.

(3) Nesvadba, P. *Encyclopedia of Radicals in Chemistry, Biology and Materials*, Volume 4; John Wiley & Sons, Inc., 2012.

(4) Fouassier, J.-P.; Lalevée, J. *Photoinitators for Polymer Synthesis*; Wiley-VCH, 2012.

(5) Fouassier, J.-P.; Allonas, X.; Lalevée, J.; Dietlin, C. In *Photochemistry and Photophysics of Polymer Materials*; Allen, N. S., Ed.; Wiley, 2010; pp 351–419.

(6) Moad, G.; Solomon, D. H. *The Chemistry of Radical Polymerization*; Elsevier, 2006.

(7) Müller, G.; Zalibera, M.; Gescheidt, G.; Rosenthal, A.; Santiso-Quinones, G.; Dietliker, K.; Grützmacher, H. *Macromol. Rapid Commun.* **2015**, *36* (6), 553.

(8) Benedikt, S.; Wang, J.; Markovic, M.; Moszner, N.; Dietliker, K.; Ovsianikov, A.; Grützmacher, H.; Liska, R. *J. Polym. Sci. Part A Polym. Chem.* **2015**.

(9) Rutsch, W.; Dietliker, K.; Leppard, D.; Köhler, M.; Misev, L.; Kolczak, U.; Rist, G. *Prog. Org. Coatings* **1996**, *27*, 227.

(10) Dietliker, K.; Jung, T.; Benkhoff, J.; Kura, H.; Matsumoto, A.; Oka, H.; Hristova, D.; Gescheidt, G.; Rist, G. *Macromol. Symp.* **2004**, *217* (1), 77.

(11) Gunersel, E. D.; Hepuzer, Y.; Yagci, Y. *Angew. Makromol. Chemie* **1999**, *264* (4604), 88.

(12) Dietliker, K. K. *Chemistry and Technology of Uv and Eb Formulation for Coatings, Inks & Paints, Volume 3: Photoinitiators for Free radical and Cationic Polymerisation*; SITA Technology: London, 1991.

(13) Matyjaszewski, K.; Davis, T. P. *Handbook of Radical Polymerization*; John Wiley & Sons, Inc., 2002.

(14) Ligon, S. C.; Husár, B.; Wutzel, H.; Holman, R.; Liska, R. *Chem. Rev.* **2014**, *114* (1), 577.

(15) Dadashi-Silab, S.; Doran, S.; Yagci, Y. *Chem. Rev.* **2016**.

(16) Sumiyoshi, T.; Schnabel, W.; Henne, a. *J. Photochem.* **1985**, *30* (1), 63.

(17) Kolczak, U.; Rist, G.; Dietliker, K.; Wirz, J. *J. Am. Chem. Soc.* **1996**, *118* (27), 6477.

(18) Jockusch, S.; Koptyug, I. V.; McGarry, P. F.; Sluggett, G. W.; Turro, N. J.; Watkins, D. M. *J. Am. Chem. Soc.* **1997**, *119* (17), 11495.

(19) Spichty, M.; Turro, N. J.; Rist, G.; Birbaum, J.-L.; Dietliker, K.; Wolf, J. P.; Gescheidt, G. *J. Photochem. Photobiol. A Chem.* **2001**, *142*, 209.

(20) Zewail, A. H. *Angew. Chemie - Int. Ed.* **2000**, *39* (15), 2586.

(21) Sluggett, G. W.; Turro, C.; George, M. W.; Koptyugjs, I. V; Turro, N. J. *J. Am. Chem. Soc.* **1995**, *117* (12), 5148.

(22) Sluggett, G. W.; Mcgarry, P. F.; Koptyug, I. V; Turro, N. J. **1996**, *7863* (96), 7367.

(23) Jockusch, S.; Turro, N. J. *J. Am. Chem. Soc.* **1998**, *120* (15), 11773.

(24) Hristova, D.; Gatlik, I.; Rist, G.; Dietliker, K.; Wolf, J. P.; Birbaum, J. L.; Savitsky, A.; Möbius, K.; Gescheidt, G. *Macromolecules* **2005**, *38* (18), 7714.

(25) Griesser, M.; Neshchadin, D.; Dietliker, K.; Moszner, N.; Liska, R.; Gescheidt, G. *Angew. Chemie - Int. Ed.* **2009**, *48* (49), 9359.

(26) Gatlik, I.; Rzadek, P.; Gescheidt, G.; Rist, G.; Hellrung, B.; Wirz, J.; Dietliker, K.; Hug, G.; Kunz, M.; Wolf, J.-P. *J. Am. Chem. Soc.* **1999**, *121* (36), 8332.

(27) Moss, R. A.; Platz, M. S.; Jones, M. J. *Reactive Intermediate Chemistry*; John Wiley & Sons, Inc., 2004.

(28) Yurkovskaya, A.; Morozova, O.; Gescheidt, G. In *Encyclopedia of Radicals in Chemistry, Biology and Materials*; John Wiley & Sons, Ltd, 2012.

(29) Hore, P. J.; Joslin, C. G.; McLauchlan, K. A. *Chem. Soc. Rev.* **1979**, *8* (1), 29.

(30) Pedersen, J. B. *Theories of Chemically Induced Magnetic Polarization*; Odense University Press, 1979.

(31) Trifunac, A. D.; Lawler, R. C. *Magn. Reson. Rev.* **1982**, *7* (2147 - 174).

(32) Hayashi, H. *Introduction to Dynamic Spin Chemistry*; World Scientific Publishing Company, 2004.

(33) Woodward, J. R. *Prog. React. Kinet. Mech.* **2002**, *27* (3), 165.

(34) Hristova-Neeley, D.; Neshchadin, D.; Gescheidt, G. *J. Phys. Chem. B* **2015**, *119* (43), 13883.

(35) Forbes, M. D. E. *Photochem. Photobiol.* **1997**, *65* (1), 73.

(36) Höfer, P. In *Electron Paramagnetic Resonance - A Practitioner's Toolkit*; Brustolon, M., Giamello, E., Eds.; John Wiley & Sons, Inc., 2009.

(37) Goudsmit, G. H.; Paul, H.; Shushin, A. I. *J. Phys. Chem.* **1993**, *97* (50), 13243.

(38) Neshchadin, D. Quantitative Applications of 1H and 31P Chemically Induced Dynamic Nuclear Polarization, University of Basel, 2003.

(39) Closs, G. L. *Adv. Magn. Reson.* **1974**, *7*, 157.

(40) Adrian, F. J. In *Chemically Induced Magnetic Polarization*; Springer Netherlands, 1977; pp 77–105.

(41) Goez, M. *Concepts Magn. Reson.* **1995**, *7*, 69.

(42) Pine, S. H. *J. Chem. Educ.* **1972**, *49* (10), 664.

(43) Muus, L. T.; Atkins, P. W.; McLauchlan, K. A.; Pedersen, J. B. *Chemically Induced Magnetic Polarization*; Reidel Publ. Comp., 1977.

(44) Kaptein, R. *J. Chem. Soc. D Chem. Commun.* **1971**, No. 14, 732.

(45) Gatlik, I. Time-Resolved ESR Investigation of Photoinitators for Radical Induced Polymerization, University of Basel, 2001.

(46) Hristova, D. Kinetic Studies of Radical Reactions using time-resolved EPR, University of Basel, 2005.

(47) Shergill, R.; Haberler, M.; Vink, C. B.; Patten, H. V; Woodward, J. R. *Phys. Chem. Chem. Phys.* **2009**, *11* (33), 7248.

(48) Ott, T. Synthesis and Application of Highly Functionalised, ETH Zürich, 2008.

(49) Huber, A. D. Synthese und Charakterisierung von Bisacylphosphanoxiden und deren Anwendung im Witterungsschutz von Holz, ETH Zürich, 2012.

(50) Neese, F. *Wiley Interdiscip. Rev. Comput. Mol. Sci.* **2012**, *2* (1), 73.

(51) Kolczak, U. CIDNP, NMR and ESR Investigation of New Radical Photoinitiators and New Antioxidants, University of Basel, 1995.

(52) Minegishi, S.; Loos, R.; Kobayashi, S.; Mayr, H. *J. Am. Chem. Soc.* **2005**, *127* (8), 2641.

(53) Mayr, H.; Ofial, A. R. *J. Phys. Org. Chem.* **2008**, *21* (7-8), 584.

(54) Zalibera, M.; Stébé, P.-N.; Dietliker, K.; Grützmacher, H.; Spichty, M.; Gescheidt, G. *European J. Org. Chem.* **2014**, *2014* (2), 331.

(55) Müller, G. Phosphorous Based Photoinitiators: Synthesis and Applications, ETH Zürich, 2013.

(56) Yağci, Y.; Schnabel, W. *Prog. Polym. Sci.* **1990**, *15* (4), 551.

(57) Moad, G.; Rizzardo, E.; Thang, S. H. *Polymer (Guildf).* **2008**, *49* (5), 1079.

(58) Guo, A.; Liu, G.; Tao, J. *Macromolecules* **1996**, *29* (7), 2487.

(59) Lapienis, G. *Prog. Polym. Sci.* **2009**, *34* (9), 852.

(60) Beuermann, S.; Buback, M. *Prog. Polym. Sci.* **2002**, *27*, 191.

(61) Voll, D.; Neshchadin, D.; Hiltebrandt, K.; Gescheidt, G.; Barner-Kowollik, C. *Macromolecules* **2012**, *45*, 5850.

(62) Lauer, A.; Fast, D. E.; Kelterer, A. M.; Frick, E.; Neshchadin, D.; Voll, D.; Gescheidt, G.; Barner-Kowollik, C. *Macromolecules* **2015**, *48* (23), 8451.

6 Appendix

6.1 Supporting Information (Chapter 3)

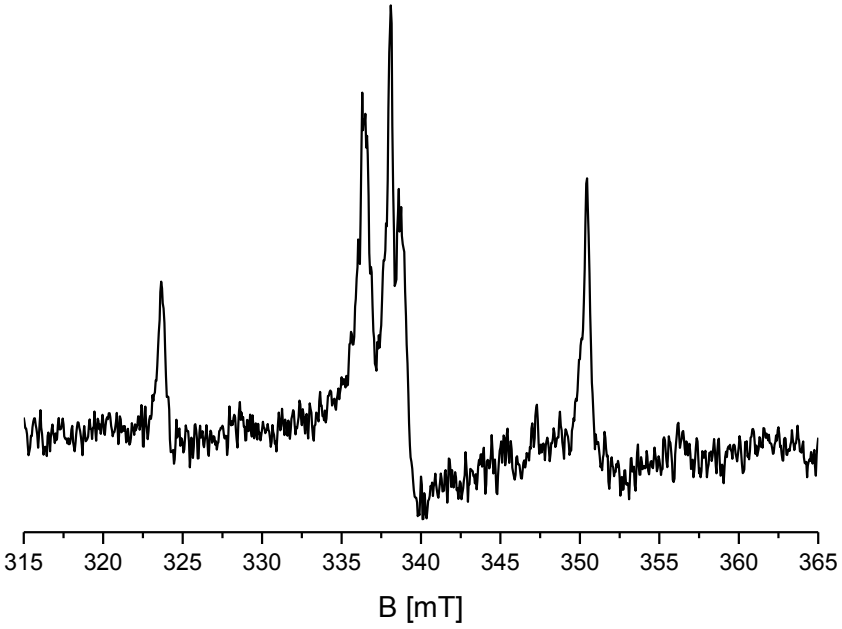

Figure 46. TR-EPR spectrum of compound **1** in presence of Et_3N observed 200 – 300 ns after the laser flash (sample: 15 mM **1**, 1.5 M Et_3N).

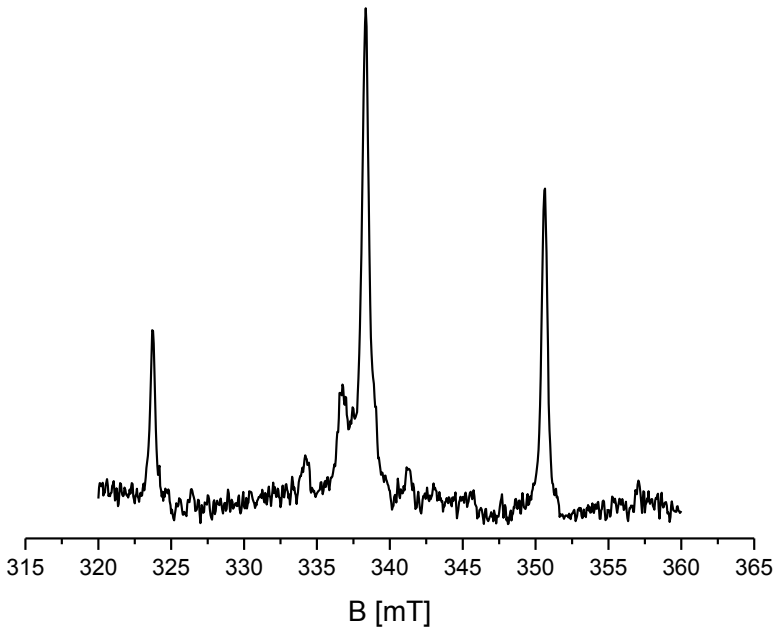

Figure 47. TR-EPR spectrum of compound **1** (15 mM) in presence of Bu_4NF*H_2O (17 mM) measured in acetonitrile 200 – 300 ns after the laser flash. The line distance of the signals marked with an asterisk is 7.1 mT. Only ~ 1 equivalent of the salt was used in the experiment, since at higher concentrations the solutions proved to be instable (precipitation during bubbling with argon).

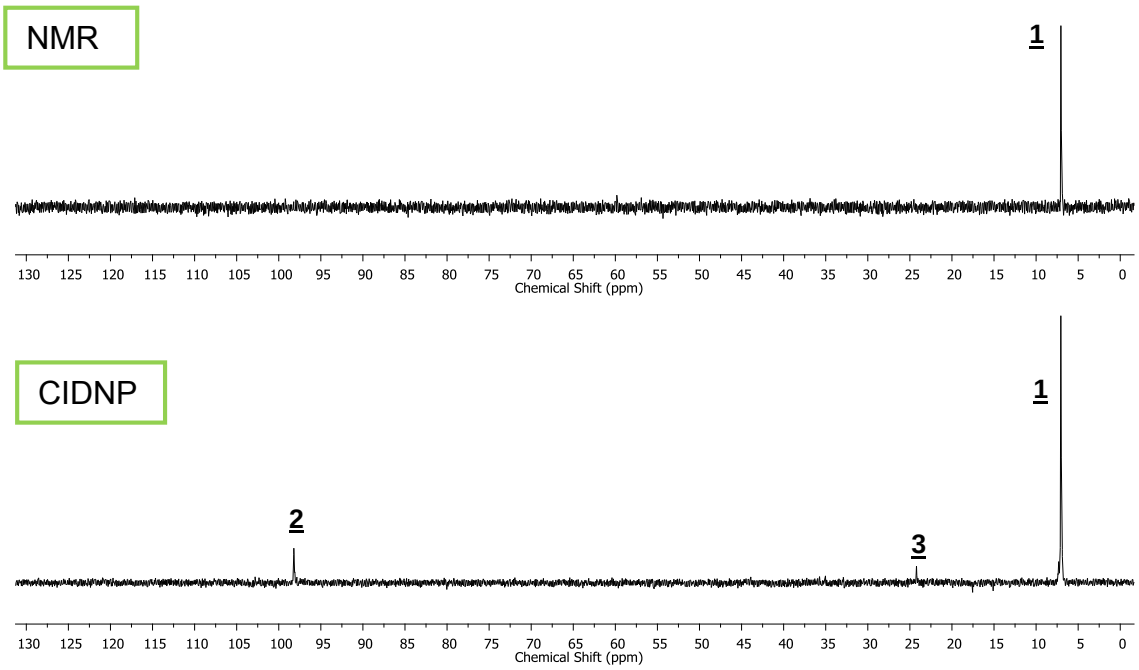

Figure 48. ^{31}P-NMR and CIDNP spectra of compound **1** (15 mM) in presence of EtOH (5 M).

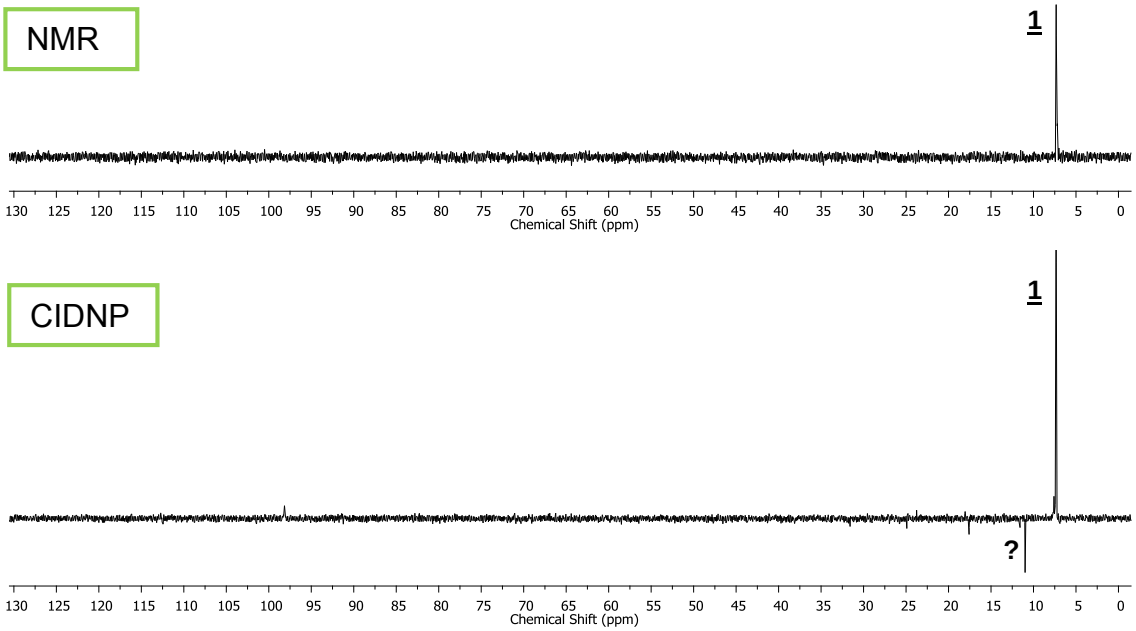

Figure 49. ^{31}P-NMR and CIDNP spectra of compound **1** (15 mM) in presence of Et_3N (1 M).

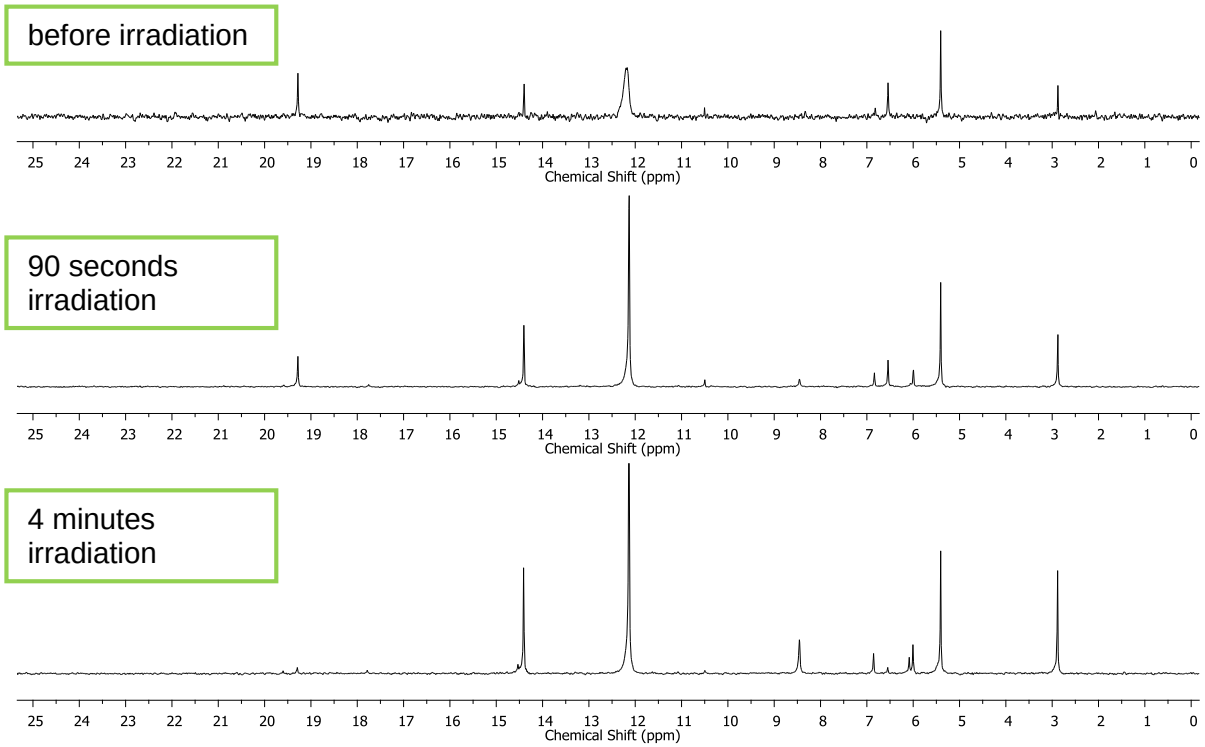

Figure 50. ^{31}P NMR spectra of BAPO (compound **1**) in presence of Bu_4NF*H_2O (sample: 40 mM **1** and 600 mM salt in deoxygenated acetonitrile-d_3).

6.2 Supporting Information (Chapter 4)

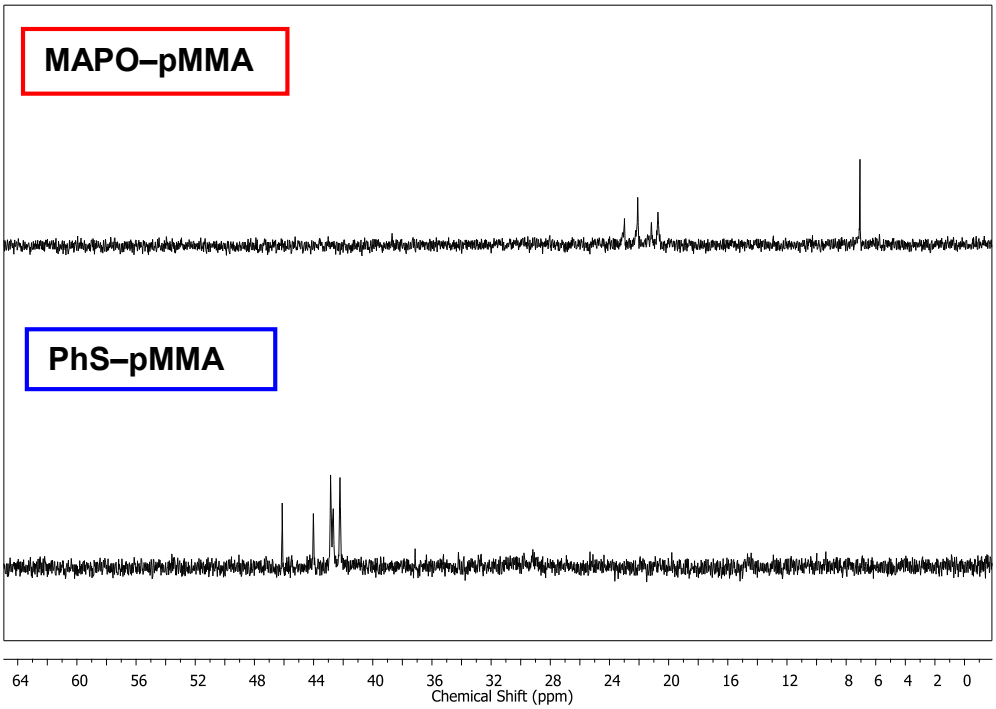

Figure 51. ^{31}P-NMR spectra of MAPO-pMMA and of PhS-pMMA (solvent: THF-d_8). Residual BAPO (7.06 ppm) is still present in the pMMA sample, which however does not interfere with end group analysis by MALDI-MS, due to the different mass range.

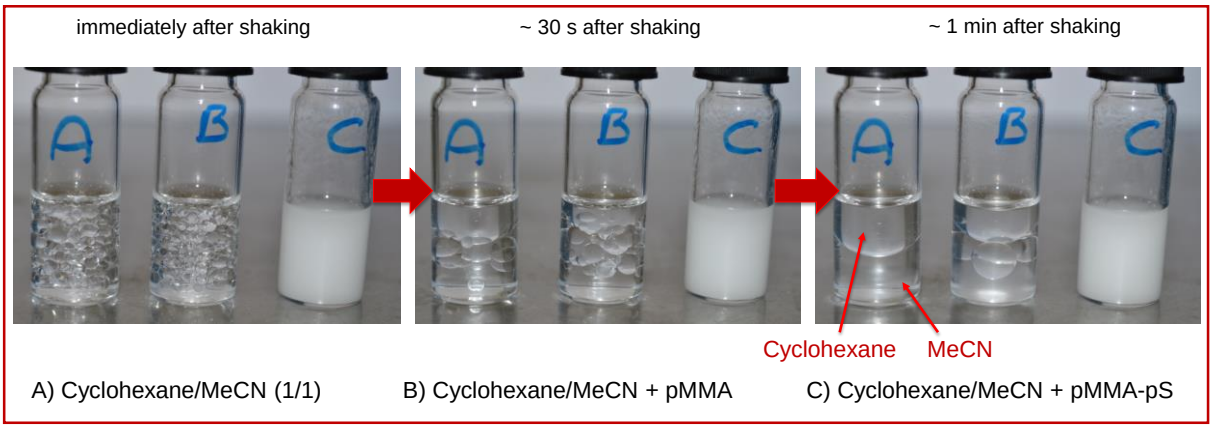

Figure 52. Emulsifying effect of pMMA-pS in the system cyclohexane-acetonitrile.

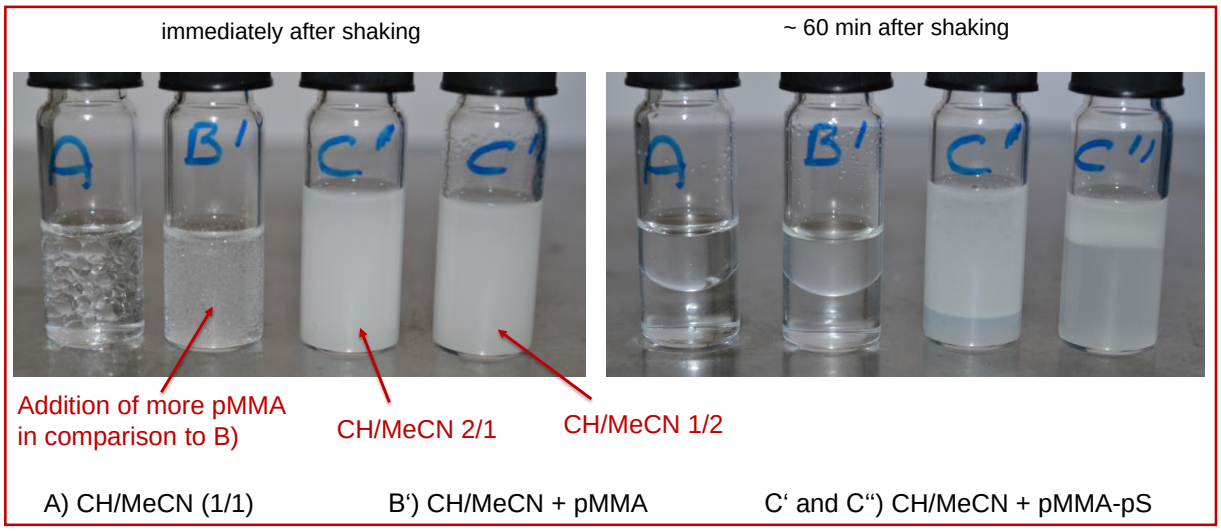

Figure 53. Emulsifying effect of pMMA-pS in the system cyclohexane-acetonitrile with different solvent ratios; observation immediately after shaking and after one hour.

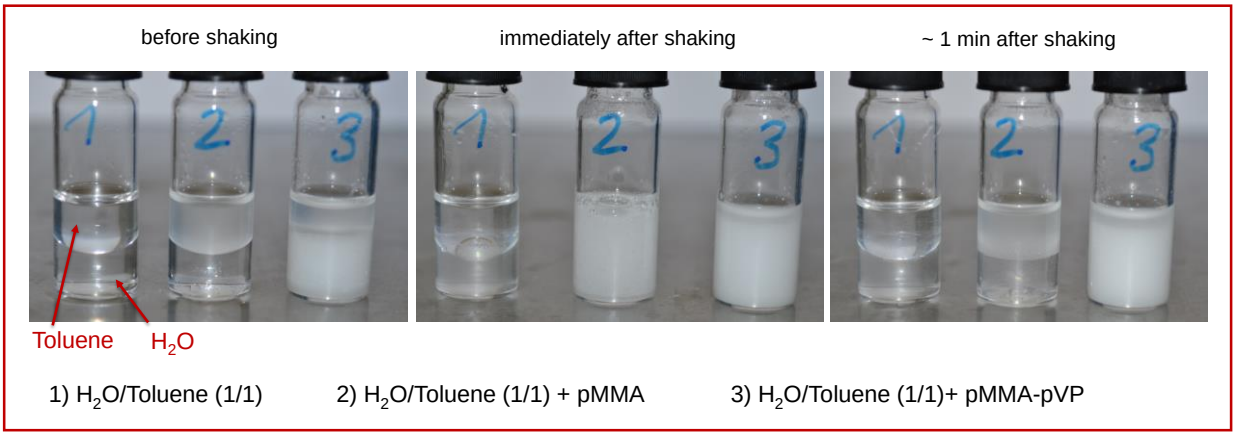

Figure 54. Emulsifying effect of pMMA-pVP in the system water-toluene.

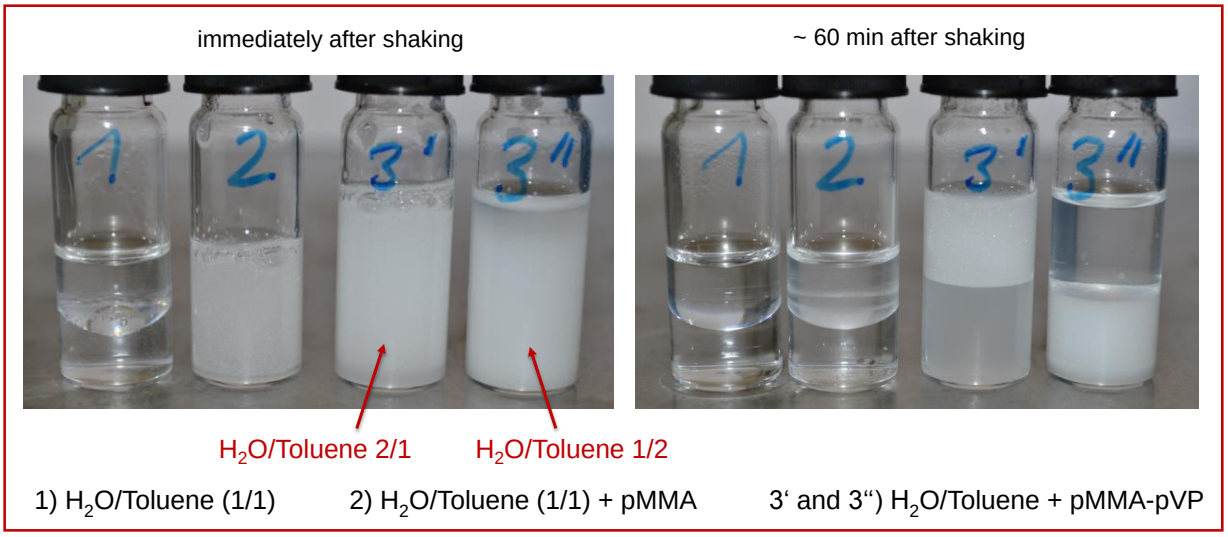

Figure 55. Emulsifying effect of pMMA-pVP in the system water-toluene with different solvent ratios; observation immediately after shaking and after one hour.

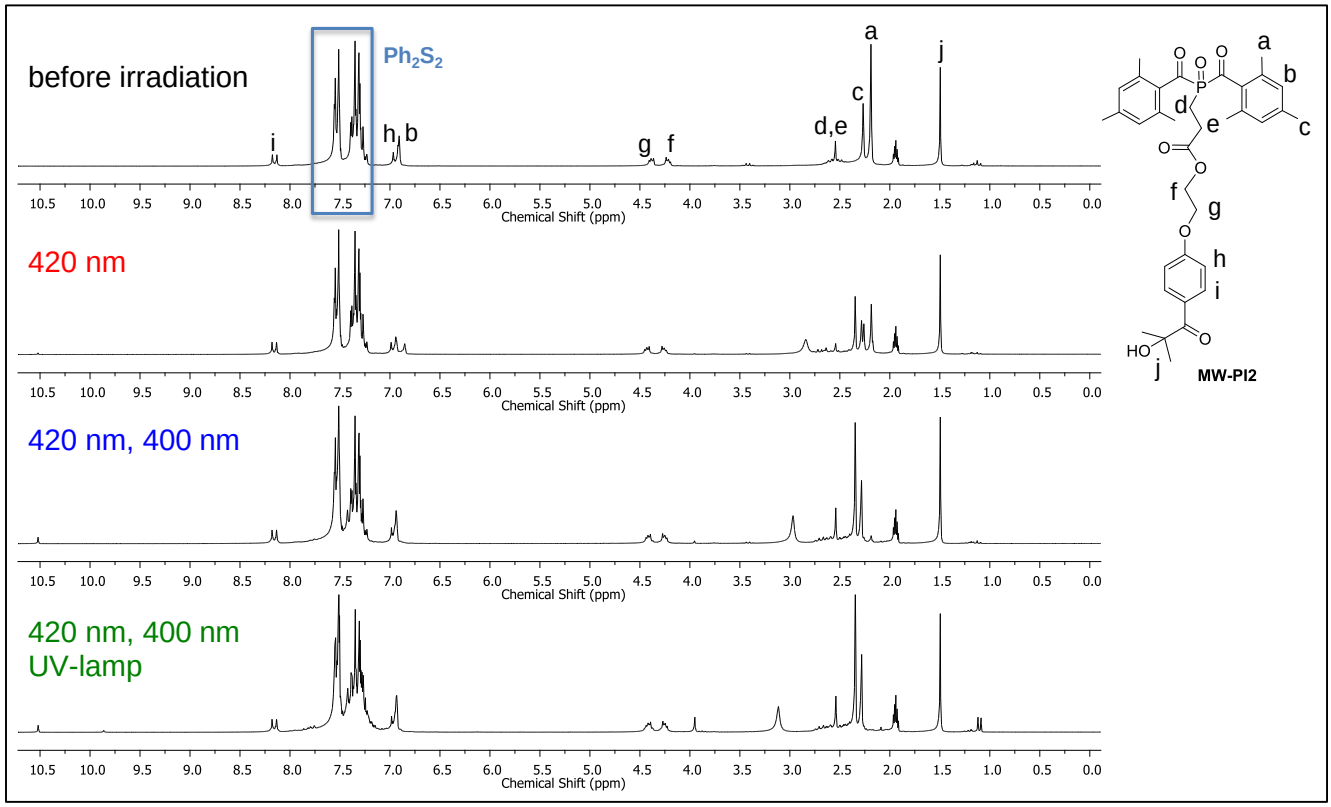

Figure 56. ^{1}H-NMR spectra of MW-PI2 in presence of Ph_2S_2. (Sample: 25 mM MW-PI2, 7 equiv. Ph_2S_2 in acetonitrile-d_3, irradiation times: 4 min at 420 nm, 20 min at 400 nm, 10 min UV lamp.)

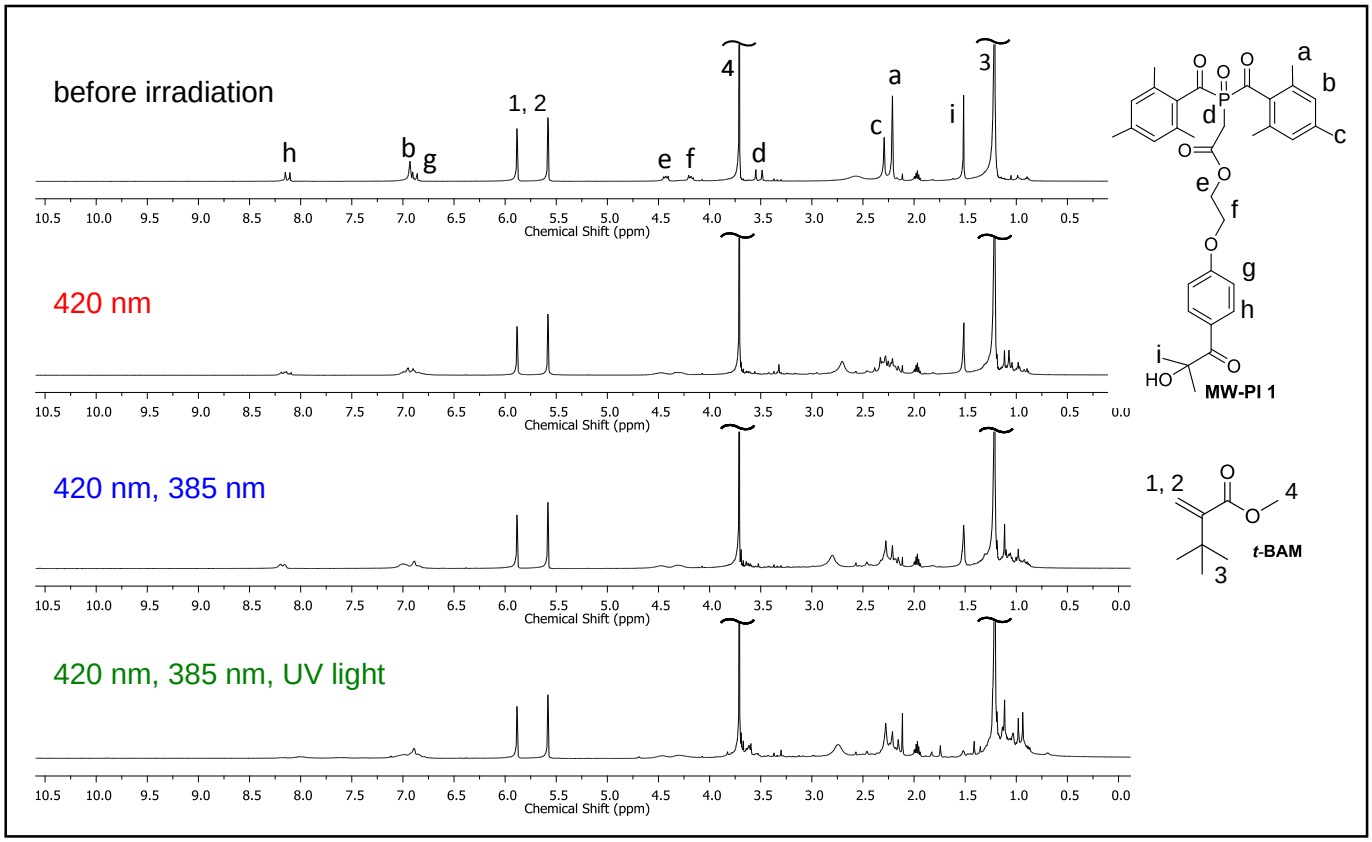

Figure 57. ^{1}H-NMR spectra of MW-PI1 in presence of *t*-BAM. (Sample: 25 mM MW-PI2, 7 equiv. *t*-BAM in acetonitrile-d_3, irradiation times: 10 min at 420 nm, 10 min at 400 nm.)

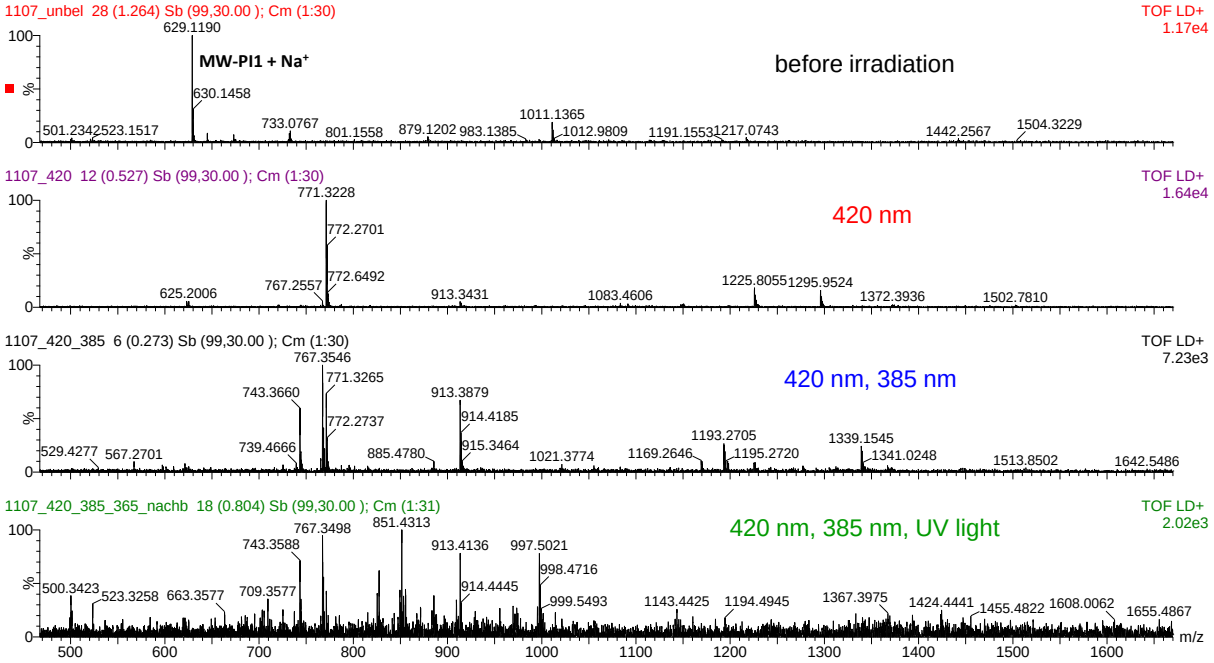

Figure 58. MALDI-MS spectra of MW-PI1 in presence of *t*-BAM (irradiation times: 6 min 420 nm, 12 min 385 nm, 220 s UV lamp).

6.3 List of Schemes

6.4 List of Figures

6.5 List of Tables